Design Synthesis Exercise

Parashuttle 2

July 2013

Group 18

TU Delft Delft University of Technology

PARASHUTTLE®

Challenge the future

Parashuttle 2

Design Synthesis Exercise 2013

Authors:

D. (Daniel) M. Atherstone	4101677
G. (Gerald) J.J. van Dalen	4002881
R. (Robert) L. Eggink	4001397
F. (Floris) H. Haasnoot	4080912
M. (Marco) E.G. van Hellenberg Hubar	1526820
K. (Koen) S. van de Kerkhof	4105737
T. (Tim) D. van Leeuwen	4094573
M. (Max) G. Roest	4084217
P. (Pieter) J.F. Verbist	4094697
D. (Daan) Westerveld	4106032

Preface

Parashuttle is a project started by Lodewijk-Jan Doensen, a general practitioner and aerospace enthusiast. Inspired by his own vision of improved powered parachutes he built a closed-cockpit paraplane for one person, which unfortunately never flew. This design has been the basis of a Delft University of Technology Design Synthesis Exercise project, the final piece of work of the bachelor of Aerospace Engineering. This group of ten Aerospace Engineering bachelor students was challenged to come up with an improved and upgraded version of Parashuttle: Parashuttle 2. Key features of an envisioned upgraded design were its ability to transport not one but two persons and its amphibious characteristics. In front of you lies the final report on the design and development of this revised Parashuttle.

Of course we would like to thank Lodewijk-Jan for trusting us with the design of a second version of his Parashuttle. Without his inspiration this Design Synthesis Exercise would not exist, also his suggestions and involvement during the design process were greatly appreciated. Furthermore we would like to thank our tutors dr. ir. Mark Voskuijl, dr. ir. Erik-Jan van Kampen and ir. Christophe de Wagter for all their valuable comments, suggestions and coaching. Furthermore there are some people within the faculty of Aerospace Engineering who helped us with facts and explanations: ir. Rolf van der Vlugt, Ali Elham MSc and ir. Jos Sinke. Finally we would like to thank Aart de Wachter and Rogier Wolff, who gave early information regarding parafoils and paragliding in general.

The team has genuinely enjoyed working on this novel product and hopes that the reader enjoys reading this report just as much.

Summary

Private flying using a paraglider or powered parachute is an activity practised by thousands of people worldwide, enabling them to enjoy the freedom and fun experience flying offers. From both this market and commercial and governmental agencies there is a need for an improved design of such powered parachutes, one that is able to operate on both land and water and incorporates a closed cockpit which does not expose the pilot to the environment. These are the main functionalities Parashuttle 2, the world's first two-person, closed-cockpit amphibian paraplane, will provide.

In this report detailed design of Parashuttle 2 has taken place, leading a vehicle with a maximum take-off weight of 490 kg and a list price of €32,660 excluding value added tax. The vehicle of 4.6 m long, 2.3 m wide and 2.65 m high is able to transport up to 180 kg of payload. Range and endurance are 198 km and 3.7 hours respectively, making this product attractive for use by commercial and governmental agencies. These two groups of customers contribute to the foreseen demand of a thousand products.

The vehicle's specially designed undercarriage (consisting of floats, wheels and rudders) allows it to operate on both land and water and provides the possibility to switch between the two. Impact handling and manoeuvrability have been ensured by a design optimised for low mass. The fuselage truss structure has been designed to handle 4.5 g loads in a variety of load cases and has been optimised for low mass and accessibility of the cockpit. The large hinging door ensures the latter. The choice of engine and propeller has resulted in a predicted maximum climb rate of 4.7 m/s. Take-off and landing distances are 37 and 32 metres and 60 and 70 metres on land and water respectively. Emissions are in the order of 700 grams of carbon dioxide per kilometre travelled. Finally stability characteristics have been investigated, showing that the vehicle is stable. Damping characteristics of oscillatory motion have not been studied however.

The vehicle's fuselage is designed to comfortably seat two passengers, with payload being stored in the fuselage as well. Instruments, a heating system and high visibility windows allow for comfortable flight for both pilot and passenger. Parashuttle 2 is controlled by the pilot using his arms in normal flight, with his legs assisting during flaring and sharp turns. The maximum arm control force is 110 N, the maximum leg force required is 800 N.

The production process, required future activities and the marketability of Parashuttle 2 have been researched as well, in order to inventory costs associated with the future development, testing and production of Parashuttle 2. It was found that a total investment of €800,000 is needed, leading to a profit of 2.15 million euros over ten years. Production will break even at 271 Parashuttles sold.

Uncertainty still remains in the current design, most importantly a suitable parafoil type has not been found yet. Research into parafoil performance and dynamics is highly recommended, together with analysis of the vehicle's dynamic behaviour during flight and its response to disturbances (such as gusts and bird strikes). Prototype testing is also recommended to validate the analytically predicted performance of Parashuttle 2.

Contents

Chapter 1 | Introduction

Ever since the origin of mankind people have dreamed of being able to fly, often associating this with the feeling of ultimate freedom or even immortality [1]. The Greek myth on Daedalus and Icarus [2] illustrates this ancient desire. Myth became reality when in 1903 the Wright brothers performed the first powered heavier-than-air flight [3], with aircraft evolving rapidly ever since [4].

Today flying is an event accessible to billions of people, with trillions of kilometres being travelled each year [5]. The joy of flying leads to many flying privately for pleasure. One of the cheapest ways of flying is using microlight aircraft [6], for example a powered parachute. These powered parachutes (also known as paraplanes) typically consist of a buggy attached underneath a parafoil and powered by a propeller. The open buggy leaves the pilot exposed to the environment, decreasing flight comfort. This problem was solved with the introduction of Parashuttle, a closed cockpit powered parachute [7]. A second drawback of several paraplanes (and of Parashuttle) is their ability to transport only one person, making flying an individual recreational activity. Also, the restriction of having to land on (level) terrain limits the usability of a paraplane. This leads to the following need statement for a new product:

"Recreational flyers would like to fly with a passenger and be able to operate on both land and water in a variety of weather conditions."

All of these problems are resolved by Parashuttle 2, the world's first two-person, closed-cockpit amphibious powered parachute. The mission statement of Parashuttle 2 thus is:

"Parashuttle 2 will be the world's first closed-cockpit, two-person amphibian paraplane, able to compete with other microlight aircraft on the market."

This report is the final one in a series of four detailing on the design of Parashuttle 2. Based on the functionalities, requirements and concept design specified in previous work [8, 9], this report will go through the process of detailed design. This process is presented in four parts in this report:

Part I of this report recaps the work performed so far, going through a market analysis for this product in chapter 3 and stating its functionalities and corresponding requirements in chapter 4. The final concept, decided on in previous work, is discussed in chapter 5.

Part II elaborates on the models used for the analysis of the performance of Parashuttle 2. Both the theory behind the models and their implementation is discussed.

Part III explains how the subsystems of Parashuttle 2 are designed, discussing a design strategy in chapter 11 and dealing with subsystem design in chapters 12 through 18.

Part IV deals with the integration of the components discussed in part III and verifies the performance of the final design of Parashuttle 2 in chapters 19 through 28. This part ends with the validation of the product through the use of a compliance matrix in chapter 29.

At the end of this report the team will have designed, verified and validated a final design for Parashuttle 2, having specified all apects of the design. The design process gone through will be reviewed and evaluated in chapter 30.

Part I - Preliminary design

Chapter 2 | Operations & logistics

Throughout this design synthesis exercise an image has been kept in mind of what the operation of Parashuttle 2 would look like. This view is largely based on customer wishes and designer ideas. Explicitly stating this vision in this chapter allows for designing (the components of) Parashuttle 2 in later chapters in this report. Therefore the reader is now taken through a typical mission of Parashuttle 2: that of an owner going out for a day and flying his Parashuttle.

Such an owner will perform all activities shown in Figure 2.1 on the right. These activities will now be discussed one by one.

Retrieve from storage - Parashuttle 2 will most probably be stored in a garage or some other protective environment, its parafoil being stored inside the cockpit. Prior to using Parashuttle 2 its brakes will first have to be disengaged, after which it can be rolled out of the garage. The handle at the front of the fuselage can be used to push and pull the vehicle. It also allows for lifting the front wheels of the vehicle, allowing the operator to turn Parashuttle 2 around its axis.

Load onto trailer - With Parashuttle 2 having to take off from a designated strip on land or water, the vehicle will first have to be transported to this location. Using the aforementioned handle Parashuttle 2 can be towed onto a car trailer, where it is secured using both its brakes and straps.

Transport - When loaded on a trailer Parashuttle 2 can be transported behind a car. If needed refuelling can be done at a petrol station.

Take Parashuttle 2 off the trailer - Upon arrival at the location of take-off, the straps with which Parashuttle 2 was secured to the trailer should be removed. Following this the vehicle can be taken off the trailer, again using the handle located at the front of the fuselage. Parashuttle 2 can be unloaded either on land or on water. In the latter case a ramp is required.

Prepare and load Parashuttle 2 for flight - Once unloaded from the trailer, the pilot should prepare his Parashuttle for flight. This means that any protective covering should be removed and the vehicle should be visually inspected for any damage. If detected, appropriate action should be taken. Should the time between overhauls have passed, the engine should be serviced.

The majority of flight preparations concerns the parafoil. In case the vehicle is to take off from land the kite remains in the fuselage for now, in case Parashuttle 2 will take off from water the parafoil should be unfolded and inflated using a compressor, which should be brought along. Its trailing edge should then be attached to the back of the floats using short lines. These lines keep the parafoil in the proximity of the vehicle during taxi. The main parafoil lines should be connected to the correct kite connection points on top of the fuselage, the exact location depending on the intended loading. Both the kite connection and control lines are placed over the fuselage and duct at this stage,

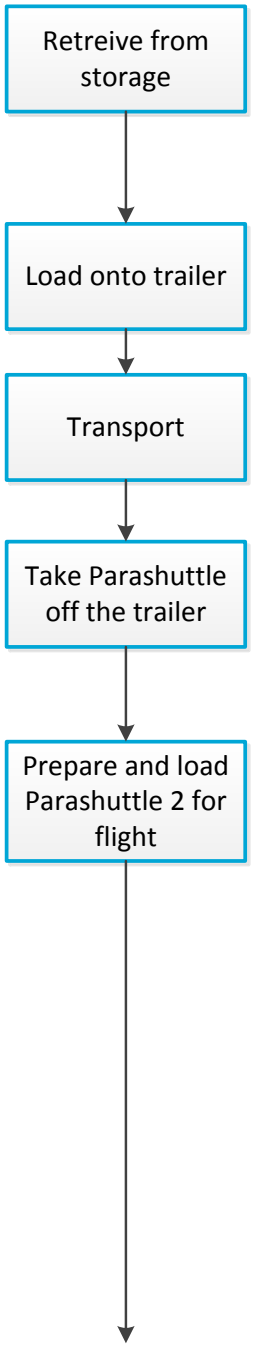

ensuring they do not have to circumnavigate the duct when the kite lifts off. Following all these preparations Parashuttle 2 can be loaded with payload (stored underneath the second seat) and the passenger and pilot can enter through doors in the side, using the floats as a step to get in.

Taxi and take-off - Following all flight preparations Parashuttle 2 can taxi to the take-off location. To do so it must be able to steer on both land and water. As the parafoil is stored in the fuselage while Parashuttle 2 moves over land, the passenger will have to walk in that case. Since it is not expected that taxi distances will be large this is not a problem. In case the vehicle taxis over water it will drag the parafoil (positioned on its top with the trailing edge close to the vehicle) with it, keeping it nearby using short lines.

In case Parashuttle 2 takes off from land the parafoil should be prepared for take-off at this moment, in the same way as was done on water. This time the parafoil will not be connected to the floats however. If positioned on water these lines will be disengaged at this instance as well, using a release system. Located at the start of the take-off strip, the pilot can now increase thrust to accelerate the vehicle. Since the leading edge of the kite (laying on its back) is positioned furthest away from the fuselage and since all parafoil connection lines are equally long, this part of the kite will be pulled first. This causes it to get into an upright position, at which point in time the kite lifts itself out of the water and over the vehicle. As the Parashuttle increases its velocity the parafoil lifts the vehicle from land or out of the water.

Fly and manoeuvre - After take-off the pilot can actually fly, being able to climb and descend by increasing or decreasing throttle respectively and turning by operating the kite control lines from the cockpit. Besides operating the vehicle the pilot should be able to communicate both with the passenger and the external environment, the latter through communication equipment. This also implies the pilot should be able to see the parafoil. The passenger should be able to enjoy the outside view and be seated comfortably.

Should an emergency occur during flight (meaning the parafoil is hard to control, or the control lines break) then the pilot should be able to revert to a secondary means of control to land the plane safely. It should be demonstrated during testing that within its flight envelope the parafoil of Parashuttle 2 will not collapse critically.

Land and taxi - After a descent Parashuttle 2 should be able to flare and land on either land or water. In case Parashuttle 2 lands on land its brakes should be applied, on water the water resistance will provide a braking force. After landing the parafoil will fall back either onto land or in the water. In the first case Parashuttle 2 should be halted as quickly as possible, to prevent the kite from scraping over the ground. Post-flight activities (discussed next) should then be performed close to the runway.

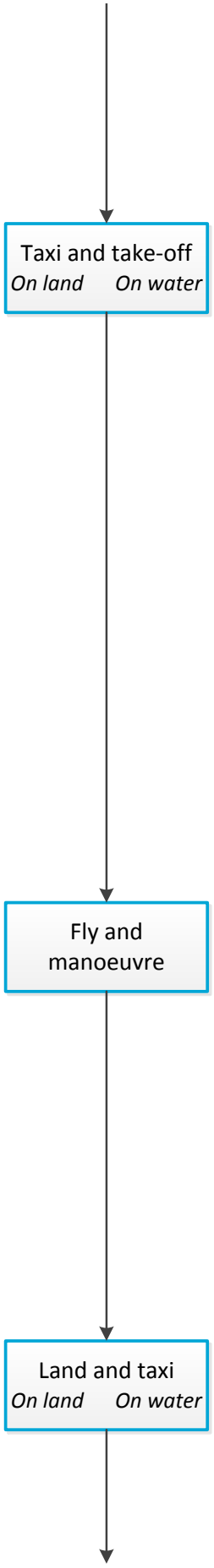

In case of landing on water Parashuttle 2 will drag its parafoil behind it, implying it requires significantly more space for manoeuvring than during earlier taxiing. Open water or a wide channel would be most suited here. Parashuttle 2 should then be taxied to a docking place, where post-flight activities can be performed.

Perform post-flight activities - Post-flight activities initially consist of dealing with the parafoil. On land this means deflating the kite, detaching its control and connection lines, folding it up and storing it in the fuselage. On water the kite should be detached as well and then brought to a location where it can dry. After it has dried it can be folded and stored. After detaching the parafoil Parashuttle 2 should be visually inspected for any damage and appropriate action should be taken in case anything is found. Finally Parashuttle's protective covering can be applied again, thus preparing the vehicle for storage or transport.

Transport and/or storage - Following the preparation, execution and aftermath of the flight, the pilot will go through the reverse of the process described in the first four blocks. In case the storage location is nearby transport is not required and Parashuttle 2 can be stored straight away. Again it can be moved and manoeuvred using the handle up front. In case Parashuttle 2 is taken back to home it shall be loaded and strapped onto its trailer again, driven back and then be stored in a protective environment.

Figure 2.1: Activities during typical operation of Parashuttle 2.

Chapter 3 | Market analysis

Parashuttle 2 will meet the market need identified in the introduction and will provide functionalities no other paraplane currently does. To assess the demand for Parashuttle 2 a market analysis has been performed previously [8], also providing insight into the price that can be charged for Parashuttle 2. The evaluation was conducted in the three phases described below. The results of the market analysis are summarised in this chapter and conclusions are given in the final section.

Phase I - Research is done to list all potential end-user groups. These groups are listed in section 3.1. Based on data an estimate will be made of the size of these groups.

Phase II - In section 3.2 a competitive product price is determined, based on prices of comparable paraplanes and alternative products like glider aircraft, paramotors or small powered aircraft.

Phase III - In section 3.3 current trends possibly influencing the design of Parashuttle 2 in future are identified together with future competitors.

3.1 Phase I

During the market analysis four groups of users of Parashuttle 2 were identified: current members of the paragliding community, microlight aircraft and light sports aircraft flyers, government agencies and commercial agencies. Combining multiple sources [10–15] it was found that the size of the first group is about 150,000, though demand in this group will not be near this number due to the fact that most paragliders prefer the silent experience of paragliding. Using information on the number of pilot licenses registered from available sources [16, 17] it was estimated the second group consists of roughly 50,000 potential customers.

Though governmental and commercial agencies are not allowed to make use of Parashuttle 2 in the Netherlands under the regulations it is to be certified for [18, 19], a sizeable number of customers (around one thousand) is foreseen in other countries. To be used by these agencies Parashuttle 2 should have similar performance to current paraplanes, implying that:

1. Parashuttle 2 should have operating costs in the region of €30/h [6].
2. Parashuttle 2 should be able to take off in less than 50 m and have a landing distance of less than 40 m [20].
3. Parashuttle 2 should have a range of around 200 km [6, 21].
4. Parashuttle 2 should have an endurance of around 3 hours [20, 21].

Going through these requirements (not considered in previous work since Dutch regulations ruled out commercial use) one observes that some of these are more strict than those defined earlier [8]. It has been decided that Parashuttle 2 will be designed for its original requirements first and if possible will be upgraded to fulfil these requirements.

From this analysis it was concluded that, although hard numbers can not be given with certainty, the potential market size for Parashuttle 2 is in the order of thousands of products. This number will be kept in mind when defining the (costs of the) production process of Parashuttle 2.

3.2 Phase II

Comparing the specifications of currently available paraplanes to those of Parashuttle 2 it was concluded that the market price of Parashuttle 2 will exceed the average price (€20,000) of these aircraft, due to its wider range of functionalities. Through an analysis of (the prices and functionalities of) microlight aircraft and light sports aircraft currently available it was concluded that the sales price of Parashuttle 2 should be in the region of €35,000 for it to be financially competitive on

the MLA & LSA market. At such price Parashuttle 2 could be attractive for commercial and governmental use as well [6]. This sales price was defined to be a driving (but not killer) requirement, as the project can not be considered a total failure if this sales price is exceeded slightly.

3.3 Phase III

In order to properly predict the marketability of Parashuttle 2 not only its market introduction should be considered, but also the first few decades after the introduction are of importance. Therefore current developments which could have a future impact on the market of Parashuttle 2 have been assessed. The combination of increased scarcity of fossil fuels and the accompanying rise in oil prices [22, 23] will lead to increasing operating costs of Parashuttle 2 in future. Additionally the improvements in the specific energy of batteries [24] make the use of an electric engine more favourable, meaning that in future Parashuttle's engine might be replaced by an electric one. Requirements on safety and navigation systems present will become more strict with personal air transport becoming more popular as well, meaning the interior of Parashuttle 2 will have to be adjustable for these developments.

Future competitors for Parashuttle 2 have been found to be gyrocopters (a crossover between a helicopter and a motorcycle), which are being developed at this point in time and will become more affordable (costing around €250,000 now) over time.

3.4 Conclusion

The market analysis for Parashuttle 2 is hampered by the fact that there is no clearly defined market for the product, furthermore it is unclear how much potential new markets have. Extending the market to governmental and commercial use leads to more requirements on Parashuttle 2, most of which do not significantly differ from requirements imposed earlier [8].

An inventory into prices of existing paraplanes and LSA and MLA references has been performed. Considering the complexity of these vehicles a list price of €35,000 has been chosen as target price for Parashuttle 2.

Diminishing fossil fuel reserves and the development of sustainable energy sources can play an important role in the future marketability of Parashuttle 2. Alternative products are still in a development stage but might become competitors in future.

Chapter 4 | Functionalities & requirements

In previous chapters the need for a closed-cockpit, amphibious paraplane design was identified and the demand for such a product has been investigated. Knowing that demand is big enough to start designing the product, functionalities Parashuttle 2 should provide have been identified at the start of this project. These functionalities will be shortly discussed in section 4.1. The desired functionalities (amongst other sources) impose requirements on the design of Parashuttle 2, these are discussed in section 4.2.

4.1 Functionalities

In essence Parashuttle 2 is designed to carry two people around in flight, however to do so Parashuttle 2 must provide a number of other functionalities. An inventory of these has been made in a functional breakdown structure, presented in appendix A. One observes that, besides flying, Parashuttle 2 shall offer eight other utilities in order to perform missions such as the one described in chapter 2: The provision of power, dealing with the external environment, maintainability, manoeuvrability, the ability to be stored, the accommodation of payload, the provision of safety and transportability. By putting these nine functions in the correct order one can build up the mission of Parashuttle 2.

This is exactly what has been done in the functional flow diagram of the product, shown in appendix A as well. Further explanation of all functionalities has been given in previous writing [8]. The functional breakdown structure and functional flow diagrams have been used to come up with the requirements imposed on Parashuttle 2, presented in the coming section. Furthermore they have been used to think of design options able to provide the desired utilities. These design options are discussed in chapter 5.

4.2 Requirements

The requirements on Parashuttle 2 originate from five sources. The sources are shortly listed below, the requirements originating from these have been ordered in a requirements discovery tree. This tree, together with the full list of requirements, is shown in appendix B. This last has later been used to validate whether the final product satisfies customer wishes.

Regulations - Parashuttle 2 should above all be certifiable under MLA regulations, this is one of the top level requirements. The product should thus meet all standards required by this set of regulations.

Market demands - As explained in chapter 3 the market for Parashuttle 2 determines for example its sales price and availability.

Safety considerations - Since officially little training is required to fly a powered parachute and Parashuttle 2 will be flown mostly by relatively inexperienced individuals [21], it is important that Parashuttle 2 is as safe as possible.

Mission requirements - Parashuttle 2 shall be able to fulfil the mission presented in the previous section. The functionalities required to do so impose many requirements on the design of Parashuttle 2.

Sustainability - Consumers are becoming more and more oriented towards sustainability, meaning that besides the aforementioned sources of regulations sustainability considerations need to be taken into account as well.

Chapter 5 | Final concept selection

Multiple design solutions providing the functionalities and meeting the requirements presented in the previous chapter can be thought of. Earlier in this project design options have been clustered into concepts, on which a trade-off has been performed to come up with a final concept [9]. This final concept is to be designed in detail in parts II, III and IV of this report. The concepts analysed are presented in section 5.1, after which trade-off results are discussed in section 5.2. The configuration and lay-out of the final concept are then discussed in section 5.3.

5.1 Concept designs

Some design choices are known to have a major impact on the rest of a concept design or on the overall lay-out of a concept. Choosing between different undercarriages might have effects on the fuselage shape and engine position. One could on the other hand think of two identical designs, distinguished only by the use of different engines. In previous writing dominant design options (which vastly influence the full design) were identified and distributed over six concepts, which were then specified in detail [9]. Below a description of these six concepts is given:

Concept 1 - A floating hull concept in which the two passengers are seated abreast. The concept's parafoil is supported by two poles to prevent it from touching the water.

Concept 2 - A vehicle supported by three floats in which passengers are seated in-line in a transparent cockpit. The concept is powered by an electric engine, with a winch allowing for automatic retraction and release of the kite.

Concept 3 - A paraplane supported by two floats incorporating wheels, carrying a rail on top of the fuselage to attach its pre-inflated parafoil to. Passengers are seated abreast.

Concept 4 - An electrically powered hovercraft in which the passengers are seated abreast. A winch provides the possibility of automatic retraction and release of the parafoil.

Concept 5 - A hovercraft in which passengers are seated in-line in a transparent fuselage. A floating kite is attached to the fuselage using a rail.

Concept 6 - A paraplane featuring a top-mounted wing producing part of the required lift. Two floats with wheels provide stability on land and water, a net mounted to the back prevents the non-inflatable parafoil from touching the water.

A trade-off has been performed to find which of the aforementioned concepts is the best option to use as a final design. This procedure is summarised in the next section.

5.2 Trade-off & final concept selection

Prior to the trade-off it was found that the electric engine of concept 4 (used for both hovering and propulsion) required a battery mass not compatible with regulations. This option was therefore discarded prior to the trade-off. During a trade-off in which all concepts were evaluated on nine trade criteria it was found that concept 3 (the 'simple' concept with floats and a floating kite) performed best, though it was also found that the electric engine of concept 2 severely downgraded it on multiple trade criteria. Replacing the electric engine by a gasoline engine, omitting the winch and storage system (considered infeasible due to the big parafoil required) for an inflatable kite and evaluating this new concept 2* led to this concept performing even better than concept 3.

To see whether concept 2* adhered most to customer wishes a second trade-off was performed, this time using customer preferences to determine the weights of the trade criteria. Again concept 2* proved to perform best, leading to the decision to choose concept 2* as a final design. From now on this concept 2* will be referred to as the final concept.

5.3 Configuration & lay-out

In the third part of this report the components of the final design will be designed in detail. To facilitate this process (elaborated on in chapter 11) the general lay-out of the final design is presented in this section, as well as the configuration of its components. These are both shown in Figure 5.1.

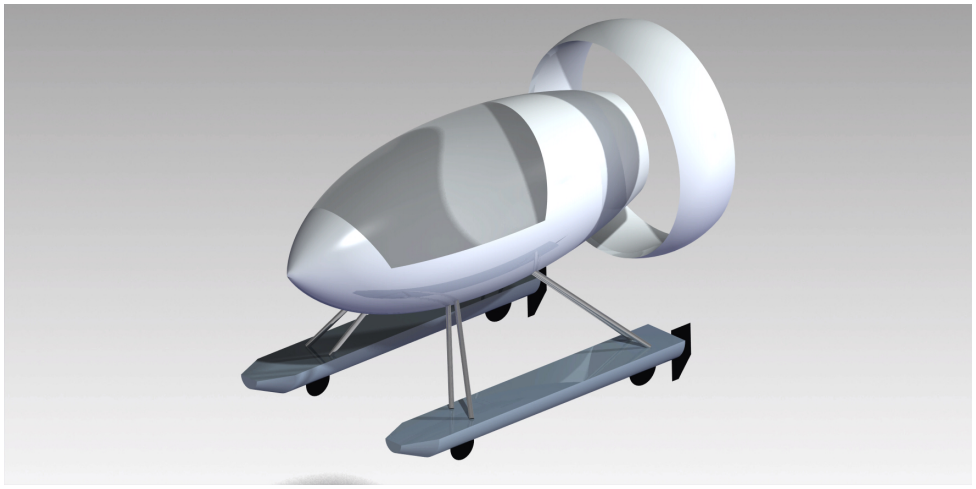

Figure 5.1: Initial configuration of the final design of Parashuttle 2.

The final concept seats the passengers in line, allowing the cockpit to be slender and thus to reduce aerodynamic drag of the fuselage. The frame structure of the fuselage guarantees its structural integrity, whereas its non-loaded transparent skin provides the passengers with high visibility. The engine and propeller are located in the back, with a duct being used around the propeller to prevent kite lines from interacting with the propeller and to improve efficiency [25, 26].

The vehicle is supported by two floats, connected to the fuselage. The floats incorporate two wheels each, one of which is fitted with a brake. By using differential braking the plane can turn on land. Turning on water is done using rudders mounted on the back of the floats.

The vehicle is lifted using a floating parafoil, which is to be inflated before take-off. During flight the parafoil will slightly deflate, however it will retain its shape due to the continuous flow of air into the kite through its designated air vents. After landing the parafoil is folded up and stored. Lateral control is obtained by warping the parafoil using control lines running from the kite's trailing edge to the cockpit.

With the lay-out of the vehicle and configuration of its components now known the team can start designing the aforementioned components into detail. This will be done in part III of this report in chapters 11 through 18. First the models used to evaluate performance of the final design on various aspects are discussed in part II.

Part II - Analysis models

Chapter 6 | Propeller model

With relatively little information available on the optimal configuration of propellers for desired performance, the team has built a model to assist in designing and analysing a suitable propeller. The number of blades of Parashuttle's propeller and their size and shape will be determined in chapter 12. The model is explained in section 6.1, with verification and validation done in section 6.2.

6.1 Model theory

The model used to predict propeller thrust for a certain rotational speed is based on blade element theory [27], programmed in MATLAB. Parashuttle's velocity V_e, the local air density ρ, the engine angular velocity ω_e, the propeller blades' shape, length, pitch angle distribution and angular velocity ω and the number of blades B are used as input. Using these one can find the thrust T produced as well as the power P required for this thrust. This is done using equations 6.1 and 6.2:

$$T = B \int_{R_{hub}}^{R_{tip}} \frac{1}{2} \rho V_e^2 c (C_l \cos(\phi) - C_d \sin(\phi)) \mathrm{d}r \tag{6.1}$$

$$P = B \int_{R_{hub}}^{R_{tip}} \frac{1}{2} \rho V_e^2 c \omega r (C_l \sin(\phi) + C_d \cos(\phi)) \mathrm{d}r \tag{6.2}$$

Here ϕ is the angle between the rotational velocity and the total velocity experienced by the blade, which is determined from the blade element pitch angle and the decrease in angle of attack due to the velocity of the vehicle. The model assumes no induced air velocity due to the propeller blades.

6.2 Verification & Validation

To verify the model discussed previously a rectangular, constant pitch, three blade propeller was analysed using both the numerical model and the analytical method (assisted by Wolfram Alpha to solve the complex integrals). The results for thrust for both cases can be found in Table 6.1. As can be seen the difference is 2%, which is small enough to be ascribed to round-off errors.

Table 6.1: Results of the verification and validation of the model

Verification		**Validation**	
MATLAB model	Analytical solution	MATLAB model	Experimental values
2658.2 N	2601.3 N	3070.8 N	1549 N

The now verified model needs to be validated as well, thus experimental values from wind tunnel tests were compared with calculations using the MATLAB model. An experiment in which a propeller with a Clark Y profile was tested in a wind tunnel was used to validate the model [28]. Running the MATLAB model using the aerodynamic characteristics of this airfoil [29] allowed for validation of the model. The results are summarised in Table 6.1. It is found that the model gives results of the same order of magnitude, however the experimental value is about half that of the model. Reasons for this discrepancy are sought in the fact that the precise distribution of twist over the propeller was unknown. Furthermore the model showed high angles of attack, which in reality would lead to flow separation, an effect which could not be incorporated in the model. Also the induced velocity will play a role in this discrepancy.

Chapter 7 | Flight models

Two flight path models will be used to analyse whether the design of Parashuttle 2 come up with fulfils requirements set on flight performance. In sections 7.1 and 7.2 the longitudinal and lateral flight path model used for analysis will be elaborated on. These models will then be referred to in later chapters to explain design options and performance characteristics.

7.1 Model for longitudinal flight

The model used to analyse the longitudinal flight characteristics of Parashuttle 2 is based on a Master Thesis of the Rochester University of Technology [30]. The model makes use of the following assumptions:

1. The parafoil is at a fixed orientation with respect to the fuselage and to be right above the fuselage when the fuselage is in horizontal position.
2. The lift coefficient of the parafoil is constant, leading to a constant total lift coefficient. Additionally the lift over drag ratio is constant.
3. The thrust vector is assumed to be aligned with the fuselage horizontal axis.
4. Lift is assumed to be perpendicular to the airspeed, drag (for both the parafoil and the fuselage) is assumed parallel to the airspeed.

The full model (including the MATLAB code and Simulink model) is given in the thesis. Here the model is verified and validated as well, giving confidence in the fact that this model accurately represents reality (steady climb rates are predicted within 20% of the actual value and flight paths are simulated very accurately, with steady-state altitude responses correct in the order of decimetres and transient response predicted within 1 metre). The model predicts the qualitative flight behaviour correctly, showing climbing flight in case engine thrust is increased and descending flight in case thrust is lowered. Additionally one observes that during flight the total velocity remains nearly constant (in trimmed flight, i.e. no deflection of the canopy), which is a common phenomenon for powered parachutes.

The determination of the pitch angle is less accurate. Since the model makes use of rigid lines, moments can be translated from the parafoil to the fuselage. Due to this, the parafoil drag and lift have significant effects on the moments about the centre of gravity. Furthermore, the inherent stability of the fuselage with respect to the parafoil is not taken into account, because the kite connection point is assumed to be clamped (i.e. the wing can not rotate with respect to the fuselage). This way, in the model the fuselage pitch angle with respect to the parafoil is zero. More elaborate investigation in the pitch response can be done by using a multi-body dynamic model. Furthermore, the pitch response should be investigated and optimised using ground tests, as described in chapter 26.

The model was copied by the team members. By ensuring that the simulation model provided exactly the same graphs as in the master thesis the model was verified. With confidence that the model functioned properly, adjustments to the simulation were made to make it applicable to Parashuttle 2. This section will elaborate on these modifications and will present an overview of the required inputs and outputs for this model.

7.1.1 Thrust setting

In the original model thrust was a direct input, with the thrust setting determining the flight path obtained. Since in Parashuttle 2 the pilot will use thrust variations to control the altitude it has been decided to specify the desired rate of climb over time and then let the model change the

thrust accordingly. To do so, use was made of a proportional controller, which adjusted the thrust level (beteen 0% and 100%) using:

$$\frac{d(T_{setting})}{dt} = k_1 \cdot (ROC_{intended} - ROC_{actual}) \tag{7.1}$$

where k_1 is a constant which is to be optimised during the analysis of flight performance in chapter 21. The thrust level is then converted to a propulsive force using the propulsion model discussed previously. The pilot's thrust setting is converted to an engine RPM, which is then converted to the thrust delivered by the propeller using the model explained in chapter 6.

7.1.2 Fuel consumption

Contrary to the electrical powered parachute used in the thesis, Parashuttle 2 uses a petrol engine which consumes fuel. To take the varying aircraft mass during flight into account (its mass will decrease by about 7% in flight) the fuel mass has been added as a state variable in the model. Its derivative is given by the fuel flow, which can be derived from the instantaneous engine RPM using the specifications of the chosen Rotax 582 engine [31]. Once the vehicle runs low on fuel a descent is instructed to the simulation, after which the vehicle lands. Investigating the flight time and touchdown position gives indications of the vehicle's range and endurance. Note that a conservative value for fuel consumption is used based on the information from an engine reseller.

7.1.3 Parafoil lift and drag

In the original model the lift curve as a function of airspeed was determined from the requirement to be able to cruise at a certain velocity. For the model of Parashuttle 2 the parafoil's lift coefficient, area and the air density will be estimated in order to evaluate the lift for a given velocity. Rather than assuming a constant lift over drag ratio for the parafoil, research is done into the drag polar of parafoils. With no wind tunnel and fuselage available to experimentally determine fuselage drag, reference fuselages will be looked for in chapter 18 to determine its drag coefficient. The parafoil and fuselage drag combined give a more accurate prediction for the drag than the value obtained using a constant lift over drag ratio.

7.1.4 Parafoil connection

In the original model the mounting location of the parafoil on the fuselage was assumed to be constant. Since the power lines (i.e. the main lines connected to the canopy) are also assumed to be perpendicular to the longitudinal body axis, this means the centres of gravity of the canopy, the fuselage and thus the total system are on one line. This leads to some simplifications in the moment equation. Because the kite connection point of Parashuttle 2 can be moved, this is adjusted in the longitudinal model. This way the pitch angle of the fuselage can be decreased by moving the kite connection backwards.

7.1.5 Take-off procedure

In case Parashuttle 2 is initially positioned on land or water the vehicle should first take off. Both on land and water the boundary condition is set that the pitch angle θ and its derivative should remain zero during take-off. Naturally the z-coordinate of the vehicle is zero. During take-off acceleration is given by Equation 7.2, in which D_{UC} is the undercarriage drag. On land this consists of the roll drag given by Equation 7.3, on water it is a combination of viscous drag and wave drag, given by Equation 7.4. For both land and water the required normal force N (called buoyancy on water) is

given by Equation 7.5.

$$a_x = \frac{T - D_p - D_f - D_{UC}}{m} \tag{7.2}$$

$$D_{UC} = \mu_{roll} \cdot N \quad \text{(on land)} \tag{7.3}$$

$$D_{UC} = f(V) \quad \text{(on water)} \tag{7.4}$$

$$N = W - L \tag{7.5}$$

The horizontal velocity a_x is integrated over time, leading to a velocity V_x and position x. Once lift is bigger than weight the vehicle will accelerate in z-direction, at which stage the regular model is run again to simulate flight behaviour.

7.1.6 Landing procedure

In case a negative rate of climb over a long period of time is given as input, the simulation will at some point predict the vehicle hitting the ground. At this point the simulation switches to landing mode, setting the pitch angle θ, pitch rate $\dot{\theta}$ and vertical velocity to zero. In this phase the following horizontal equations of motion apply:

$$a_x = \frac{-D_p - D_f - D_{UC}}{m} \tag{7.6}$$

$$D_{UC} = \mu_{roll} \cdot N + 0.65\mu_{brake} \cdot N \quad \text{(on land)} \tag{7.7}$$

$$D_{UC} = f(V) \quad \text{(on water)} \tag{7.8}$$

$$N = W - L \tag{7.9}$$

These equations are similar to those on water, though now thrust is set to zero and the drag of the undercarriage on land features a braking component as well. Here it is assumed that the rear wheels (those used for braking) carry 65% of total vehicle weight. The simulation of landing runs until the horizontal velocity has been reduced to zero.

7.1.7 Flight simulation procedure

The flight simulation model requires input on Parashuttle 2, its parafoil and the intended rate of climb over time. Furthermore a set of initial conditions is required. The simulation model will implement these values into the equations of motion and integrate the resulting accelerations to obtain the velocity and position of Parashuttle 2. The data flow of this flight model thus is as shown in Figure 7.1, where the orange arrow represents a feedback loop.

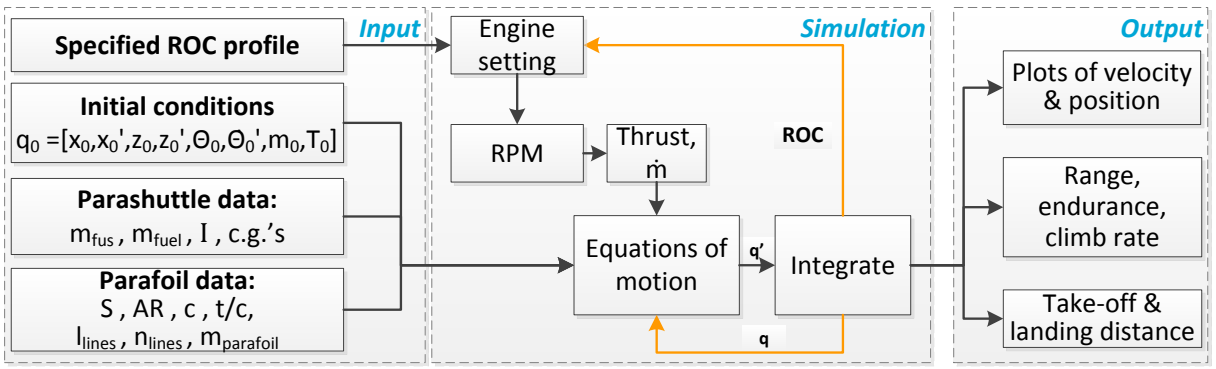

Figure 7.1: Flow of data through the simulation model for longitudinal flight.

The output of this model will be used to comment on Parashuttle's performance in chapter 21 and its control characteristics in chapter 22.

7.2 Model for lateral flight

Besides the model for longitudinal flight presented earlier a model describing the turning behaviour of the vehicle is also required to analyse its performance. Since such a model does not exist yet the team has decided on building an own simulation tool. A visit to kite expert Rolf van der Vlugt (member of the TU Delft Wind Energy Research group) has taught that a parafoil provides a paraplane with turning capabilities through three effects:

Asymmetric lift - In case one pulls the control lines of the left side of a parafoil (as seen from behind) this side of the parafoil will camber more, providing additional lift. This lift will produce a clockwise moment, roll the vehicle in clockwise direction and cause it to turn to the right due to the centripetal part of the lift force.

(Induced) drag - The increase in lift force mentioned above will result in additional (induced) drag on the left side of the parafoil. This will cause a yawing moment which turns the vehicle left.

Parafoil warping - When shortening the control lines the left part of the parafoil will tilt backwards and the front part will tilt forwards. This twist causes the resultant lift force to tilt backwards on the left part of the kite and forwards on the right part. This again induces a yawing moment which turns the paraplane left.

Naturally all effects are reversed in direction when the right control lines are shortened. Rolf van der Vlugt told that for parafoils the effect of asymmetric lift on a turn is negligibly small, meaning this cause is not taken into account. According to Mr. van der Vlugt leaving out the third effect results in a model adequately predicting turning behaviour, yet not feeling entirely natural. However for ease of simulation (and since according to Mr. van der Vlugt this is the effect which is primarily responsible for turning) only the second effect will be taken into account. This also implies that it is assumed that the vehicle does not roll.

The free body diagram used as a basis for the simulation model for lateral flight is shown in Figure 7.2. It is assumed that the aircraft does not sideslip (β represents the angle between the instantaneous and initial velocity) and that the orientation of the parafoil with respect to the aircraft remains constant. This implies that an increase in drag on the parafoil is directly transferred to the fuselage through the parafoil lines. The increase in drag ΔD causes a yawing moment and a yawing acceleration, given by Equation 7.10. The additional induced drag force in turn is given by Equation 7.11.

$$\ddot{\beta} = \frac{\left(F_{k,right} - F_{k,left}\right) \cdot \Delta y}{I_{zz}} \tag{7.10}$$

$$\Delta D = \frac{1}{2}\left(\frac{C_{L_2}^2 - C_{L_1}^2}{\pi A}(1+\delta)\right)\rho S V^2 \tag{7.11}$$

Equation 7.11 is derived from the equation for parafoil drag (discussed in more detail in chapter 17), in which C_{L_1} is the initial lift coefficient, C_{L_2} is the lift coefficient after deflection of the parafoil, A is the aspect ratio and δ is a coefficient dependent on the aspect ratio [32]. Once required details on the parafoil are known the angular acceleration found in Equation 7.10 can be integrated to find the vehicle's angular velocity and orientation. The latter parameter can be used to determine the instantaneous velocity, using:

$$V_x = V\cos\beta \tag{7.12}$$

$$V_y = V\sin\beta \tag{7.13}$$

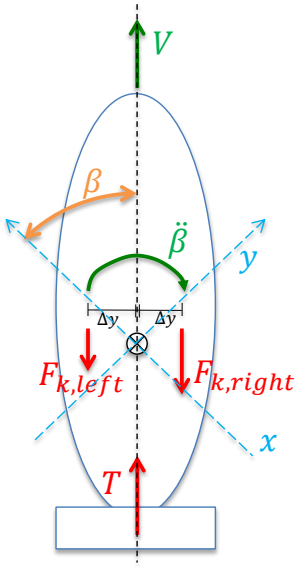

Figure 7.2: Free body diagram for turning flight.

Here it is assumed that during all manoeuvres the velocity remains constant. Equations 7.12 and 7.13 can finally be integrated to find the x- and y-position of the vehicle to reconstruct its flight path.

This model requires a relation between the pilot's control stick deflection and the change in lift coefficient used in Equation 7.11. Keeping in mind possible lever functions of the control system, it is known that the pilot's control stick deflection will result in the parafoil's trailing edge being pulled down with a deflection

$$\delta_{TE} = \delta_{Pilot} \cdot \frac{\delta_{TE}}{\delta_{Pilot}} \tag{7.14}$$

where $\frac{\delta_{TE}}{\delta_{Pilot}}$ is the stick ratio, which is based on the control forces required by the parafoil and the forces a pilot can exert. Modelling the parafoil as a flat plate of which the trailing edge is deflected by a distance δ_{TE} due to the shortening of the control lines, thin airfoil theory is used to determine the change in lift coefficient. This whole process is described in chapter 13. This method is then also used to design the control system such that the pilot is able to operate the vehicle using no auxiliary devices.

The angular acceleration obtained in Equation 7.10 will again be used to form a proportional controller. This proportional controller will determine the action to be taken by a pilot by comparing the current rotational rate to the desired rotational rate. In case the rotational rate is bigger than desired the left line should be pulled, in case the rotational rate is smaller than desired the right line should be pulled. This is reflected in equations 7.15 and 7.16:

$$If\ \dot{\beta} > \dot{\beta}_{intended}: \qquad \delta_{Pilot_L} = k_2 \cdot (\dot{\beta} - \dot{\beta}_{intended}) \tag{7.15}$$

$$If\ \dot{\beta}_{intended} > \dot{\beta}: \qquad \delta_{Pilot_R} = k_2 \cdot (\dot{\beta}_{intended} - \dot{\beta}) \tag{7.16}$$

where k_2 is again constant which is to be optimised in chapter 21. The full simulation flow of this lateral model thus is as shown in Figure 7.3:

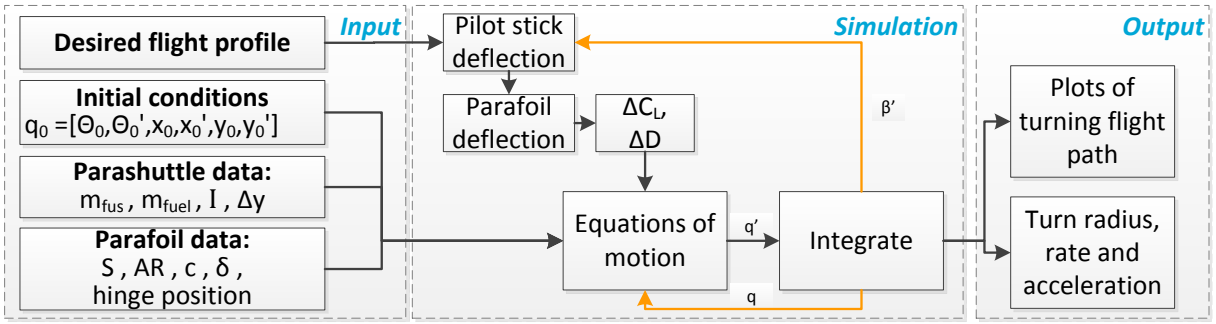

Figure 7.3: Flow of data through the simulation model for lateral flight.

Chapter 8 | Finite elements analysis

To analyse frame structures (such as the fuselage) finite elements method (FEM) is required. In statics, truss and frame analysis is very similar to the discretisation of solid beams. Since the fuselage structure is a frame structure it can be analysed using such methods, hence in this project a FEM analysis program has been used. The program Frame3DD [33] was chosen for its MATLAB interface and output capabilities. The program is discussed in section 8.1 and verified in section 8.2.

8.1 Frame3DD

Frame3DD is an open-source software tool used for both static and dynamic analyses of three-dimensional frame structures, compute static reactions and displacements as well as determining natural frequencies, mode shapes and more dynamic responses. The MATLAB interface however only provided access to the static analysis capabilities.

8.1.1 Input structure

The program requires the following inputs:

Nodal locations - The nodal locations are specified as x, y, z and r. In two-dimensional analysis the y-direction is upwards, in three dimensions the z-direction is upwards. r depicts the rigid radius and is unused in this project.

Element connections - For n elements in the structure this is a 2×n matrix. Each beam is an element and is described as an connection between two nodes.

Element property matrix - A 10×n matrix, which gives cross-sectional properties of each element. The properties to be specified are the frontal area, shear area in y-direction, shear area in z-direction, torsional moment J_{xx}, I_{yy}, I_{zz}, elastic modulus, shear modulus, roll angle and mass density.

External forces and moments - For J nodes this is a 6×J matrix, giving the external forces and moments applies to each node. Each node has 6 degrees of freedom. The order of forces are: force in x-, y- and z-direction and the moments around the x-, y- and z-axis. These forces and moments are specified in the global frame of reference (z upwards).

Distributed load matrix - A 3×n matrix for distributed loads in the local x, y and z directions of the elements. The local direction means that x is along the longitudinal axis of the beam.

Constrains matrix - A 6×J matrix, where each degree of freedom may be restricted and will thus result in a reaction force at this node in the direction of the degree of freedom.

8.1.2 Outputs of the model

The outputs of the model include the deflection and rotation of each node for each degree of freedom, the reaction forces at the constraints specified previously and a matrix containing all forces and moments on each element.

8.1.3 Extension of Frame3DD

The program outputs mentioned above are not yet sufficient to determine whether a structure is strong enough to deal with the loads it experiences during flight. Modifications to the structural analysis tool are needed to ensure the program can be used to determine the maximum stress imposed on a structures component, which in turn can be analysed to assess whether a structure fails.

To determine the maximum stress inside beams shear and moment distributions have to be found along the local axes of the beams. Since the reactions on both beam ends are outputs of the FEM analysis and the distribution of force along the local axes are inputs, the internal force and moment distributions can be found.

For hollow beams with a circular cross-section the computation of stress distribution was also added. Once the shear and moment distributions are known the beam is segmented in 20 pieces longitudinally, each cross-section is then split in 30 pieces radially. Then for each of the 600 pieces of the beam stresses are determined and finally the Von Mises stress is computed. Here it is assumed that for each segment only shear and normal stresses are present.

8.2 Verification

To see whether this program gave correct results verification was performed. This verification consisted of two parts. The first would test the full program for its prediction of the generation of stresses along a clamped beam loaded in shear. A second step is checking whether the reaction forces on the end of the beams are correct. The combination of these two verifications should prove whether the program can be used in more complex structures.

8.2.1 Euler beam under loading

A simple beam of 1 meter length was loaded under a distributed force of 1000 N/m. The beam was a hollow tube with an outer radius of 3 cm and an inner radius of 2.5 cm. The test case can be seen in Figure 8.1. The beam was approximated as a two element beam in the FEM program.

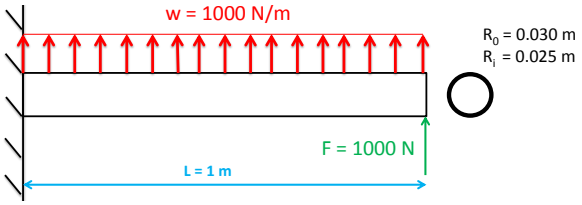

Figure 8.1: Free body diagram of the verification beam for Frame3DD.

The moment of inertia was determined using equations 8.1 through 8.4. Analytical solutions for beam deflection and internal stress are given in Equation 8.5 and 8.6.

$$I_{xx} = \frac{\pi}{64}(r_o^4 - r_i^4) \tag{8.1}$$

$$I_{yy} = I_{xx} \tag{8.2}$$

$$J_{zz} = I_{xx} + I_{yy} \tag{8.3}$$

$$A = \pi(r_o^2 - r_i^2) \tag{8.4}$$

$$v_y(x) = \frac{x^2\left(12\,\mathrm{F_y} + 6\,w - 4\,\mathrm{F_y}\,x - 4\,w\,x + w\,x^2\right)}{24\,E\,I_{zz}} \tag{8.5}$$

$$\sigma_x(x) = -\frac{r\,(x-1)\,(2\,\mathrm{F_y} + w - w\,x)}{2\,I_{zz}} \tag{8.6}$$

For shear, the distribution of maximum shear has been found analytically in Equation 8.7, where V is the shear force. The maximum shear is located at the neutral axis of the beam, with the first moment of area given by Equation 8.8:

$$\tau = \frac{VQ}{It} \tag{8.7}$$

$$Q = -r^2 t \tag{8.8}$$

Reaction forces at the nodes are given in Table 8.1, the sign convention for these forces can be seen in Figure 8.2. One observes that results are exactly equal for both cases. Figure 8.3 shows the shear and bending distributions along the local axis of the beam. Figure 8.4 shows the displacement of the nodal point in the FEM analysis versus the analytical results that followed from the euler bending equations.

Figure 8.2: Positive direction of normal(green)and shear forces (orange) and moments(red).

Table 8.1: Reaction forces at the nodes.

	Node 1 (x = 0 m)	**Node 2** (x = 0.5 m)	**Node 3** (x = 1 m)
Analytical Shear [N]	-2000	-1500	-1000
Analytical Moment [Nm]	1500	625	0
Numerical Shear [N]	-2000	-1500	-1000
Numerical Moment [Nm]	1500	625	0

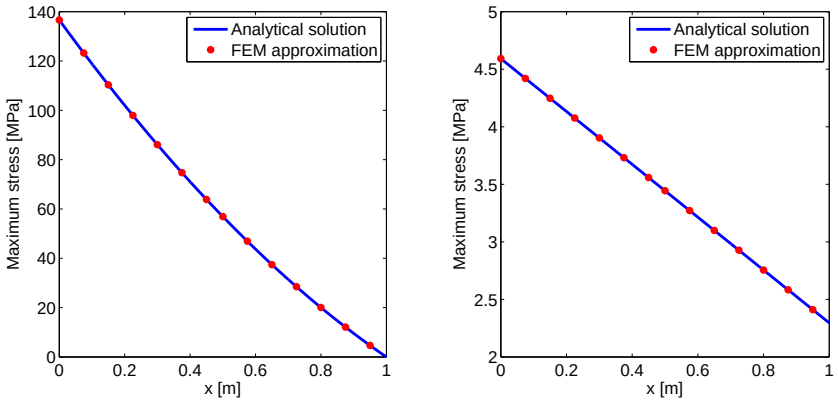

Figure 8.3: Numerical and analytical bending stress (left) and maximum shear stress (right) results over the beam.

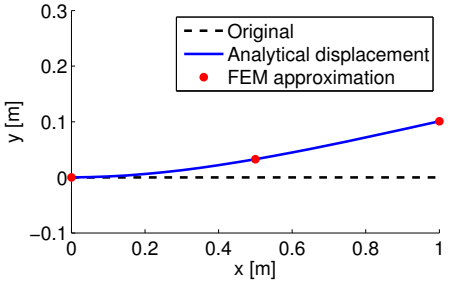

Figure 8.4: A comparison of deflection results, deflections are amplified five times.

8.2.2 Frame structure

A second verification step has been performed to see whether the numerical analysis of an assembled frame structure gives correct results. The frame structure analysed can be seen in Figure 8.5. In this case the error between analytical results and the Frame3DD results was non-existent in the reaction forces as well as the internal load distributions.

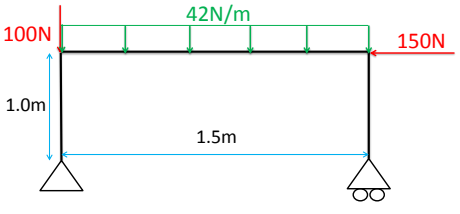

Figure 8.5: Frame structure for verification of the Frame3DD program.

Chapter 9 | Hydrodynamic models

Several computer software tools will be used to assist in the design of the floats. For designing and drawing the floats Maxsurf will be used, after which their stability and water resistance will be calculated using Hydromax and Hullspeed respectively. In this chapter the latter two programs (which are those used for the analysis of performance) are verified.

9.1 Hydromax

Hydromax is a computer program used to analyse the stability of the floats. It requires a certain float geometry, a mass and the centre of gravity of the vehicle as input, then the program will determine the roll angle the ship will attain when in a stable position. It does so by determining whether the centre of buoyancy (the point of action of the upward buoyancy force) is located exactly under the centre of gravity. If not, the program will give an error.

To verify this program an object with easy geometry is provided as input. A box measuring 4.33 m long, 0.30 m wide and 0.40 m high with a mass of 225 kg and its centre of gravity located 50 cm above the waterline was analysed. This means its centre of gravity will not be within the box, however this is also the case for the floats when supporting a relatively heavy fuselage. As a test its centre of gravity was given a 30 cm offset from the middle of the box. The program predicts that for this case the box will have a roll angle of 2.0 °. To verify this outcome another method is chosen, one which is acceptable for small angles [34]. A roll angle of 2 degrees is considered small, meaning this method can be used to verify this program.

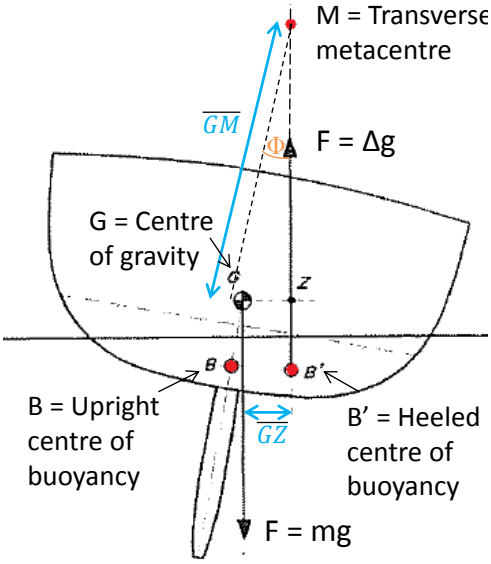

Figure 9.1: Points used during the calculation for roll angle due a centre of gravity shift (from [34].)

When looking at Figure 9.1 from geometry one observes that the sine of the roll angle Φ is equal to the distance $\overline{GZ}$ divided by the distance $\overline{GM}$. To determine the latter ratio, the first step in this method is to calculate the distance between the centre of buoyancy and the metacentre (see Figure 9.1). This distance can be calculated using Equation 9.1, where I is the moment of inertia and ∇ is the displacement of the centre of gravity.

$$BM = \frac{I}{\nabla} = \frac{\frac{bL^3}{12}}{\frac{m}{\rho_{water}}} = \frac{\frac{0.3 \cdot 4.33^3}{12}}{\frac{225}{1000}} = 9.02\ m \tag{9.1}$$

The distance between the centre of gravity and the metacentre ($\overline{GM}$) can now be found by subtracting the distance BG from the distance BM just found. BG is the distance between the upright centre of buoyancy and the centre of gravity. In case the box used for verification has its centre of gravity right in the middle (resulting in a zero roll angle), this distance is half of the draft of this box, as shown in Equation 9.2:

$$B = 0.5 \cdot \frac{\nabla}{bL} = 0.5 \cdot \frac{m/\rho_{water}}{bL} = 0.5 \cdot \frac{225/1000}{0.3 \cdot 4.33} = 0.0866\text{m} \tag{9.2}$$

With the overall centre of gravity located 0.5 m above the water line and the upright centre of buoyancy located 0.087 m beneath it, one can find that the distance $\overline{GM}$ is 8.43 m. Knowing the distance $\overline{GM}$ one can now divide the initial offset of the centre of gravity (equal to the distance $\overline{GZ}$ by this distance $\overline{GM}$ to find the analytical roll angle:

$$\phi = sin^{-1}\frac{\overline{GZ}}{\overline{GM}} = sin^{-1}(0.30/8.43) = 2.04^{\circ} \tag{9.3}$$

Comparing the analytical roll angle (2.04°) and the numerically predicted roll angle (2.0°) one observes that these are nearly equal. This gives confidence that the software tool Hydromax works as desired.

Hydromax is validated by the makers of the program themselves ([35]), so the program is assumed to be valid.

9.2 Hullspeed

To evaluate the water resistance of the floats use will be made of Hullspeed, a numerical software pack for estimating hydrodynamic drag predictions. Hullspeed will be verified here to obtain confidence in the correct functioning of this model. For this purpose the drag coefficient of a beam was evaluated analytically and numerically. If the numerical and analytical solution match then it is assumed that the program works properly and that the drag of the actual designed floats will be correct as well. Water resistance is defined as [36]:

$$R_w = \frac{1}{2}C_{R_w}\rho A V^2 \tag{9.4}$$

Where C_{R_w} is the coefficient of water resistance and is composed of two sub-coefficients, namely the coefficient of viscous resistance C_v and the wave coefficient C_w:

$$C_{R_w} = C_v + C_w \tag{9.5}$$

Viscous resistance is due to the body's friction with water and can be calculated using Equations 9.6 and 9.7. The wave coefficient resembles the resistance due to the formation of waves and is obtained from water tank tests. It is assumed that C_w equals 60% of C_v, as is done in other research [36].

$$C_v = (1+K)\cdot C_{f_v} \tag{9.6}$$

$$C_{f_v} = \frac{0.075}{[\log(Re)-2]^2} \tag{9.7}$$

$$C_w = 0.6C_v \tag{9.8}$$

Re is the Reynolds number (calculated to be $64.8\cdot 10^6$) and $(1+K)$ is the form factor. This form factor is hard to determine, being a function of the slenderness ratio SLR, the length to beam ratio L/b, the longitudinal position of the hull centre Δ_0/L^3 and the prismatic coefficient C_p (as detailed on in chapter 14) [37]. Hullspeed indicated a value of the form factor of 1.284. This value was used as an input into the calculations used to verify Hullspeed.

Hullspeed offers the user the choice of several resistance estimation methods, which one to use will be determined next. Table 9.1 indicates for what velocity range, which drag estimation methods are accurate. The velocities are indicated using Froude numbers. There are three Froude numbers: the length Froude number (most common Equation 9.9), volume Froude number (Equation 9.10)

and the beam Froude number (Equation 9.11). More on Froude numbers in chapter 14.

$$Fr_L = \frac{v}{\sqrt{g \cdot L}} \tag{9.9}$$

$$Fr_V = \frac{v}{\sqrt{g \cdot \Delta_0^{1/3}}} \tag{9.10}$$

$$Fr_L = \frac{v}{\sqrt{g \cdot b_{max}}} \tag{9.11}$$

Based on Table 9.1 it is still unsure what method to use, as there are still a lot of possibilities (the

Table 9.1: Resistance methods verified for various Froude number ranges [38].

Method	Lower speed limit	Upper speed limit
Savitsky (pre-planing)	1.0[a]	2.0[a]
Savitsky (planing)	1.0[b]	None
Blount and Fox	1.0[a]	None
Lahtiharju	1.5[a]	3.8[a]
Holtrop	0.0	0.80[c]
Van Oortmerssen	0.0	0.5[c]
Series 60	0.282[a]	0.677[a]
Delft	0.0	0.75[c]
Compton	0.1[c]	0.6[c]
Fung	0.134[c]	0.908[c]
Slender body	0.0	Up to 1.0[c] depending on SLR

[a] Volume Froude number.
[b] Beam Froude number.
[c] Length Froude number.

Froude number of Parashuttle 2 will range from 0 to approximately 2.2. Another table provided in the same reference, one which states ranges of float dimensions for which the different methods are applicable, is used therefore. Due to its size this table is not included here, one can find it in Appendix B of the user manual of Hullspeed [38]. The selection of a method was done using this table as well. The best option is to use the Holtrop method for speeds up to 10 knots. And For higher speeds the Lahtiharju method is most applicable. Both methods are validated, the Holtrop method is validated by I. Ortigosa [39] and the Lahtiharju method is validated by Michel de Vos [40].

Results of the verification procedure are shown in Table 9.2. One can see that the resistance computed by Hullspeed is larger for every velocity. At higher speeds drag predictions were found to be closer together, with deviations being around 20%. The deviations and varying predictions can be explained from the assumption that the wave coefficient is linearly dependent on the viscous resistance (60%, see Equation 9.8), which in real life will not be the case.

Table 9.2: Results of the Hullspeed verification.

Velocity [kts]	**Analytical solution** [N]	**Numerical solution** [N]	**Error** [%]
5	49	77	36
10	174	247	30
15	366	549	33
20	622	830	25
25	940	1167	19

Chapter 10 | Aerodynamic model

For aerodynamic analysis it is chosen to use an off-the-shelf Computational Fluid Dynamics package, namely Ansys FLUENT. This package is chosen for its ability to import CATIA models, such that Parashuttle 2 can easily be completely analysed. The theory behind the program is explained in section 10.1, while the verification and validation of the program is done in section 10.2.

10.1 Theory

FLUENT is a Computational Fluid Dynamics program based on solving conservation equations for mass and momentum [41], given by Equations 10.1 and 10.2.

$$\frac{\partial \rho}{\partial t} + \nabla(\rho \vec{v}) = S_m \tag{10.1}$$

$$\frac{\partial}{\partial t}(\rho \vec{v}) + \nabla(\rho \vec{v}\vec{v}) = -\nabla p + \nabla \bar{\tau} + \rho \vec{g} + \vec{F}. \tag{10.2}$$

Here S_m is any mass added in the flow (e.g. water droplets), p is the static pressure, $\bar{\tau}$ the stress tensor, $\rho \vec{g}$ the gravitational body force and $\vec{F}$ the external body forces. The model needs to be meshed (dividing the solution space into polygons, where on each polygon the equations will be solved). Then the user specifies the air inflow place, the wall (the model to be analysed) and the outlet. Together with free stream air properties and boundary conditions (the air cannot flow through the object) the equations are solved (using a finite-volume method [42]).

10.2 Verification and validation

In order to verify the program a simple airfoil is analysed, both with FLUENT and using thin airfoil theory [43]. The airfoil under consideration is a NACA 0012 airfoil. This is a symmetric airfoil for which (using thin airfoil theory) $C_l = 2\pi\alpha$. The airfoil is put under an angle of attack of $\alpha = 5°$. The values of both thin airfoil theory and Computational Fluid Dynamics analysis are shown in Table 10.1. As can be seen the difference is 0.037, which is small enough to be ascribed to the assumptions used for thin airfoil theory.

The validation data used is that of Abbott [44]. The airfoil used is again the NACA 0012 profile. Wind tunnel data from Abbott is applicable to a Reynolds number of $3 \cdot 10^6$. The results of both the wind tunnel data and the FLUENT solution can also be found in Table 10.1. As can be seen the values calculated using FLUENT are reasonably close to the measured values. During the validation however, it appeared that the results of FLUENT can fluctuate by quite a large margin. Due to the fact that FLUENT can import models made in CATIA and the relatively small time span of the project these fluctuations are accepted, however the results of FLUENT should be taken with a substantial uncertainty, between ±80-100%.

Table 10.1: Verification and validation of FLUENT for a NACA 0012 profile at $\alpha = 5°$, validation $Re = 3 \cdot 10^6$.

	Verification		**Validation**	
	Thin airfoil theory	FLUENT	Wind tunnel measurement [44]	FLUENT
C_l	0.548	0.511	0.52	0.35
C_d	-	-	0.007	0.003

Part III - Subsystem design

Chapter 11 | Design strategy

Having specified the final design choice in chapter 5 and in previous work, the team is now able to design this final concept of Parashuttle 2 into detail. This means that all components of Parashuttle 2 are to be designed and integrated into the final product. Part III of this document deals with this design phase. The design strategy followed is described in this chapter, after which chapters 12 through 18 deal with the design of all components of Parashuttle 2. These are then integrated into a final design, which is analysed in part IV of this report.

The design process to be followed at this stage is gone through in section 11.1, after which this design process is implemented and discussed in sections 11.2 through 11.4.

11.1 Design process

Detailed design of Parashuttle's final design is complicated by the fact that many of its components are interrelated, meaning the design of one influences others. Besides all components require different fields of expertise to design them. To facilitate the design process the group members' fields of expertise are identified first (in section 11.2), after which the group members are assigned different components to design (in section 11.3). Finally the interfaces between the components are evaluated in section 11.4. This process is summarised by the diagram shown in Figure 11.1:

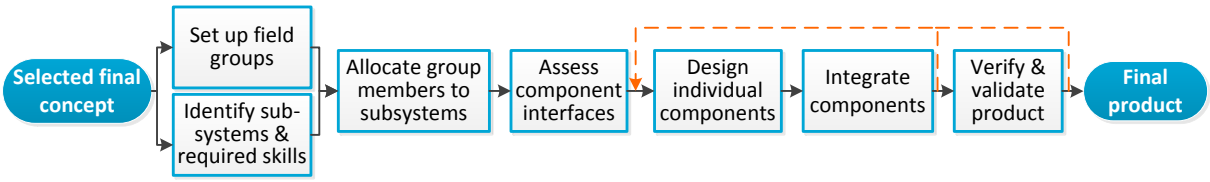

Figure 11.1: The design process of the final design of Parashuttle 2.

Following the assessment of component interfaces, all components identified in section 11.3 will be designed in chapters 12 through 18. Integration, verification and validation of the components will then take place in part IV of this report, with a feedback loop (shown in orange) being gone through should it appear that components cannot be integrated or that the system does not function properly. This whole process eventually results in a final product.

11.2 Field groups

As mentioned the fields of expertise of all group members have been identified in order to be able to allocate group members to the design of components (the second part of the diagram shown in Figure 11.1). The table below presents an overview of the team members' specialisms:

Table 11.1: Overview of the distribution of group members over the field groups.

Field of expertise	Group members
Aerodynamics	Daan, Daniel, Koen & Pieter
Control & Stability	Daniel, Gerald, Marco & Tim
Hydrodynamics	Daan & Floris
Performance	Daan, Pieter, Robert & Tim
Propulsion & Power	Daan & Marco
Structures	Floris, Koen, Max & Robert

11.3 Product groups

The final design of Parashuttle 2, presented in chapter 5, can be split up into seven parts. For these seven parts the fields of expertise required to design them have been identified. The seven parts, as well as the subjects involved in their design and the people allocated to the design of these parts are shown in Table 11.2 below:

Table 11.2: Overview of the different components of Parashuttle 2, as well as the skills required to design them and the group members allocated to their design.

Component	Required resources	Allocated group members
Propulsion unit	Aerodynamics, Propulsion & Power	Daan & Marco
Fuselage	Aerodynamics , Structures	Floris, Koen & Max
Undercarriage	Control, Hydrodynamics , Structures	Koen, Floris & Pieter
Parafoil connection	Control & Stability, Structures	Daniel, Gerald, Robert & Tim
Control system	Aerodynamics, Control & Stability	Daniel, Gerald, Robert
Cockpit	Ergonomics, Structures	Daan & Marco
Parafoil	Aerodynamics, Performance	Tim

11.4 Interdependencies

The components identified in the previous section can not be designed without keeping the interfaces between them in mind. To facilitate the detailed design of subsystems in the coming chapters use has been made of an N^2-chart to make an inventory of the interrelations between these components. When designing a component these connections are to be kept in mind, in order to facilitate the integration of all subsystems into the final design in later stages of the design process. The interdependencies between the components of Parashuttle 2 are shown in Figure 11.2.

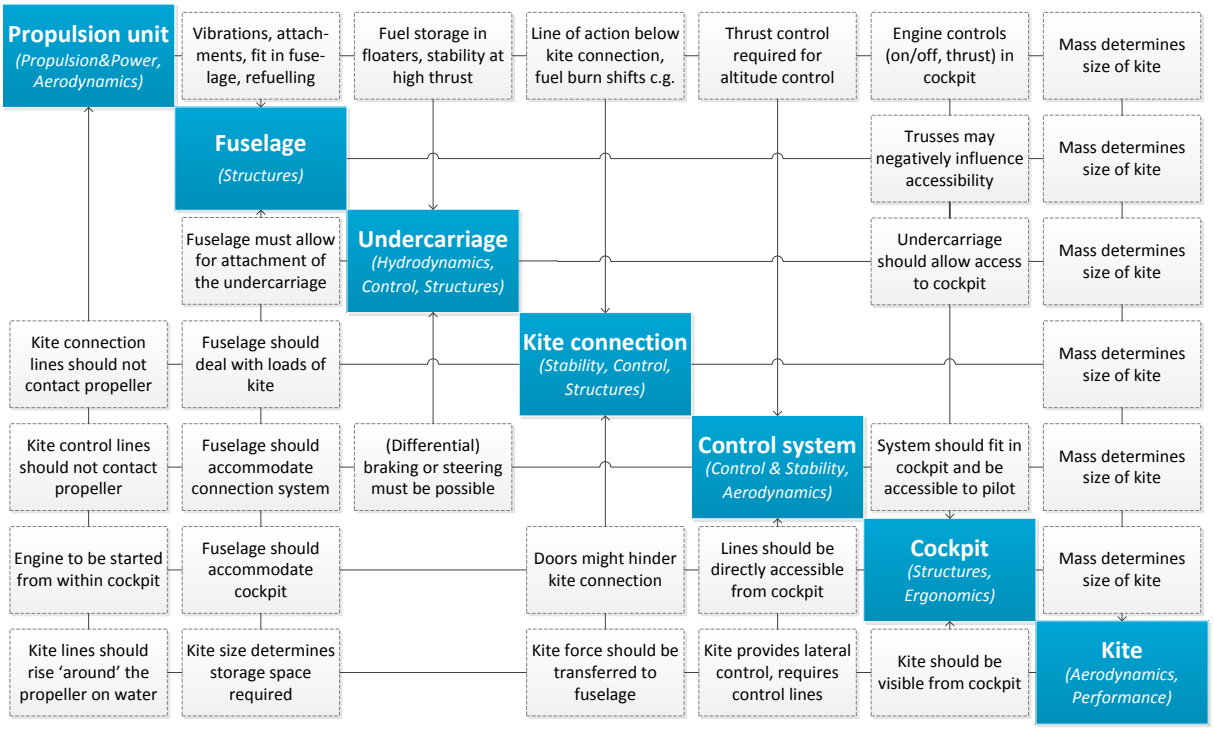

Figure 11.2: An N^2-chart showing the interfaces between subsystems of Parashuttle 2.

11.5 Design using CAD

Though technical design will be the larger part of this project, stakeholder requirements also require a marketable design to be made. The looks of a product largely determine its marketability. Using Dassault Systems CATIA, a Computer Aided Design (CAD) program, an evaluation can be done of how technical parameters can be integrated in a good looking design. A feasibility and requirement compliance analysis is conducted by visualising the integration of subsystems of the product. From such 3D visualisation design considerations could flow as well. In order to have a successful implementation of CAD design of Parashuttle 2, the points in subsections 11.5.1 through 11.5.5 are of importance.

11.5.1 Design breakdown

Because of the large number of systems, subsystems and parts of Parashuttle 2 the design of Parashuttle 2 was broken down to part level. From separate parts the model was built bottom-up again for a suitable CAD structure. Parts were combined into subassemblies after which the subassemblies combined into the total assembly. For each subassembly compliance was checked to assure no top-level requirements (such as the ability to land or take off) were violated. Next to that any apparent design flaws were communicated with other group members to be able to find better design solutions. The same process of checking compliance and checking for optimal design solutions was repeated for the final integration of the total assembly. In Figure 11.3 an overview is presented of the CAD model integration.

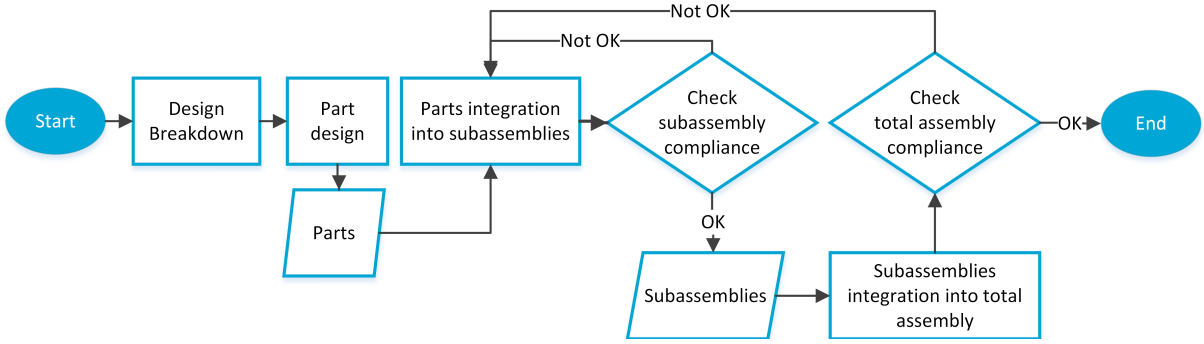

Figure 11.3: Flowchart visualising the CAD integration process.

11.5.2 Parametric constraints

To ensure the CAD model can be altered in case of design changes and can be used as input for analysis programs, several parameters have to be taken into account. Most important is the use of parametric constrained dimensioning. This means that all dimensions are directly linked to a few main dimensions. While dimensional constraining can be faster compared to parametric constraining, it will have a higher probability of causing update cycles and misalignments in the model when a certain dimension has to be changed.

Parametric constraints were used where possible. This resulted in a model to which, within normal design dimensioning, design changes could be implemented immediately. Examples of changes that could be made during design are:

- Making the fuselage more slender for drag considerations, without limiting available passenger space.
- Changing the distance between the floats.
- Alter the engine location/height for in-flight stability.
- Move the wheels for stability or manoeuvrability purposes.

11.5.3 Part connections

A second important parameter for a CAD model to be used as input for analysis programs is the connection of parts. While the FEM method discussed in chapter 8 gives a good first estimate of structural integrity, it does not take into account problems associated with the connection of beams or the positioning of subassemblies such as chairs. Connecting beams of different radii requires limitations on the design optimisation and dimensioning. For connecting beams several connection options are possible, the three main options are shown in Figure 11.4. Only the option of single continuity allows for proper meshing of the structure for using the structural analysis workbench in CATIA. The other options have proven inaccurate because of bad meshing capabilities. Next to that single continuity would be the most structurally reliable and manufacturable.

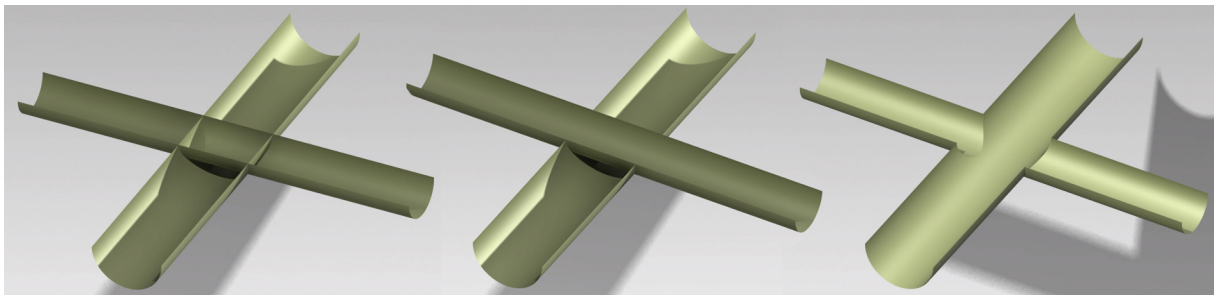

Figure 11.4: Truss connection options: both continuous (left), single continuity (middle) and double split (right).

11.5.4 Simulation model integration

While the CAD model is mainly used for design evaluation and visualisation as described in section 11.5.1, it can also be used as input for technical design analysis such as structural analysis and CFD. For structural analysis the CAD model can be used to verify the FEM methods discussed in chapter 8. Next to that the model can be used as input for CFD analysis, as discussed in chapter 10.

11.5.5 Design visualisation and looks

As explained in the introduction of this chapter one of the aspects defining the marketability of a product is its overall looks. The main stakeholder of this project indicated several preferences for the overall looks of the vehicle, examples of these are listed below:

1. A 'cigar' shaped fuselage.
2. A retractable landing gear, which ensures a streamlined shape in flight.
3. A product with a modern looking cockpit.
4. A vehicle incorporating a ducted fan.

Most design preferences as indicated above are discussed in the corresponding chapters. The 'cigar' shaped fuselage was mainly designed using CATIA. Continuous exchange of pictures of the latest design with the main stakeholder allowed for checking whether this shape fulfilled expectations. Based on these exchanges it has for example been decided to place the fuselage's skin outside of the fuselage truss structure (both are discussed later in this report).

Using all methods described above the use of CAD models will greatly assist in coming up with a design which is both feasible and fulfils customer expectations regarding the looks of the vehicle.

Chapter 12 | Propulsion

The propulsion unit of Parashuttle 2 consists of its engine, the propeller including duct and a fuel tank. From Figure 11.2 it was seen that the propulsion unit influences all other subsystems and is affected by only three. Therefore this subsystem is discussed first. In this chapter an engine and propeller will be chosen and their mass and cost will be evaluated. To do so an inventory is made of all requirements imposed on the propulsion system in section 12.1, after which the actual design takes place in sections 12.2 through 12.4. First the engine and gearbox are specified (section 12.2), after which the propeller and the duct are designed (section 12.3). The fuel tank is designed in section 12.4 and, finally, a design summary is given in section 12.5.

12.1 Subsystem requirements

In section 4.2 mention was made of all requirements imposed on Parashuttle 2. Many of these (indirectly) affect the design of the propulsion subsystem, meaning an inventory of requirements posing limitations on this subsystem is to be made first. Summarising, the requirements to be met by the propulsion subsystem are:

1. The engine of Parashuttle 2 shall be able to be started up, controlled and shut down from within the cockpit.
2. The propulsion system shall provide Parashuttle 2 with a range of at least 100 km and an endurance of at least 2.5 hours.
3. The propulsion system of Parashuttle 2 shall be able to produce at least 40 kW of power and 2,000 N of thrust.
4. The propulsion system of Parashuttle 2 shall be accessible for maintenance.
5. The propulsion system of Parashuttle 2 shall produce less than 60 dB of noise at full power and full RPM, when measured at 150 m distance.

The third requirement was obtained from the MATLAB performance model set up in previous work [9]. For the propulsion system budgets of €6,000 and 110 kg were allocated. Keeping in mind both the requirements and interfaces determined previously the design process can be executed.

12.2 Engine and gearbox

In previous reports it was established that the engine should be able to provide at least 40 kW of power. Preferably the engine is as small and light as possible to accommodate fitting in the fuselage. It has been decided to equip Parashuttle 2 with a 48 kW Rotax 582 engine, a model commonly used on powered parachutes. The engine can be equipped with an electric starter (allowing the engine to be started from within the cockpit) and requires a gearbox (chosen in section 12.3). Table 12.1 provides all relevant information on this engine model, as specified by the manufacturer [45].

Table 12.1: Specifications of the Rotax 582 engine and accompanying gearbox [46].

Specification	Value
Length	771 mm
Width	571 mm
Height	578 mm
Power	65 hp / 48 kW (at 6000RPM)
Maximum RPM	6800 min^{-1}
Mass (including accessories)	63.2 kg
Cost	€7,000
Time between overhauls	300 hr

12.3 Propeller and duct

Choosing a suitable propeller for an aircraft is a complex process, for which no standard recipe exists. The team has decided on first performing a preliminary calculation on the required propeller diameter to assess whether it is possible to give the propeller sufficient clearance from ground and water. Once the propeller has been sized and a blade geometry has been chosen the duct can be designed.

12.3.1 Propeller

An initial estimate of the propeller diameter D can be made using the method given by Roskam [47]. Using the maximum power P_{max} (in hp), the number of blades n_p and the 'blade-power-loading' number P_{bl} (estimated to be 2.0 from reference aircraft) the propeller diameter is estimated using

$$D = \sqrt{\frac{4P_{max}}{\pi n_p P_{bl}}} \tag{12.1}$$

Entering the maximum engine power of 48 kW in Equation 12.1 for a 2-bladed and 3-bladed propeller gives propeller diameters of 1.4 m and 1.12 m respectively. For more detailed design of the propeller the model predicting propeller thrust as described in chapter 6 was used. Since the NACA 16 series of airfoils is often used for propeller blades this airfoil was chosen [48, p.216]. The aerodynamic coefficients of the NACA 16-509 profile in a Mach 0.6 flow (the propeller tip speed during climb) are known [49], making this airfoil a suitable choice.

Using the model predicting propeller thrust it was found that a pitch distribution ensuring an angle of attack of 7° was optimal, as it ensures the highest lift without having separation of flow [49]. Using such a distribution it was found, by running the model, that the propeller diameter should be larger than estimated previously; in the order of 1.7 m and 1.4 m for a 3-bladed and 5-bladed propeller respectively.

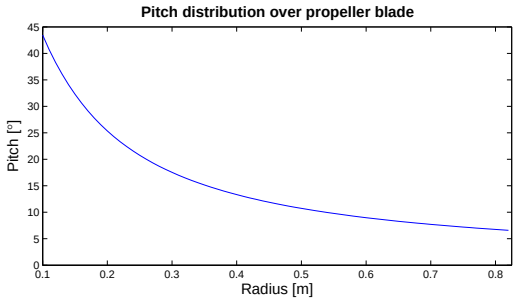

Figure 12.1: Ideal propeller pitch distribution.

Keeping in mind the propeller mass moment of inertia (the chosen gearbox can only withstand 6000 kg · cm^2) one can now design the propeller. Analysing various propeller designs showed that a 4-bladed propeller of 1.7 m in diameter, with a pitch and chord distribution as shown in figures 12.1 and 12.2, provides the required thrust for all flight phases while being optimised for cruise (i.e. a low engine RPM is needed during cruise, thus improving fuel consumption). Since the propeller's tip speed will not exceed Mach 0.65 at full engine power specialised tip shapes to bring down shocks are not necessary [50], allowing for the use of rectangular tips. The gearing ratio required is 2.62, which is provided by the 'E' gearbox [45].

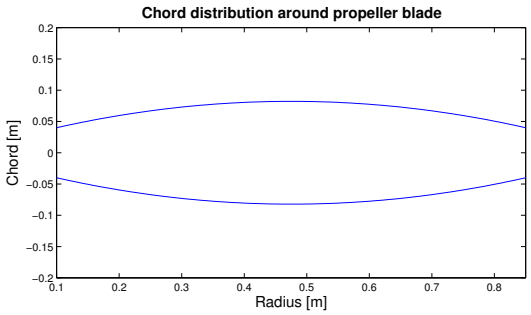

Figure 12.2: Propeller chord distribution.

Engine performance parameters for cruise, climb at 3 m/s and maximum power are shown in Table 12.2. These are parameters a Rotax 582 engine is capable of producing [51]. Propeller properties in cruise are shown in Table 12.3. The advance ratio is a measure for the forward velocity compared to the blade velocity [27] ($J = V_\infty/\omega D$, with ω is the propeller rotational speed)

and will decrease with more power applied, since the kite wants to stay at the trim velocity (i.e. V_∞ stays constant, while ω increases).

Table 12.2: Performance parameters of a 4-bladed, 1.7 m diameter propeller.

		Cruise	**Rate of climb = 3 m/s**	**Maximum power**
Engine RPM	[min^{-1}]	3,300	5,200	6,500
Thrust	[N]	817.7	2011.7	3136.1
Torque	[Nm]	80.7	128.8	163.1
Power required	[kW]	10.6	26.7	42.4

Table 12.3: Propeller properties during cruise.

Advance ratio [-]	**Tip Mach number** [-]	**Moment of inertia** [$kg \cdot cm^2$]
0.36	0.65	6,000

The propeller will be made of a foam core with a carbon fibre outer shell. This is because carbon fibre can withstand water (both fresh and salt [52]), while at the same time yielding mass savings and damage tolerant blades when compared to aluminium blades [53].

To give the propeller a 'plug-and-play' ability and to save on the development and testing cost of a brand new propeller it is chosen to use an off-the-shelf propeller. Ideally this propeller should have the same properties as the propeller designed above. The propeller chosen is manufactured by Powerfin, an American propeller manufacturer specialised in paraplanes [54]. The propeller blades are made of carbon fibre with a foam core, meeting material requirements. The blades will be slightly smaller than designed earlier and will not have the same pitch distribution. Therefore a contingency from the calculated thrust and the actual thrust is taken into account. This difference in thrust is accepted for the lower costs associated with an off-the-shelf propeller. The properties of the final propeller are stated below, where the price is for a single order (not taking into account discounts for batch orders):

- Four carbon fibre 'C' blades and hub
- Diameter: 1.65 m / 65 in
- Gearing ratio: 2.62
- Total mass: 4.52 kg (including hub)
- Total cost: €800 (excluding shipping and assembling)

12.3.2 Duct

The duct used in this design is primarily included to prevent the kite lines from getting cut by the propeller. Besides a duct can improve performance (at low speeds) [55] and, if aerodynamic requirements are met, may reduce the sound produced by the propeller [56].

An airfoil-shaped duct will be used to improve propeller performance. Several different parameters influence propeller performance, most of which are a function of the advance ratio J. For cruise the advance ratio will be approximately 0.36, decreasing as engine thrust is increased (as explained previously). Important parameters are the duct thrust coefficient, propeller thrust coefficient, power coefficient, inlet and outlet velocities and the efficiency [57]. During both cruise and land or water operation the propeller and duct will be in a horizontal configuration and hence have a zero angle of attack.

An airfoil performing well in cruise on all parameters mentioned previously is the NACA 7312 airfoil

[57]. A duct with this profile gives a better efficiency, a lower power coefficient and accelerates the flow in front of the propeller, which is beneficial when flying at low speeds (it provides a higher static thrust). There are some disadvantages for this profile though, the first being that this airfoil is hard to manufacture in an annular form due to the fact that it is not symmetric. Also it was now assumed that the duct will be at zero angle of attack, but during flight the angle of attack will actually fluctuate between -8 and 6 degrees. The NACA 7312 airfoil will have a relatively high drag in that case.

An alternative is the use of the simple and symmetric NACA 0012 airfoil [57], which is easy to manufacture and its relatively low thickness results in low drag. The important performance parameters of the two airfoils do not differ much [57], so due to the fact that the NACA 0012 will be easier and cheaper to manufacture the duct of Parashuttle 2 will have a NACA 0012 profile [58].

Another consideration is the shape of the cross-section of the duct. For an efficient duct boundary-layer losses should be minimised. Boundary-layer losses are a function of wetted area, surface roughness, pressure gradients and losses due to streamwise vortex filaments. The ideal cross-section shape for minimising skin-friction losses is a circle, because a circle has the smallest perimeter length to area ratio [55]. The length L of the duct should be in the range of $0.3D_{Prop}$ to $0.5D_{Prop}$, where the propeller diameter D_{Prop}, which is given in the propeller section, is 1.65 m. A higher length results in slightly better performance, however adds significant mass and cost. Hence the duct will have a chord length of $0.3D$, which is equal to 0.495 m. The propeller is located at the narrowest cross-section of the duct. Since the NACA 0012 airfoil has its maximum thickness located at 30% of its chord length, the propeller is located at 0.1485 m from the ducts leading edge. The maximum thickness of the duct is $0.12L$ or 0.0594 m.

Now that the shape of the duct is specified, the mass and cost can be estimated. The duct will consist of a polystyrene (PS) foam core and 1 mm glass fibre skin. From CES EduPack the densities for the PS foam and glass fibre are extracted, these are 20 kg/m^3 and 1800 kg/m^3 respectively. This will give a skin mass of 10.322 kg, a core mass of 2.278 kg and a total duct mass of approximately 13.2 kg. Also the material prices are found in CES EduPack. The foam core costs 2 €/kg and the glass fibre skin will cost 27 €/kg, which will result in a material cost of approximately €283.

For noise considerations it is estimated that propeller tip clearance should be approximately 1% of the total propeller diameter [56]. This way noise will be reduced significantly without too much loss of thrust and also this offers offering clearance for potential vibrations of the propeller. Finally, ground clearance should also be taken into account. Water should not be sucked up by the propeller (this could degrade the propeller and/or duct) and the duct should not touch the land or water during take-off or landing. This should be kept in mind during the design of the fuselage and undercarriage. In Table 12.4 the properties of the duct can be found.

Table 12.4: Duct properties

Airfoil profile	Chord length L	Thickness t	Thickness location x/L	Tip clearance d	Propeller location x/L	Cost	Mass
NACA 0012	0.495 m	0.06 m	0.3	1.65 cm	0.3	€283	13.2 kg

12.4 Fuel tank

The Rotax engine of Parashuttle 2 is powered by automotive fuel, allowing Parashuttle 2 to be fuelled up at a petrol station. This is beneficial in terms of operating comfort since little effort is required to fuel the vehicle. Through an analysis of Parashuttle 2 in cruise flight it was found (taking the specific fuel consumption of the engine and drag on the vehicle into account) that to obtain a range of 100 km and an endurance of 2.5 hours 28 kg of fuel is required. This computation

did not take into account take-off and landing however, for these procedures 2 kg of fuel is added. Using a petrol density of 0.7 kg/L one now finds that 43 litres of fuel are required.

It is desired to have the fuel tank placed at the bottom of the fuselage (to keep the centre of gravity of the vehicle low) and to have the fuel tank located longitudinally near the centre of gravity. The latter feature ensures the centre of gravity does not shift much when fuel is burned, leading to better flight characteristics. It is estimated that 15 cm of space will be available below the rear passenger. Using 80 cm of the roughly 1.0 m wide fuselage results in a fuel tank of 40 cm long, 80 cm wide and 15 cm high. The fuel tank will be made of a multi-layered high-density polyethylene and a barrier of ethylene vinyl alcohol. These materials are chosen due to their low density (compared to metals), small footprint [59] and good impermeability [60]. Fuel tanks are desired to have good deformation capabilities in case of a crash [61] (i.e. it is desired that they do not rupture during a crash), which a thermoplastic material possesses.

Two layers of polyethylene of 2 mm thick, with a 1 mm thick layer of ethylene vinyl alcohol will yield a fuel tank of 5.0 kg, costing €12.4 [62] in pure material costs. From the fuel tank fuel needs to be supplied to the engine and the fuel tank should provide the capability for refuelling. In order to comply with this a filler cap is located on the fuselage, connected to the fuel tank. It is estimated that the filler cap will weigh 0.5 kg while the 25 cm long connection (with an estimated diameter of 5 cm and made from the same materials) will weigh 0.12 kg and cost €0.25 in material cost. The connection to the engine will be a 1 m long tube made, again, from the same material. The diameter will be sized such that the maximum fuel usage can be supplied to the engine [45] leading to a diameter (keeping manufacturability in mind) of 1 cm. This leads to a mass and cost of 0.1 kg and €0.2 respectively. The total mass and cost of the complete fuel system will thus be 5.72 kg and €13 in material costs.

12.5 Summary

In Table 12.5 a final overview of the cost and mass of the propulsion system can be found.

Table 12.5: Propulsion cost and mass

Part	Cost	Mass
Engine (incl. gearbox and electric starter)	€ 7,000	63.2 kg
Propeller	€ 800	4.5 kg
Duct	€ 283	13.2 kg
Fuel tank (excl. fuel)	€ 13	5.7 kg
Total	€ 8,096	86.6 kg

Chapter 13 | Control system

Parashuttle 2 operates in three conditions: in flight, on land and on water. This chapter will elaborate on the design of a control system for all these operations. The flight simulation models discussed in chapter 7 are used to do so. Requirements on the control system are discussed first in section 13.1. Next in section 13.2 the control forces and displacements to be imposed on the wing will be calculated using an aerodynamic model of the parafoil. Finally the detailed design of the control mechanisms will be explained with all its components in sections 13.3 through 13.6.

13.1 Requirements

Many of the requirements shown in appendix B imposed by the mission of Parashuttle 2 have influences on the design of the control system. Not all will be repeated here, instead a brief overview of the key requirements for the control system are given:

1. The control system shall be operated by one pilot.
2. The pilot shall be able to operate the engine from within the cockpit. This includes starting the engine and controlling the thrust level.
3. The pilot shall be able to operate Parashuttle 2 on land, entailing turning (with a maximum turn radius of 6 m), braking (from 3 m/s to standstill within 5 m) and accelerating.
4. The pilot shall be able to operate Parashuttle 2 on water, entailing turning (with a maximum turn radius of 8 m), accelerating and decelerating.
5. The pilot shall be able to perform manoeuvres, accelerate and decelerate during flight. Manoeuvring entails turning (a rate 4 turn, or a turn with a minimum turn radius of 40 m), flaring before touchdown and controlled climb and descend.
6. The control system shall allow for easy maintenance by an individual, with the possibility to replace components.
7. The control system shall have a back-up system to control the kite in case the primary controls fail.

For the control system budgets of €340 and 9 kg were allocated, defined in previous work [9]. Keeping the requirements and budgets in mind, the detailed design steps can be conducted next.

13.2 Control forces and displacements

As mentioned earlier the pilot of Parashuttle 2 has to be able to decrease airspeed and perform turns using the control lines of the parafoil. To achieve this freedom of movement the pilot must be able to deflect both ends of the kite both separately (to turn) and simultaneously (in order to decelerate or flare before landing). This section describes the determination of control forces and surface deflections needed to manoeuvre the parafoil and with it the vehicle.

In section 7.2 three factors were described which influence a parafoil's turn. In the simplified lateral model only the difference in induced drag is considered as the force needed for turns. Equation 7.11 showed the equation for this difference in induced drag:

$$\Delta D = \frac{1}{2}\left(\frac{C_{L_2}^2 - C_{L_1}^2}{\pi A}(1+\delta)\right)\rho S V^2 \tag{7.11}$$

This change in drag results in a yawing moment on the vehicle. Since in this equation all other parameters are (assumed to be) constant, only a change in lift coefficient $\Delta C_L = C_{L_2} - C_{L_1}$ causes the turn. The lift induced to obtain this required increase in lift coefficient at one side of the

parafoil (or both sides when decelerating) is caused by a pilot input in one of the control lines. This will give a certain deflection to the parafoil and involves a required control force.

Since the parafoil is flexible calculations for its deflection and induced lift force (and control force) are quite complicated. This section elaborates on a simple aerodynamic model to obtain these forces, using a certain deflection as input. As the longitudinal model described in section 7.1 only uses the thrust setting as control input to determine the pitch setting and vertical speed, this aerodynamic method is only implemented in the lateral model. In a further stage of design flight path predictions can be optimised by implementing the effects of control line deflections in the longitudinal model as well.

Note that it was assumed that the steering lines at the back of the canopy are the only controls needed to make turns. Though weight shifting is often used as well [63], it is not accounted for since the turns performed by Parashuttle 2 will be relatively slow (rate 4).

To find the lift force exerted given a certain trailing edge deflection, thin airfoil theory [43] is used. The canopy is modelled as a flat plate with a hinge at 75% of chord length, shown in Figure 13.1. This deflection is modelled as a camber line in the airfoil. The change in lift due to the deflection of the canopy's trailing edge determines the force to be applied on the steering lines, by assuming this force has to counter-act part of the total increase in lift. Since only this change in lift is of interest, the angle of attack of the plate is set to zero. This gives (of course) zero lift when there is no input given on the control lines. To find the change in lift the fundamental equation of thin airfoil theory is used, which is stated in Equation 13.1.

$$\frac{1}{2\pi}\int_0^{\pi}\frac{\gamma(\theta)\sin\theta d\theta}{\cos\theta-\cos\theta_0}=V_\infty\left(\alpha-\frac{dz}{dx}\right) \tag{13.1}$$

A solution for the vorticity distribution γ is obtained using a Fourier series expansion shown in Equation 13.2. According to the Kutta condition (which makes the plate's camber a streamline of the flow) this solution should be set to zero for $\theta=\pi$:

$$\gamma(\theta)=2V_\infty\left(A_0\frac{1+\cos\theta}{\sin\theta}+\sum_{n=1}^{\infty}A_n\sin n\theta\right) \tag{13.2}$$

Coefficients A_0 and A_n are a function of the slope of the camber line $\frac{dz}{dx}$. The camber line used is depicted in Figure 13.1. The camber line and its slope are given in Equations 13.3 and 13.4.

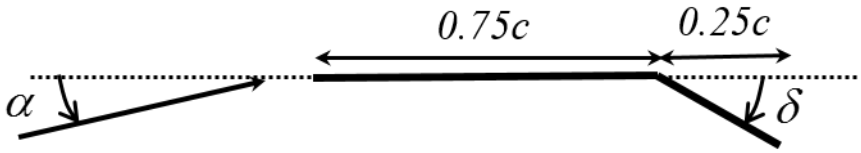

Figure 13.1: Deflected plate at 0.75c [64]

$$z=\begin{cases}0, & \text{if } x\leq 0.75c\\ -\sin\delta(x-0.75c), & \text{if } x>0.75c\end{cases} \tag{13.3}$$

$$\frac{dz}{dx}=\begin{cases}0, & \text{if } x\leq 0.75c\\ -\sin\delta, & \text{if } x>0.75c\end{cases} \tag{13.4}$$

Using this slope the total circulation due to the vortex sheet can be found. This circulation can be used to find the lift force per unit span and with it the airfoil lift coefficient. The final expression for this lift coefficient is given in Equation 13.5.

$$C_l = 2\pi \left[\alpha + \frac{1}{\pi} \int_0^{\pi} \frac{dz}{dx} (\cos\theta_0 - 1) d\theta_0 \right] \tag{13.5}$$

In this equation α is the angle of attack (which is zero) and $\frac{dz}{dx}$ is the slope of the camber line. Since the hinge is at 0.75c and the slope of the camber before the hinge is zero, the lower boundary of the integral in Equation 13.5 changes to $\frac{2\pi}{3}$ (a graphical method to obtain this is given in [64]). Substituting the expression found in Equation 13.4 for $\frac{dz}{dx}$ gives a change in lift coefficient due to the deflection as stated in Equation 13.6.

$$\Delta C_l = -2 \sin\delta \int_{\frac{2\pi}{3}}^{\pi} (\cos\theta_0 - 1) d\theta_0 = \left(\frac{2\pi}{3} + \sqrt{3} \right) \sin\delta \tag{13.6}$$

Since it is assumed that the control force is part of this change in lift (i.e. the pilot has to constrain the surface from deflecting back due to a moment around the hinge point), the lift coefficient can be used to approximate the control force needed. For this the change in parafoil lift coefficient is approximated to be the same as the airfoil lift coefficient, i.e. $\Delta C_L = \Delta C_l$. From this change in lift coefficient a reference lift force can be calculated using the lift formula:

$$L = C_L \frac{1}{2} \rho V^2 S_{ref} \tag{13.7}$$

In here $C_L = C_{L_0} + \Delta C_L$, where C_{L_0} is the cruise lift coefficient and ΔC_L is the change in lift coefficient due to the described control line deflection.

For the control force calculation only the parafoil area deflected by the pilot should be taken into account; therefore an approximation of the lift force on that part of the canopy is required. This lift force is the control force which has to be exerted on the wing. The equation for this control force on the kite is shown in Equation 13.8, where S_δ is the deflected area of the parafoil, estimated to be 3 m^2 (asymmetric deflection). Table 13.1 shows the control forces for different deflections.

$$F_{kite} = \sin\delta \left(\frac{2\pi}{3} + \sqrt{3} \right) \frac{1}{2} \rho V^2 S_\delta \tag{13.8}$$

Table 13.1: Different control deflections and forces on the kite control lines, with ρ = 1.225 kg/m^3, V = 15 m/s and S_δ = 3 m^2.

Deflection [m]	δ [°]	ΔC_L	F_{kite} [N]
0.165	8.4	0.5612	232
0.3	15.5	1.0204	422
0.465	24.4	1.5816	654

The parafoil deflections displayed in the table are chosen based on the distance the arms and legs a pilot can (realistically) move in Parashuttle 2. The last entry in the Table 13.1 is the total deflecion of the arms and the legs. Note that the control system is designed such that the deflection is both done by the arms and the legs, whereas the force in that case is carried by the legs only. This is explained in section 13.3.

The calculation results presented in this section are estimated based on a simple analytical method. Control forces found are comparable to results found in [65]. Still the uncertainty of the values is quite large, especially because the exact layout of the parafoil is not known yet. Ground tests should be performed in order to validate the results, as explained in chapter 26.

13.3 Flight controls

In this section the mechanism used to control Parashuttle 2 in flight is discussed. In order to control the vehicle in flight the pilot requires controls inside the cockpit on which control forces can be exerted. These mechanisms consist of two levers for control using arms and two pedals for control using legs. The control levers are located to the left and right of the pilot and serve to control the parafoil during normal turns in flight. The pedals are located left and right under the dashboard in front of the pilot, providing additional control required during steep turns and flaring. In order to size these levers and pedals the maximum force a pilot may exert has to be identified. For the arms this was found to be 220 N; hence 110 N per arm. For one leg this maximum force is 800 N [66]. When sizing the control levers and pedals these forces are kept in mind.

As stated in section 13.2 the force required to deflect the parafoil sufficiently is 232 N on the levers and 654 N at the pedals without friction. Taking friction into account the design forces are 300 N and 800 N for the levers and pedals respectively. Knowing these forces it is possible to use the balance of moments around the hinge of the lever or pedal to compute the stick ratio κ_{lever} (or κ_{pedal}):

$$\kappa_{lever} = \frac{d_1}{d_2} = \frac{F_{control}}{F_{stick}} \tag{13.9}$$

Using the aforementioned, values for forces and stick ratios are shown in Table 13.2. In order to get absolute values for d_1 and d_2 (the lengths above and below the hinge) the total lever length has to be determined based on the space available inside the cockpit. The total lever length will be 0.5 m, since this height is needed to provide sufficient comfort for the pilot when he moves his arms. Based on space available the total pedal length will be 0.3 m. The arm deflection is also limited by the amount of space in the cockpit and becomes 0.45 m. Equations 13.10 and 13.11 are now used to compute lever lengths. Using the stick ratios computed earlier it is now possible to compute the control line deflection by the levers and pedals, again shown in Table 13.2.

$$d_1 = \frac{l_{lever}}{1 + \frac{1}{\kappa_{lever}}} \tag{13.10}$$

$$d_2 = l_{lever} - d_1 \tag{13.11}$$

Table 13.2: Sizing parameters of both the levers and pedals used for control.

Lever parameters	Results	Pedal parameters	Results
F_{stick}	110 N	F_{pedal}	800 N
$F_{control}$	300 N	$F_{control}$	800 N
κ_{lever}	2.73	κ_{pedal}	1
l_{lever}	0.5 m	l_{pedal}	0.3 m
d_1	0.3659 m	p_1	0.15 m
d_2	0.1341 m	p_2	0.15 m
Arm deflection	0.45 m	Leg deflection	0.30 m
Control line deflection	0.165 m	Control line deflection	0.30 m

To complete the sizing cross-sections of the pedals and levers have to be determined. To do so first the maximum moment within the levers/pedals has to be determined; this is done using the moment formula $M_{max} = F_{stick} d_1$. With this maximum moment it is possible to calculate the maximum stress using the flexure formula [67], where the moment of inertia I for a ring is given by $\frac{\pi}{4}(R_o^4 - R_i^4)$. The results are shown in Table 13.3.

For designing the levers and pedals a safety factor of 1.5 is implemented on the maximum stress. The maximum stresses including safety factor are 38.6 MPa and 60 MPa for the levers and pedals respectively. Using CES Edupack it was found that a suitable material to deal with these loads is Aluminium 6060, which has a compressive strength of 86 MPa and a tensile strength of 152 MPa. With both lever material and dimensions known the mass of the pedals and levers combined can be computed, which is 1.3 kg. Using aluminium costs of 2.30 €/kg the total material cost is €3. If it is bought off the shelf the costs will increase to €300 for both the levers and pedals [68].

Table 13.3: Lever and pedal cross-section dimensions and imposed stresses.

Lever parameters	Values	Pedal parameters	Values
R_o	0.015 m	R_o	0.020 m
R_i	0.012 m	R_i	0.017 m
M_{max}	40.25 Nm	M_{max}	120 Nm
σ_{max}	25.7 MPa	σ_{max}	40 MPa

The levers are connected to the control lines of the parafoil directly, using only a small pulley to pull the cable in the right direction. Figure 13.2a shows the lay-out of the system linking the lever and the pedals to the control cable. It can be seen that the pedals are not directly attached to the main control line, since the pedals are only used for flaring or steep turns and are not supposed to interfere with normal control of the parafoil. It can also be seen that eight pulleys are included per side to guide all the cables in the correct direction. The pulleys have a radius of 2.5 cm and an average thickness of 1.4 cm. They are made of aluminium. The mass of these pulleys is estimated to be 1.2 kg in total. Figure 13.2b shows where the main control lines are guided to. In these figures it can be seen that the levers have a handle at the top with the motorcycle brake included at the top. An anti-slip material is included on the surface of the pedal in order to prevent feet from slipping of.

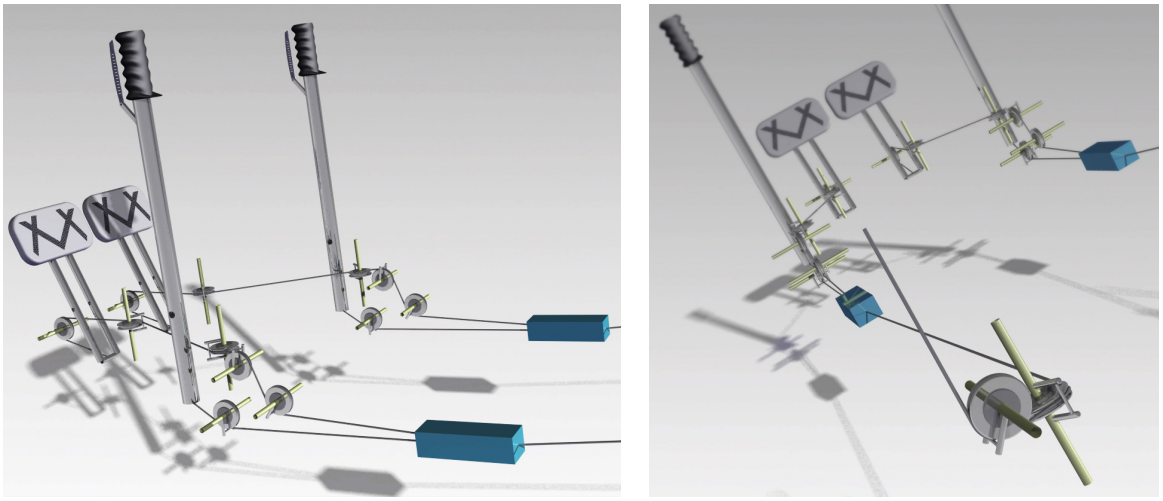

(a) Render of the connection of the pedals and the levers to the control line.

(b) Render of the main control line guided to the parafoil.

Figure 13.2: The control system shown with different components.

Figure 13.3a shows the clamp system connecting the pedals to the main control lines, which was already shown by the blue box in Figure 13.2. This system makes use of a lever which clamps itself onto the main control line when tension is exerted on the pedal line. The system will be able to pull the control line due to the friction force induced between the end of the lever and the control line. In order to have sufficient friction force a suitable material has to be chosen for the end of the lever. This material should have a sufficiently high friction coefficient with steel, of which the control line is made [69]. It is found that rubber's friction coefficient with steel is 0.7 [70]. To prevent the system from sliding over the control line a safety factor of 1.5 is used for the friction force with regard to the pedal force. With a friction coefficient of 0.7 and a maximum pedal force of 800 N this gives a normal force of 1714 N using Equation 13.12.

With these forces known it is possible to calculate the ratio of the height of the lever above the hinge h_1 and the width of lever below the hinge w_2 using Equation 13.13. Since the height below the hinge (h_2) does not contribute to the force transfer it is determined to be 0.05 m to bring the end of the lever closer to the main control line. In Figure 13.3a the lever of the clamping system is shown. The lever of the clamp system needs to bear the loads induced on it. Using equations 13.14 to 13.16 the maximum stress on the lever is computed. Making use again of Aluminium 6060 t4 and a safety factor of 1.5 one obtains a square cross section of 0.027 m wide. This results in a total lever mass of 0.7 kg. Table 13.4 gives a small summary of the forces on and dimensions of the clamp system. This system includes a slider guiding the clamp system along the main control line and also makes sure the clamp system can not retreat further than its rest position. The length of this slider must be at least 0.30 m long (the maximum deflection allowed by the pedals). The front view of this slider is shown in Figure 13.3b, where the outer contour represents the cross section of the slider. The slider is also made out of aluminium. This will give a mass of 4.3 kg.

$$F_N = \frac{F_{friction}}{\mu_{friction}} \tag{13.12}$$

$$\kappa_{lever} = \frac{F_N}{F_{pedal}} \tag{13.13}$$

$$M_{max} = F_{pedal} \cdot h_1 \tag{13.14}$$

$$\sigma_{max} = \frac{M \cdot y_{max}}{I} \tag{13.15}$$

$$I = \frac{1}{12} \cdot b \cdot h^3 \tag{13.16}$$

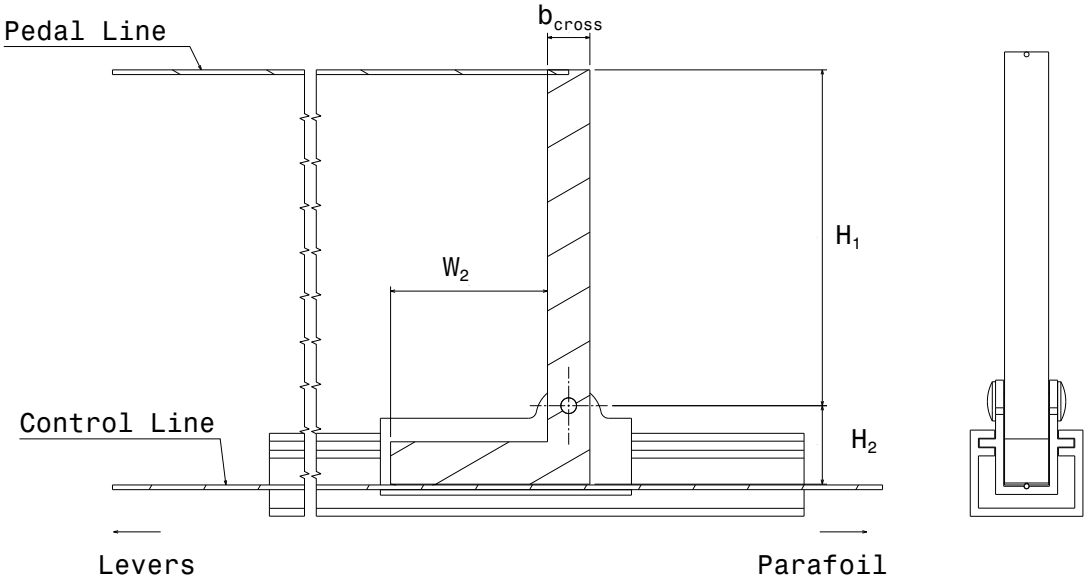

(a) Side view of the lever that clamps the main control line.

(b) Front view of the slide that guides the clamp lever.

Figure 13.3: The system used to connect the pedals to the main control line.

Table 13.4: Dimensions and forces for the clamp system.

Parameters	Value
F_{pedal}	800 N
$F_{friction}$	1200 N
F_N	1713 N
κ_{lever}	2.14
h_1	0.214 m
h_2	0.05 m
w_1	0 m
w_2	0.1 m
h_{cross}	0.027 m
b_{cross}	0.027 m
Mass	5.7 kg
Material cost	€1.61

The control lines are made of stainless steel with a tensile strength of 619 MPa [71]. With an ultimate pulling force of 800 N and a safety factor of 5.0 the control lines should have a diameter of at least 2.9 mm. These lines (one for right side and left side of the parafoil) will be lead to the parafoil connection location by the the fuselage trusses at the side of the vehicle. At the parafoil connection these lines will be connected to the control lines of the parafoil itself. As the control lines in the fuselage connect the pedals and levers to the parafoil control lines they require a length of 5 meters each, resulting in a total control line length of 10 m. With a density of stainless steel of 8030 kg/m^3[71] and a diameter of 2.9 mm this gives a mass of 0.55 kg. It is found that stainless steel control cables have a cost of 3.05 €/m, hence a total cost of €30.50 for the control cables is included [72]. Since the control system is a very important part of Parashuttle 2 it is decided to also have safety control lines, which directly enter the cockpit through the top plate of the cockpit. These lines can be controlled direct and manual by the pilot in case of a failure of the original control system.

13.4 Steering on land

In this section the control of Parashuttle 2 on land will be discussed. Control on land consists of two parts: steering and braking. As mentioned in section 5.3 the final design has four wheels integrated in the floats for driving on land. Differential braking will not be possible with four fixed wheels, since the free-rotating wheels will get dragged laterally over the ground in this case. Therefore it has been decided that only two wheels (those with brakes) are fixed and that the other wheels can rotate. These wheels are held in/brought back to a straight position by rotational springs, in order to prevent the wheels from being misaligned when touching down.

The decision made was to place the steering wheels in front, due to the fact that rear wheel steering is only used for very low speed vehicles. This is because in order to induce the side force needed for turning, the whole vehicle needs to be rotated in yaw first. This rotation and the fact that the vehicle has not started turning yet causes the vehicle to roll. At high speeds this can cause the vehicle to roll over [73].

Part of the requirements for steering is that Parashuttle 2 should have a turn radius of at most 6 m. In order to achieve this the front wheels should be able to turn a certain amount based on the wheelbase and wheel track. This can be seen in Figure 13.4

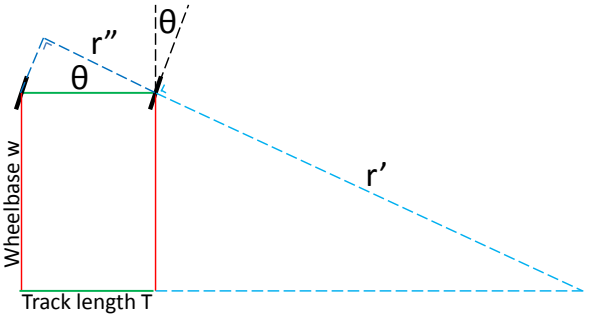

Figure 13.4: Schematic of turning radius

$$r' = \frac{W}{\sin\theta} \tag{13.17}$$

$$r'' = T \cdot \cos\theta \tag{13.18}$$

$$R = r' + r'' \tag{13.19}$$

$$R = \frac{W}{\sin\theta} + T \cdot \cos\theta \tag{13.20}$$

Using a wheelbase of 2.49 m and a wheel track of 2.0 m, a turn radius of 6 m would require a deflection angle of 35 °. The requirement for braking is that Parashuttle 2 should come to standstill in 5 m from an initial speed of 3 m/s. As Parashuttle has a slightly higher mass but a lower speed compared to a motorcycle it has been decided that the same type of brakes would be used. The braking force required can be calculated with energy conservation. The kinetic energy of the vehicle should be equal to the work done by the frictional forces on the two rear wheels:

$$\frac{1}{2}mv^2 = 2F_{friction}s \tag{13.21}$$

Having found the required friction force from the relation above, one can compute the force applied to the brake disc by the brake pads (C) using Equation 13.22:

$$C = \frac{F_{friction}}{4\mu_b n} \cdot \frac{R}{r_d} \tag{13.22}$$

where μ_b is the coefficient of friction between the brake pad and disc (according to Roskam Part IV [74] this is around 0.7), n is the number of fictional surfaces (2), R is the outer radius of the tyre and r_d is the radius of the brake disc. The latter is constrained by the radius of the rim, both are defined in section 14.3. The maximum frictional force between the wheel and the ground is determined by the normal force on the rear wheels and the coefficient of friction. It was calculated that the force needed on the brake pad was 1020 N. In order to apply this force a hydraulic cable is implemented, the cross section of which can easily be estimated using basic hydraulics:

$$A_{Cable_{Pilot}} = A_{Cable_{Brake}} \cdot \frac{F_{Pilot}}{F_{Brake}} \tag{13.23}$$

In case a hydraulic cable with a radius of 3 cm at the brake and a radius of 1 cm at the pilot (which results in a $A_{Cable_{Pilot}} : A_{Cable_{Brake}}$ ratio of $3^2 = 9$) is used, the required hand force is 113 N or 11.5 kg force. According to the TNC-CDAAR [75] the average non-dominant grip strength of a 50 year old female is 16.5 kg, meaning such a cable allows for braking by most pilots.

Table 13.5: Cost and mass of the steering mechanism.

Component	**Mass** [kg]	**Cost** [€]
Brake Disc	0.4 ± 0.1	30 ± 8
Brake Caliper	1.0 ± 0.1	80 ± 10
Brake Pads	0.3 ± 0.1	20 ± 5
Hydrualic Cables	0.6 ± 0.2	24 ± 4
Fluid Reservoir	0.5 ± 0.1	30 ± 6
Hydrualic Fluid	0.5 ± 0.05	6 ± 1
Total	3.3 ± 0.65	190 ± 34

The cost and mass can be seen in the Table 13.5, there are quite large uncertainties due to the fact that the exact values are hard to find for complete braking systems. Prices were taken from off the self products and then adjusted for the capabilities required by Parashuttle 2. The components will be made of water resistant aluminium. Regular inspection of the brake discs and pads must be done to look for wear. The level of hydraulic fluid in the reservoir must also be checked in order to have the sufficient pressure.

13.5 Steering on water

In this section the mechanism used to steer on water is elaborated on. Steering on water is done using two rudders attached to the back of the floats. The control of these rudders is linked to the wheels' differential brake control, hence pulling the right brake will move the both rudders to the right and vice versa for pulling the left brake. The design of the rudder itself is elaborated on in subsection 14.2.5. Figure 13.5 shows a schematic of the rudder system. The rudder (2) is controlled by pulling the control cables (4) connected to the brake levers. To turn right the right brake lever is deflected, causing the rudder to rotate, inducing a moment and in turn causing the vehicle to turn. The rudder can hinge upwards at the hinge point (5) allowing it to be retracted by pulling on the retraction cable (6); this ensures that the rudder does not come into contact with the ground during land operation. The whole mechanism is connected to the back of the float by the fixed attachments (1). The T-lever (3) is able to rotate freely in the fixed attachments.

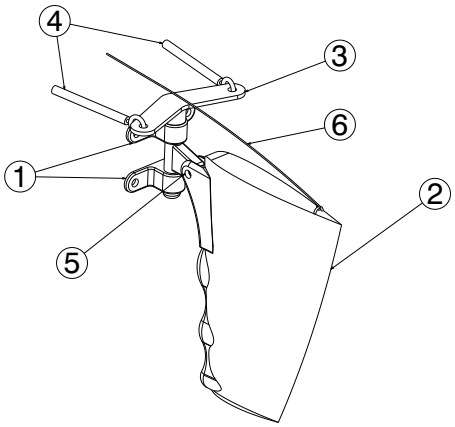

Figure 13.5: Schematic of the rudder mechanism, highlighting: 1.Attachments, 2.Rudder, 3.T-lever, 4.Control cables, 5.Hinge point, 6.Retraction cable.

The force required on the brake lever to deflect the rudder is dependent on the speed, the deflection of the rudder, the length of the T-lever, the moment arm of the rudder and the area of the rudder (found in subsection 14.2.5). Taking a hand force slightly lower than that of a fifty year old female (mentioned in section 13.4) allows for computation of the required length of the T-lever. The force exerted on the rudder by the flow of water can be calculated using the lift formula. This lift will induce a moment about the hinge point. Using the hydraulics formula seen in section 13.4 one can calculate the force that can be exerted on the T-lever, this force will also produce a moment. Rearranging all terms of the lift, moment and hydraulics formulas one gets Equation 13.24

$$l = \frac{\rho V^2 S C_L x_{ac} A_{in}}{F_{hand} A_{out}} \tag{13.24}$$

In subsection 14.2.5 it can be seen that the rudder was designed for a speed of 2 m/s, having a C_l of 1.3 and an area of 0.105 m^2. Assuming x_{ac} (distance to aerodynamic centre) to be 0.15 m and the same hydraulic cable to be used, the length, l of the top bar of the T-lever would be equal 0.066 m.

An estimate has been made on the total cost and mass of the complete steering mechanism, this estimate is shown in Table 13.6. The total cost is estimated to be €72 ± 16, excluding the cost of the rudders which can be found in section 14.6. The mass is estimated to be $2.55kg \pm 0.6$. All costs and masses were based on similar products found on the market as well as simple volume calculations.

Table 13.6: Total mass and cost of rudder mechanism.

Component	Quantity	Mass [kg]	Cost [€]
T-lever	2	0.5 ± 0.1	8 ± 2
Float Attachments	4	0.4 ± 0.1	10 ± 4
Hinging Attachment	2	0.3 ± 0.1	8 ± 2
Retraction Cable	2	0.3 ± 0.05	15 ± 3
Hydrualic Cable	2	0.6 ± 0.2	24 ± 4
Hydrualic Fluid	0.5 l	0.5 ± 0.05	6 ± 1
Total		2.6 ± 0.6	72 ± 16

13.6 Thrust control

In this section the thrust control is elaborated on. As described in section 7.1 thrust variations are used to adjust the climb/glide rate and thus the altitude. The Rotax 582 engine is provided with various accessories, including a throttle cable, choke cable and a throttle and choke quadrant. It is decided to use a simple knob on top of the handle to increase (push it up) and decrease (push it down) the thrust. Therefore only the throttle cable is needed to connect this knob to the engine. The cable will be led along the fuselage trusses. The thrust level is shown on the screen described in section 16.2.

The main thrust control part is the throttle cable, which has a total cost of €63 [46]. The cables are made of 1.2 mm stainless steel with a nylon coating. With a total length of 4 meters and a density of 8000 kg/m^3(found in CES Edupack) this will add up to 0.2 kg.

13.7 Summary

The complete control of Parashuttle 2 is accomplished by four different control systems, the total cost and mass of these control systems are summarised in Table 13.7

Table 13.7: Summary of control systems

Part	Cost	Mass
Kite Control	€365	8.1 kg
Wheel Control	€190	3.3 kg
Rudder Control	€72	2.6 kg
Thrust Control	€63	0.2 kg
Total	€690	14.2 kg

Chapter 14 | Undercarriage

The undercarriage is an important subsystem, since one of the most challenging and innovative aspects of Parashuttle 2 is its amphibious characteristics. The undercarriage will provide the vehicle with this novelty. This chapter is structured in the following way: first the subsystem requirements are discussed in section 14.1, after which the complete design of the floats (without wheels) will be detailed on in section 14.2. In section 14.3 the wheels will be designed and integrated into the floats. Section 14.4 determines the water resistance acting on the floats. Next a sensitivity analysis will be performed in section 14.5. Lastly the mass and material cost of the floats is determined and summarised in section 14.6.

14.1 Subsystem requirements

A detailed list of requirements for Parashuttle 2 has already been established in appendix B. Many requirements on this list are, either directly or indirectly, applicable to the undercarriage. The most important ones are listed below:

1. Parashuttle 2 shall fit on an internationally road-legal trailer.
2. Parashuttle 2 shall be able to drive over both land and water.
3. Parashuttle 2 shall be able to brake during manoeuvring on both land and water.
4. Parashuttle 2 shall be able to turn during manoeuvring on both land and water.
5. Parashuttle 2 shall be able to land on and take off from both land and water.

The main design philosophy is to first make sure that the loads involved in taking off, landing and cruising can be withstood by the structure and that the vehicle is stable both land and water. When the structure is able to do so, the focus is put on optimising for mass. Mass is considered to be more important than water resistance, because resistance only occurs during take-off and landing. Mass is of importance during the complete flight and its effect on performance and sustainability will be larger than the effect of water resistance.

Of the cost and mass budget made in previous work [9], €8,000 and 43 kg were allocated to the undercarriage respectively. These values will be strived for in the forthcoming detailed design.

14.2 Float design

This section is dedicated to the design of the floats. Section 14.2.1 describes how the geometry of the floats is obtained. It also compares the designed geometry with existing floats as a means of validation. In subsection 14.2.2 the material to be used for the floats is determined, after which the structure will be designed in subsection 14.2.3. Next, the stability of the floats will be assessed in subsection 14.2.4. Lastly, the rudders are designed in subsection 14.2.5.

14.2.1 Design and validation of float geometry

This subsection will explain how the geometry of the undercarriage is determined. The method and equations are explained first, with a summarising table containing all calculated values given at the end of the first subsection. Next the obtained geometry will be compared to the geometries of reference floats to validate the results.

Design of the float geometry

The first thing to do is to decide on the number of floats to be used. A boat hull provides little water clearance for a propeller, the same goes for a trimaran. This make a twin float (or catamaran) configuration seem to be a good option. In hydrodynamic analysis the Froude number is often

used, which has a similar meaning to the Reynolds number in aerodynamics. The Froude number is defined as $Fr = \frac{v}{\sqrt{g \cdot L}}$ (v = velocity, $g = 9.81 m/s^2$ and L = length of the float, for now set to the length of the vehicle). For Parashuttle 2 this number will be around 2.2 at take-off speed. For this Froude number a catamaran produces less resistance than a monohull, for a trimaran drag is even lower [76]. However, because of the floating hull providing little engine clearance and the increased complexity this configuration causes structurally, this configuration is not desirable. Hence for the design of Parashuttle 2 a twin float configuration will be used.

Figure 14.1 shows the definition of angles and dimensions of floats and hulls. A step generally reduces the body's friction with water, however at speeds lower than 30 knots ($\approx$ 15.5 km/h) a step has no beneficial effect and only adds drag [77]. Since Parashuttle's maximum velocity on water is lower than 15.5 km/h no step will be used.

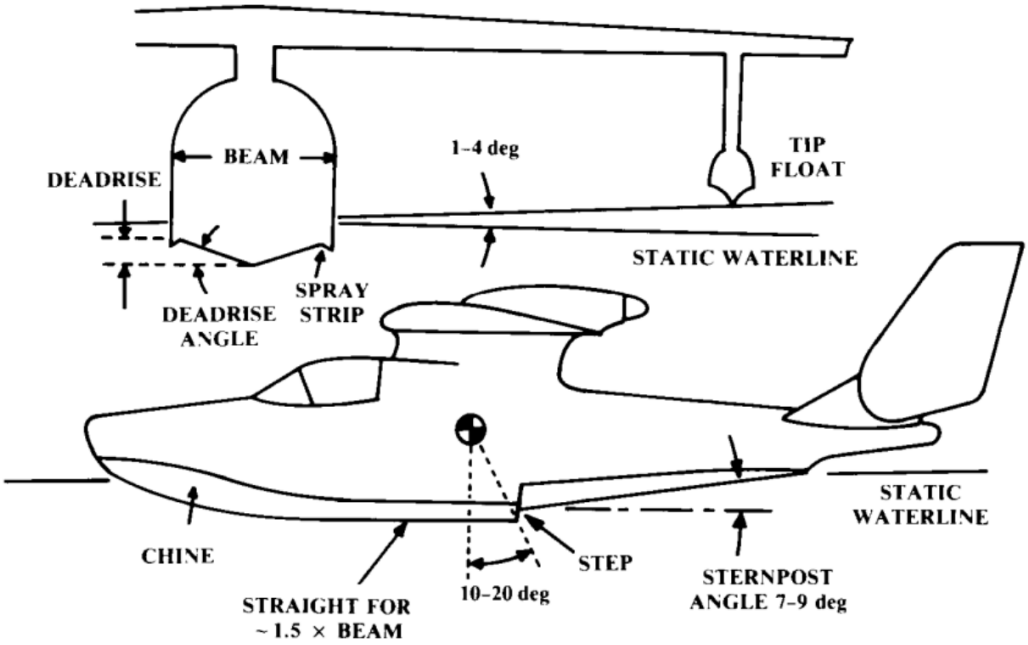

Figure 14.1: Nomenclature of angles and dimensions of floats and hulls [78].

According to [79] the first step in designing floats is estimating the mass the floats and of the complete vehicle in order to determine the required water volume to be displaced. The mass of one float can be estimated using

$$W_f = 0.0365 \cdot \Delta_0 + 43.5 \tag{14.1}$$

where Δ_0 is the gross vehicle mass in kg. This formula was determined using empirical data in the year 1935 [79]. Materials back then were not as advanced as nowadays, which is why the estimated mass will be multiplied with a factor 0.75. Furthermore the mass per float determined by Equation 14.1 incorporates a "reserve buoyancy" factor of 100%. Because of requirement P2-Mis-2-2-1 (see appendix B) this factor should be reduced to 90%. Next the floats' volume can be determined using

$$V = \frac{\Delta_0}{\rho}. \tag{14.2}$$

This calculation is based on Archimedes' principle, with ρ the density of water. Since the paraplane is required to be able to take off from and land on both salt and fresh water, the density of fresh water (the lower of the two) is used in this calculation, its density being 1000 kg/m^3.

Now actual sizing can begin. First the equations will be provided, then an explanation of how these equations were used will be given. The beam is defined as the width of the float (see Figure 14.1).

Typically the beam varies along the length of the floats. The maximum beam can be computed using Equation 14.3 [80].

$$b_{max} = \sqrt[3]{\frac{\Delta_0}{C_{\Delta_0} \cdot \rho}} \tag{14.3}$$

in which b_{max} is the maximum beam width and C_{Δ_0} is the static beam loading coefficient. For a configuration of floats, the slenderness ratio is an important parameter. With L being the length of the floats, it is defined as:

$$SLR = \frac{L}{b_{max}} \tag{14.4}$$

The forebody and afterbody of a hull are the part upstream and downstream of the (often used) step respectively. The afterbody normally is inclined by an angle called the sternpost angle (see Figure 14.1 on page 46). Since no step is included in this design, the forebody length is considered to be the distance between the tip of the float and the start of the inclination, and the afterbody is the part between the start of the inclination and the tail. For a given static loading coefficient, the forebody length is defined as [80]:

$$l_f = b_{max} \cdot \sqrt{\frac{C_{\Delta_0}}{k}} \tag{14.5}$$

in which k is the spray coefficient. The spray coefficient is an indication of the amount of water "sprayed" in the air along the sides of the floats. An empirical formula (Equation 14.6) for the forebody length can be deduced from [81]. Combining Equations 14.4 and 14.6 and knowing that $L = l_f + l_a$ gives Equation 14.7.

$$l_a = 1.11 \cdot l_f \tag{14.6}$$

$$\frac{l_f}{b_{max}} = \frac{SLR}{2.11} \tag{14.7}$$

Rewriting Equation 14.5 results in:

$$C_{\Delta_0} = k \cdot \left(\frac{l_f}{b_{max}}\right)^2 \tag{14.8}$$

At this point all equations required to get the main geometry dimensions have been established. Now it will be shown how they must be used.

First one assumes a slenderness ratio, which can be substituted in Equation 14.7 to get the l_f/b_{max} ratio. Parashuttle 2's maximum velocity on water is relatively low compared to seaplanes, however it is not a slow cruising vessel either. Therefore an SLR of 12 (something between these 2 categories was used) [82]. The acquired l_f/b_{max} ratio can now be substituted in Equation 14.8. This equation needs the spray coefficient k as an input, so k must be estimated as well. According to [80] satisfactory spray is a good enough standard for design, hence a spray coefficient of 0.0675 was used. This results in a value for C_{Δ_0}, which together with the density of fresh water ρ and the displacement mass Δ_0 can be substituted in Equation 14.3 to retrieve a value for the maximum beam. Knowing b_{max} the length of the floats can be determined using Equation 14.4.

The deadrise angle is the angle at the bottom of the floats (shown in Figure 14.1 on page 46). This angle is mostly between 10 and 30 degrees. It is decided to keep the deadrise angle the same throughout the whole length because this will keep the production process simple. What the angle should be is a trade-off: a flatter bottom allows for faster take-off, however it will increase impact during landing [83].

The maximum induced load due to slamming on the water can be calculated using Equation 14.9 [84], where ρ is the density of water, V_0 the vertical speed and β the deadrise angle. Running

the model discussed in chapter 7 a preliminary value for the descent rate was found to be 2.0 m/s. After designing the general shape of the floats the impact area when landing straight is estimated to be 1.27 m^2. It is decided that both floats and struts between the floats and fuselage are designed for a maximum loading of 2 g. Now the maximum pressure P_{max} can be estimated ($m \cdot g \cdot 2/area$). Filling in the descent rate of 2.0 m/s a dead rise angle of 26 degrees is computed with Equation 14.9.

$$P_{max} = \frac{\rho V_0^2 \pi}{2} \cot(\beta) \tag{14.9}$$

The sternpost angle usually is between 7 and 9 degrees. It was decided to use an angle of 7 degrees because then the trim angle is smaller than for higher sternpost angles [85] and it will give more stability to the vehicle.

A summary of the obtained parameter values is given in Table 14.1, mass is here the first approximation.

Table 14.1: Overview of obtained dimensions for Parashuttle's floats.

Parameter	Value	Parameter	Value
Float mass W_f	24.9 kg	Afterbody length l_a	2.28 m
Maximum beam b_{max}	0.362 m	Required displacement volume V	0.423 m^3
Length L	4.34 m	Deadrise angle β	26°
Forebody length l_f	2.06 m	Sternpost angle ϕ	7°

Validation of the float geometry

Now that the geometry of the floats is established one can check whether the design came up with is feasible. The floats will be compared to existing seaplane floats as a means of validation. In Table 14.2 a comparison of characteristics can be found.

Table 14.2: Float verfication with Aerocet 2200 and MEAD M-1430 Amphibious Float.

Parameter	Parashuttle 2	Aerocet 2200 [86]	MEAD M-1430 [87]
Displacement mass [kg]	495	639	612
Length [m]	4.34	5.40	4.42
Maximum height [cm]	37	63.4	-
Maximum beam [cm]	36.2	70.6	56.5
Sternpost angle [°]	7	7	6
Deadrise angle [°]	26	25.5	22
Step	No	Yes	Yes

One can see that the numbers for the Aercet 2200 floats are generally higher than the numbers for Parashuttle 2. This is because the mass of the Piper is considerably larger than Parashuttle's mass. The MEAD floats have to provide more buoyancy than Parashuttle's, but are almost equally long. Therefore the MEAD float should get its extra buoyancy from other larger dimensions such as the maximum beam. It can also be seen that the reference floats both have a step. It was previously explained that for the speeds at which Parashuttle 2 takes off a step would only increase drag. Seaplanes' take-off speeds are a lot higher [88], hence for those a step is an efficient way to decrease drag. The sternpost and deadrise angle were not explicitly mentioned in [86] and [87]. These references only contain scaled figures that could be used to measure the angles.

Since the dimensions of the floats are related to the required water displacement, it seems that the geometry of the floats of Parashuttle 2 is feasible. It has the smallest geometry but also the smallest required water displacement.

14.2.2 Material selection

The material that will be used for the floats will be determined in this subsection. Research has been done into aircraft float materials, investigating carbon fibre, fibreglass with an epoxy resin, an aluminium alloy with silicon and magnesium, and GLARE [89, 90]. Making use of CES EduPack 2012 (a program containing all properties of almost all materials) the team could decide which material to use by means of a trade-off table. The trade-off is performed in Table 14.3. One can see that cost is the driving factor in the trade-off. Salt water resistance is only 15% of the grade because there are ways to enhance salt water resistance, using for example coating.

Table 14.3: Float material trade-off table. As can be seen Aluminium performs best.

Material property	**Carbon fibre**		**Fibreglass with epoxy**		**Aluminium 6061 T651**		**GLARE**	
Density ρ [kg/m^3] (15%)	$1.61 \cdot 10^3$	5	$2.0 \cdot 10^3$	4	$2.73 \cdot 10^3$	2	$\pm\ 2.8 \cdot 10^3$	2
Costs [€/kg] (40%)	83.6	1	22.2	3	2.73	5	$\pm$ 5	5
Young's modulus E [GPa] (15%)	50.7	3	31	2	71.5	5	67.9	4
Shear modulus G [GPa] (15%)	19.5	4	11	2	27.3	5	16	3
Salt water resistance (15%)	Excellent	5	Excellent	5	Acceptable	3	Acceptable	3
TOTAL GRADE	**2.95**		**3.15**		**4.25**		**3.8**	

It can be seen that the Al 6061 T651 comes out best. A sensitivity analysis must now be done to check whether this result is susceptible to small changes in trade weights. For the sensitivity analysis each weight is set to 20%. The results are tabulated in Table 14.4.

Table 14.4: Sensitivity analysis results

Material	**Grade**
Carbon fibre	3.6
Fibreglass with epoxy	3.2
Al 6061 T651	4.0
GLARE	3.4

It is clear that again the aluminium alloy is the best option. The indicated alloy is chosen because its magnesium and silicon atoms improve salt water resistance.

14.2.3 Design of the structure

In this section the method to define the structure of the floats will be explained. Five load cases were defined first, these are listed below. The floats' structure should be strong enough to deal with all forces in any of these load cases. The minimum force Parashuttle 2 should hold is 3g. Because landing exactly on both floats at the same time is rare the minimum force per float is set to 2g. For analysis the following loadcases are distinguished:

1. Landing straight with 2 g per float and a water resistance when having the float carry 50% of weight.
2. The front 1 meter experiences a 2 g landing impact and a water resistance when having the float hold 50% of the weight.
3. The last 1 meter will be subjected to a 2 g landing impact and a water resistance when having the float hold 50% of the weight.
4. Moving on water with a float carrying 90% of weight (the maximum load) and the water resistance when the float is fully submerged.

5. Standing still with one person standing on the float and the float holding 90% of weight.

The float drawn using CATIA is split along its length, at each cut the width and height are calculated. Interpolating these numbers allows for computation of local width and height at any location.

The projected area of the entire float as seen from above is determined using the step width and the average beam of each step. Dividing the total applied force by the total area gives the distributed load. Multiplying this distributed load with the area of each section gives the normal force on that section.

This distributed load and the water resistance computed using Hullspeed are now implemented in Frame3DD (the structural analysis model discussed in chapter 8) to get the shear force and moment at each point in the floats and at the four struts. Now for each point the critical case is taken (maximum moment and shear), shown in Figure 14.2.

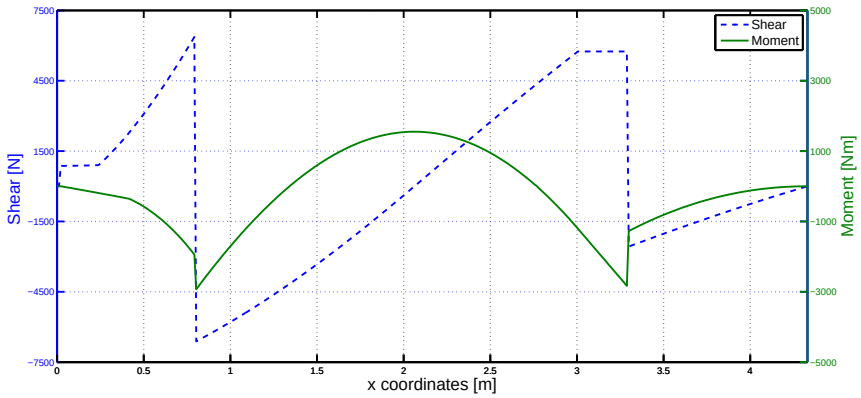

Figure 14.2: Maximum shear and moment at each point.

To calculate internal stresses boom theory is used at each float section. In Figure 14.3 the floats' simplified shape and place of the booms can be seen. For this method first the centre of gravity has to be calculated. This is done by summing the products of the bars' areas and moment arms around a reference point and then dividing this by the total area. Knowing the centre of gravity, the area of booms can be calculated using Equation 14.10, in which the ratio of $\frac{\sigma_2}{\sigma_1}$ is calculated using Equation 14.11, where P is the force in x-direction. In this case this compressive force is assumed to be only due to drag.

To be sure the structure will be able to hold both the maximum moment and maximum force in x-direction, both maximum values (which do not necessarily occur in the same load case) are taken into account simultaneously. The moment of inertia of each bar parallel to an axis is calculated using Equation 14.12. For the bottom part the moments of inertia are calculated using Equation 14.13, since these are not parallel to any axis. In this equation t represents thickness, a is the length of the beam and β is the angle between the horizontal axis and the beam. The total moment of inertia is the summation of the moments of inertia for each bar.

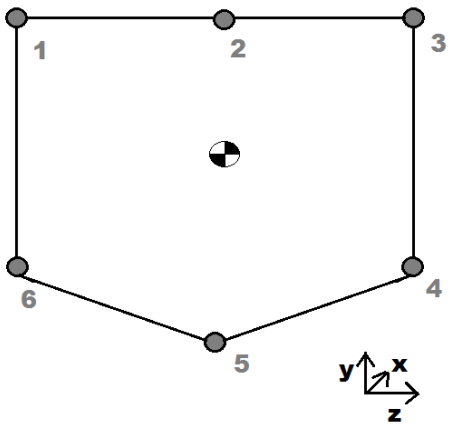

Figure 14.3: The simplified case with booms.

$$B_1 = \frac{t_d b}{6}\left(2 + \frac{\sigma_2}{\sigma_1}\right) \tag{14.10}$$

$$\frac{\sigma_2}{\sigma_1} = \frac{\frac{P}{A} + \frac{My_2}{I_{zz}}}{\frac{P}{A} + \frac{My_1}{I_{zz}}} \tag{14.11}$$

$$I_{zz} = \frac{bh^3}{12} + A \cdot dy^2 \tag{14.12}$$

$$I_{zz} = \frac{1}{12} t a^3 \sin^2(\beta) \tag{14.13}$$

The moments of inertia of the booms shown in Figure 14.3 can be calculated using Equation 14.14 and Equation 14.15. With this the shear flow can be calculated using Equation 14.16. The first part of this equation is calculated by making a cut between booms 4 and 5. Then q_{s0} is calculated using the knowledge that the moment at each point has to be zero. Finally the shear stress is obtained by dividing the shear flow by the bar's thickness.

$$I_{zz} = \sum B_r \cdot y_r^2 \tag{14.14}$$

$$I_{yy} = \sum_{r=1}^{n} B_r \cdot z_r^2 \tag{14.15}$$

$$q_s = \frac{S_y}{I_{zz}} \sum_{r=1}^{n} B_r y_r + q_{s0} \tag{14.16}$$

Not only the applied moment, but also the water pressure and resistance create a stress. Stress due to the applied moment is shown in Equation 14.17. Assuming water resistance is horizontal, the stress in x-direction due to hydrodynamic drag can be found by dividing this drag by the frontal area of the section.

$$\sigma_x = \frac{My_2}{I_{zz}} \tag{14.17}$$

Pressure on the floats' bottom is the generated by the buoyancy force, creating both the shear and moment stress calculated earlier whilst also applying pressure on the floats' sides. This pressure will create a normal stress in the bottom and top part. This is calculated using Equation 14.18, with p the pressure [91]. It is estimated that two-thirds of this stress will be carried by the bottom skin and one-third by the top skin, since pressure increases with depth.

The applied pressure also creates a bending stress, which can be calculated using Equation 14.19 [91]. Here it is assumed that the float's cross-section is a square. The value of β used in this

equation is estimated to be 0.35 [91] .

$$\sigma_z = \frac{ph}{t} \tag{14.18}$$

$$\sigma_z = \beta \cdot \frac{pb^2}{t^2} \tag{14.19}$$

Having found both shear stress, normal stress and internal stress due to the applied internal moment, the Von Mises stress can be calculated on each bar at each x-location of the float using Equation 14.20. Comparing this Von Mises stress to the material yield strength (keeping in mind a safety factor of 1.5) allows for a decision on whether to increase or decrease bar thickness. To allow for rapid solving of this optimisation strategy the structure may be at most 10% overdesigned. The optimised distribution of bar thickness is shown in Figure 14.4.

$$VM = \sqrt{\frac{(\sigma_x - \sigma_y)^2 + (\sigma_x - \sigma_z)^2 + (\sigma_x - \sigma_z)^2 + 6 \cdot (\tau_{xy}^2 + \tau_{yz}^2 + \tau_{xz}^2)}{2}} \tag{14.20}$$

Such a structure (with many discrete thickness steps) will be hard to manufacture however, though

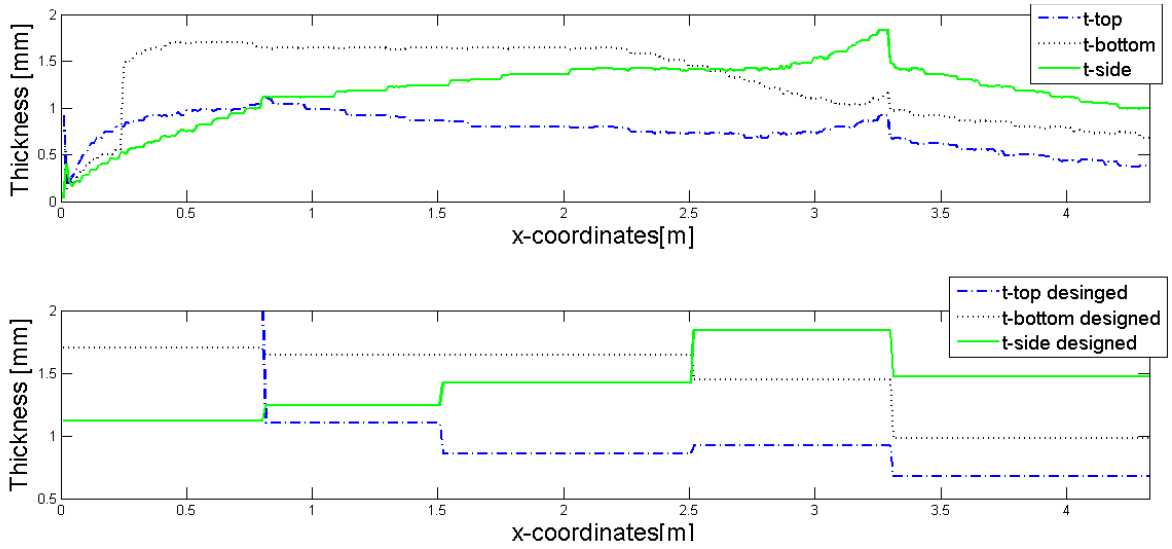

Figure 14.4: Skin thickness distributions over the floats.

it does offer the lowest mass possible (5.69 kg). An option allowing for easy manufacturing is a structure with a constant thickness, based on the maximum required thickness. This option is nearly twice as heavy though, with the aluminium skins weighing 15.24 kg. A final option is to have a constant thickness between adjacent ribs, located at 0.8, 1.5, 2.5 and 3.29 m from the front. This option will lead to a mass of 11.03 kg per float. Due to its combination of relatively low mass and relatively good manufacturability this option is chosen.

To assess whether the design come up with is susceptible to buckling under the loads of hydrodynamic drag, Equation 14.21 is used to compute the maximum distance between ribs.

$$\frac{\sigma}{A^2} \cdot 1.5 > P_{crit} = \frac{\pi^2 EI}{k^2 L^2} \tag{14.21}$$

Using the thicknesses computed previously it is found that only the front 6 cm of the floats would require ribs to be placed. Since the nose of the floats will be a rubber cap longer than 6.0 cm, the structure needs no ribs at all. However due to safety considerations (the float should still operate in case of a leak) the float requires at least four separate sections of roughly equal volume. For this reason there will be at least three ribs placed in the floats. One will be placed beneath each

strut connecting the floats and fuselage. After placing those there is one big compartment and two smaller ones. It is decided to have two ribs in the big compartment, resulting in a total of five compartments providing even more protection against leaks. The distance from the float's nose to the ribs is then 0.8, 1.25, 2.5 and 3.29 meters respectively. To prevent the ribs from leaking their thickness will be 2 mm. This will give the floats an additional mass of 2.52 kg.

14.2.4 Design for stability

To assess stability on water the program Hydromax has been used. The verification of the program was done in chapter 9. In this section the stability of the designed floats will be evaluated, explaining the use of software in the process.

During preliminary design it is estimated that the centre of gravity will be located between 0.9 and 1.0 m above the water. Should the centre of gravity shift this would produce a moment on the vehicle, one which has to be countered by the floats. Since a higher centre of gravity has a larger displacement for a similar roll or pitch angle, it is desirable to have a low centre of gravity. The floats of Parashuttle 2 will be assessed for a centre of gravity at 1.0 m above the water, to account for a worst-case scenario.

To check for what centre of gravity range the floats offer stability, a trial and error method is used. Specifying the location of the centre of gravity in Hydromax allowed to program to determine the orientation of the vehicle in stable position. These outcomes allowed for commenting on the stability and comfort characteristics of the vehicle on water (part of the floats submerging in stable position is not deemed comfortable when stepping in). Analysis was performed for both flat water and sea state 2 conditions.

Results of the analysis are shown in Table 14.5, where longitudinal distance is measured from the vehicle's nose and lateral distances are measured from the vehicle's symmetry plane. Classifications have been given to the ranges: 'critical' meaning that the vehicle will capsize in case the centre of gravity exceeds the specified range, 'uncomfortable' means that in such situations uncomfortable equilibrium angles are attained, 'wet feet' means that outside this range parts of the floats submerge. Naturally one should take into account that the centre of gravity should always be located somewhere between the two floats.

Table 14.5: Allowable centre of gravity ranges on water.

	Flat water	**Sea state 2**
Longitudinal		
Critical	190cm < x < 265cm	205cm < x < 265cm
Uncomfortable	190cm < x < 260cm	205cm < x < 250cm
Wet feet	190cm < x < 245cm	205cm < x < 235cm
Lateral		
Critical	-35cm < z < 35cm	-35cm < z < 35cm
Wet feet	-30cm < z < 30cm	-15cm < z < 15cm

Not only do persons standing on the floats of the vehicle cause the vehicle to roll, also the parafoil (which is attached at the top of the fuselage and therefore has a large moment arm) can cause the vehicle to topple over. The basic drag equation was used to determine the maximum lateral force of the parafoil. Modelling the 50 m^2 parafoil as a flat plate (for which C_D is 2) in a 5.4 m/s stream (corresponding to the wind in sea state 2 conditions) results in a force of 1.8 kN. Multiplying this by the moment arm of the parafoil connection point with respect to the centre of gravity (0.8 m) results in a moment of 1.4 kNm. Such an applied moment corresponds to an effective centre of gravity shift of 0.29 m. Since such a shift is still within the range specified in

Table 14.5 the vehicle will be able to handle such loads. The maximum sidewind Parashuttle 2 could handle without toppling over is 5.7 m/s.

In case the rolling effect of sidewind is accompanied by a person standing on one float, the effective centre of gravity will laterally move by 31 cm. Since such a shift brings the vehicle dangerously close to toppling over, it has been decided to further separate the floats. Allowable wind speeds for the vehicle not to topple over are shown in Table 14.6. One observes that for a separation of 2.3 m wind velocities can exceed the maximum velocity in sea state 2 conditions by 1 m/s, these are sea state 3 wind speeds. It has thus been decided to separate the floats 2.3 m instead of 2 m.

Table 14.6: Allowable centre of gravity ranges on water.

Outer distance [m]	**Allowed centre of gravity displacement [cm]**	**Allowable wind speed [m/s]**	**Allowable wind speed with a person on side [m/s]**
2.10	-40<z<40	5.97	5.82
2.20	-45<z<45	6.32	6.18
2.30	-50<z<50	6.67	6.53

14.2.5 Rudder design

This section discusses the design of the rudders mounted on the floats. The rudder will be used for manoeuvring on water, done at an estimated speed of 2 m/s. For this speed an optimal airfoil was designed using Javafoil. It is taken into account that this program normally calculates the drag and lift produced by an airflow instead of a waterflow. Characteristic values in the program were changed in the option menu and set to values for water. The velocity of approximately 2 m/s corresponds to a Mach number (in water) 0.00135. After testing a variety of profiles in this program and inspecting their lift and drag polars, the NACA-014-53 airfoil was chosen, since it is capable of producing high lift with low drag, the drag only increasing from a deflection of 10 degrees onwards (as seen in Figure 14.5).

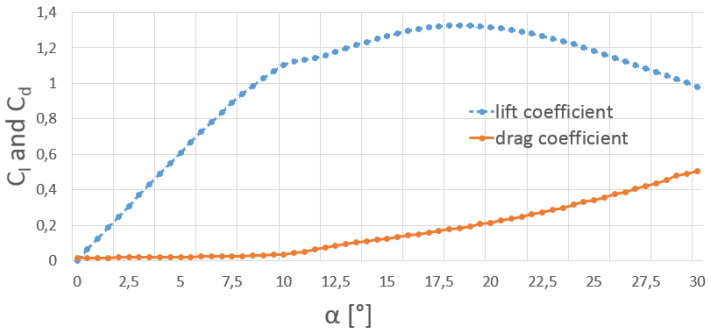

Figure 14.5: Lift and drag polar of NACA 016-53.

The rudder area is computed using Equation 14.22 [92]. The formula provided in this article is shown in Equation 14.22. This results in a rudder area of 0.105 m^2.This is the total area required because there are two rudders, one on each of the float. he area per rudder is 0.053 m^2.

$$\frac{K}{T} = \frac{\frac{1}{2}\rho g C_l cos(\delta)}{\frac{W}{L^2} d\ \delta} \frac{A}{Ld} \frac{\bar{GR}/L}{\left(\frac{k}{L}\right)^2} \left(\frac{V}{L}\right)^2 \tag{14.22}$$

where:

- K/T= Ratio of the moments of inertia of the rudder and the floats ($\pm$ 100)
- δ = Angle of deflection of the rudder corresponding to the C_l
- k = Virtual radius of gyration of ships, normally around 1.25 m
- A = Rudder area [m^2]

The rudder will have a taper ratio of 0.45, an average sweep angle of -3 degrees and an elliptical shape because this is most efficient [93]. Its front will look like a whale fin (see Figure 13.5 on page 43) because this will increase the L/D ratio, especially for higher angles of attack [94]. The bumps on the front will have an amplitude of 0.025 times the chord length and a wavelength of 0.25 times the chord length, because such rudders performed best on tests that have been done so far [95].

To see whether the turn radius of the vehicle is less than eight meters a simple calculation is required. Assuming that during the turn the centre of gravity is on the same circle as the rudder of the float that describes the inner circle, and deflecting the inner rudder assuming over 20°deflection, the turn radius will be 6.1 m. This value gives an idea of the radius and is small enough to assume that the real turn radius will be less than 8 meters as well.

14.3 Wheel design and integration

This subsection is about the selection of wheels for manoeuvring on ground, and their implementation in the floats. First an analysis of requirements on the wheels is performed in subsection 14.3.1, then the wheel unit is designed in subsection 14.3.2. After this, the decision is made on whether to use shock absorbers in subsection 14.3.3, followed by the implementation of the wheel units in the floats in subsection 14.3.4. Thereafter, the location of the wheels along the length of the floats will be determined in subsection 14.3.5. Lastly, the issue of maintainability will be discussed in subsection 14.3.6.

14.3.1 Wheel system requirement analysis

It was decided in section 13.4 to use four wheels, each float having one at the front and one at the rear. The requirement of being able to sustain a 3g impact will be met in the following way. The two back wheels together should be able to withstand a 2g impact, i.e. the back wheels should each carry 1g, which is the gross weight of the vehicle. The front wheels should each withstand 0.5g, or half the weight of the vehicle. So if Parashuttle 2 lands on its four wheels together, it can bear an impact of 3g.

In section 13.4 it was discussed that differential braking will be used to manoeuvre the vehicle on land. The back wheels should be rigid, i.e. they are not allowed to rotate around the local z-axis. They should contain the brakes for the differential steering. The front wheels will be able to swivel around a pivot. They must be designed in such a way that they are not completely unconstrained, to keep them aligned with the velocity vector and to make sure the front wheels do not flutter while the paraplane is in flight.

A decision has to be made on whether or not the wheels should be retractable. Retractable wheels offer better performance on water, and prevent any contact between the water and the wheels, brakes and other landing gear mechanisms, except if one would transfer the vehicle from land to water or vice versa. However the system would become more complex and more time would have to be spent on its design. A non-retractable landing gear on the other side significantly reduces the mass and cost of this subsystem. The drag induced by the non-retractable wheels in flight is small, since they only have a small frontal area compared to the rest of the vehicle and drag is a relatively minor issue when flying as slow as Parashuttle 2. However drag in water, corrosion and wear would be prominent issues. Due to limited cost and mass budgets it is chosen to have a non-retractable landing gear.

The FAA imposes a safety requirement on the floats of seaplanes that affects their structural behaviour. For safety considerations t is required to have four distinct, watertight compartments on the inside of the floats [96]. This way, if a compartment fails, the vehicle should still provide enough buoyancy for it not to sink. This could be done in such a way that the loads on the wheels are directed through the ribs (separating the compartments) to the top of the floats, where they are guided to the struts connected to the fuselage.

Summarising, attention should be paid to the following aspects in the design of the wheel mechanism:

1. The back wheels should each be able to bear 1g (gross weight). The front wheels should each be able to bear 0.5g (half the gross weight).
2. The part of landing gear that comes into contact with water should be anti-corrosive.
3. The drag in water should be able to be overcome by the engine during take-off.
4. The inside of the floats should remain watertight.
5. The front wheels should have some mechanism to keep them aligned with the velocity vector, and to restrain them from fluttering when they are not in contact with land.
6. The back wheels should be equipped with brakes.

14.3.2 Wheel unit

First the type of tires should be determined. The maximum loading of the front wheels is $495\ \text{kg} \cdot 0.5 \cdot 9.81\ \text{m/s}^2 = 2428$ N. The same can be done for each of the rear wheels, giving a load of $495\ \text{kg} \cdot 1 \cdot 9.81\ \text{m/s}^2 = 4856$ N. No safety factor is included in these load calculations, because it is assumed that safety factors are already incorporated in the specified maximum loading of tires, a value provided by the manufacturers. Tires, together with their characteristics, are listed in [74]. Tires are selected based on maximum loading and maximum velocities. Table 14.7 shows information on the selected tires, which are capable of landing on rough surfaces such as grass. The price of these tires could not be found, so an interpolation was done using tires of Goodrich that could be found for various maximum take-off weights.

Table 14.7: Tires used on Parashuttle 2 (from [74]).

	Front	**Back**
Model	Goodrich 10"	Goodrich 12.50"
Outer diameter	0.256 m	0.318 m
Rim diameter	0.0810 m	0.100 m
Loaded radius	0.0991 m	0.1372 m
Maximum load	2900 N	8000 N
Width	0.106 m	0.137 m
Maximum velocity	193 km/h	193 km/h
Mass	1.36 kg	2.27 kg
Price	€131	€179

The rims have to be made of an anti-corrosive and strong material. They will experience high loads during landing, since they are the only load path from the tire to the rest of the structure. Stainless steel provides these characteristics. The rim area is 0.00515 m^2 at the front and 0.00785 m^2 at the back, resulting in an estimated rim mass of ($\rho At = 8000 \cdot 0.00515 \cdot 0.005 =$) 0.206 kg and ($8000 \cdot 0.00785 \cdot 0.005 =$) 0.314 kg at the front and back respectively.

In section 13.4 it was determined that the deflection of the front wheels required to make a turn is at least 35°. It should be checked whether this is possible with the current front wheel diameter and float width at 0.8 m from the tip (the front wheel location). The model in CATIA proofs that it is possible.

It was also discussed that the brakes of the rear wheels (mounted on the axle) should remain within the wheels (in the inner circle). For the front wheels, there are several options to keep them aligned with the velocity vector:

1. There could be a rotational spring on the strut connecting the wheel to the float.
2. There could be a linear spring, attached to the side of the wheel and connected the the float.
3. Use could be made of the friction of materials at the points they make contact, e.g. at the point where the strut goes into the float.

Since it is clever to keep all small and vulnerable parts inside the vehicle (and out of contact with the environment), it is best to use rotational springs located on the struts on the inside of the floats (as indicated in section 13.4).

14.3.3 Shock Absorbers

Having designed the wheels one can now think of whether to use shock absorbers. Shock absorbers are redundant on water, because the deadrise angle (see Figure 14.1 on page 46) 'cuts' through the water. On land shock absorbers could be of use. Using Equation 14.24 [74], the length of the shock absorbers can be determined. The values used in Equation 14.24 stem from Table 14.7, W_L as the MTOW, V as the vertical speed of 2 m/s, $\eta_s = 0.6$ for air springs [74] and a tire efficiency $\eta_t = 0.47$ [74]. For the back wheels the length of the shock absorbers is 0.5 mm for a design landing gear load factor N_g of 3. For the nose gear, which then only carries half the weight, with the same load factor of 3, only 3.8 mm is required. If the struts supply these displacements, then shock absorbers are not necessary.

$$s_t = D_0 - 2 \cdot R_{load} \tag{14.23}$$

$$s_s = \left[\frac{0.5 W_L V^2}{g n_s P_m N_g} - \eta_t s_t\right] \frac{1}{\eta_s} \tag{14.24}$$

14.3.4 Implementation of wheel units into floats

Since the tires are quite large, the wheels will have to be buried in the floats. The wheels will be partially visible from the outside, though they will not actually enter the inside of the float. The bottom skin of the float will follow the shape of the wheels. In Figure 14.6 this design is shown.

The design of the supporting struts can best be made clear by running through the load path of the ground reaction forces. The layout of the wheel system is shown in Figure 14.7. When he tires hit the ground the load created is guided through the rim, which in turn passes the load to the axle (on which for the back wheels the brake is attached). This causes the axle to bends upward. The vertical strut goes through the skin of the float and connects to the floats' struts. The hole through which the strut enters the float is made watertight using well-fitted rubber rings. Inside the floats the strut is attached to one of the ribs used to create different compartments. This is to guide the shear force applied to the floats directly to the upper surface. Inside the floats a rotational spring is attached to the strut.

The rotational spring stiffness has to be such that the wheels do no not show oscillatory behaviour during flight and offer good manoeuvrability on land. There is still too much uncertainty involved to be able to give an estimate of the spring stiffness at this stage.

The dimensions and material of the supporting, vertical struts must be determined. It is chosen to use aluminium with an anti-corrosive coating. Other non-corrosive materials (like fibreglass reinforced epoxy or stainless steel) are either impractical to produce or too heavy. It is assumed there is no bend in the strut, unlike shown in Figure 14.7. The front struts have to carry a maximum load of 2.4 kN (determined when selecting tires), the back struts carry a maximum of 3.2 kN. The

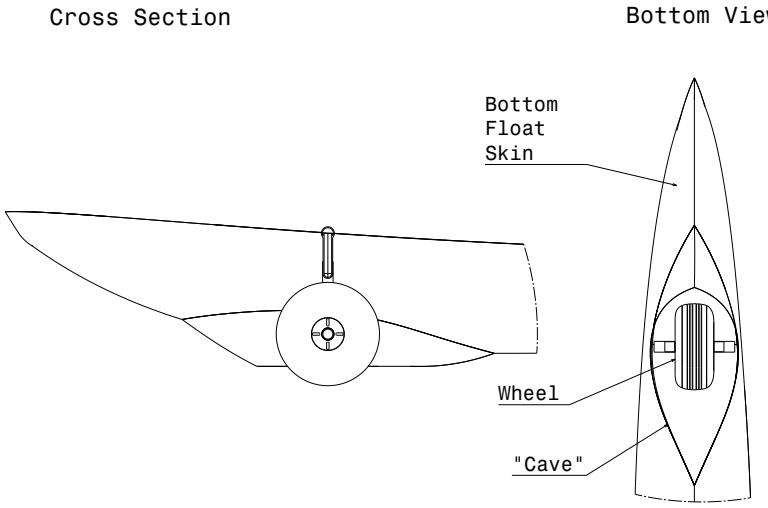

Figure 14.6: Buried wheel design.

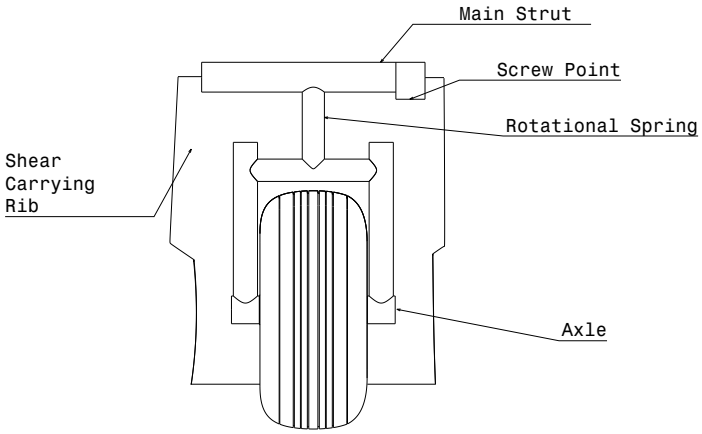

Figure 14.7: Cross-section of the wheel system of a front wheel.

struts will have an annular shape, their length being approximately the height of the float (i.e. the centre of the wheel is at the same level as the bottom of the float). Two requirements apply to the struts. The first one is that they should not yield in compression. Next to that, they should not buckle. Condition 1 is written as in Equation 14.25:

$$\sigma_{y,c} > \frac{P_{max}}{A_{cross}} \tag{14.25}$$

where $A_{cross} = \pi \left(R_o^2 - R_i^2\right)$. The second condition can be written as [97]:

$$P_{max} < \frac{\pi^2 E I}{k^2 L^2} \tag{14.26}$$

where k is the effective length factor. For clamped beams this factor is 0.5. However, to be conservative and to take safety into account, this factor is taken to be 0.65. I is $\frac{\pi}{4}\left(R_o^4 - R_i^4\right)$. The most critical of these conditions will be the standard for design. If an inner radius of 1 cm is assumed, it is clear that the buckling condition is much more limiting. The thickness and outer radius of the front wheel struts are 1.02 cm and 2.02 cm respectively, the thickness and outer

radius of the back wheel struts are 1.15 cm and 2.15 cm. The mass of the four struts together would be $2 \cdot A_{cross_{front}} L_{front} \rho_{Al} + 2 \cdot A_{cross_{rear}} L_{rear} \rho_{Al} = 1.33$ kg + 1.25 kg = 2.58 kg.

The location of the wheels, hence the location of two of the (at least) three ribs will be determined in subsection 14.3.5.

14.3.5 Wheel location

One of the downsides of current shape of the floats (with a sternpost angle) would be that the back wheels have to stick out further in order to ensure enough ground clearance. This will cause additional drag, since more frontal area is in the water. The plus side of the sternpost angle is that it decreases the drag of the whole float quite drastically. It is investigated whether the drag decrease due to the sternpost angle outweighs the drag increase of the additional wheel area in the water in comparison with the wheel area with no sternpost angle. First the difference in drag with and without sternpost angle is computed with the program Hullspeed. The reference speed for this computation is 7 m/s, which is the average cruise speed on water. The drag is 288 N less with a sternpost angle included in the floats. To calculate the increase in wheel area under the floats it is first necessary to determine the back wheel location and the height of both the front and back wheel sticking out beneath the floats. To determine the location of the back wheels under the floats a ground clearance angle χ of 15° is taken into account between the back of the floats and the back wheels. In Table 14.1 the dimensions of each float are stated. These dimensions are used in Figure 14.8, where 7° is the sternpost angle ϕ and 2.283 m is the afterbody length, l_a. In Equation 14.27 b is calculated in order to be able to calculate d with Equation 14.28. Now the location of the back wheel is known, measured from the back of the float. With d known it is possible to compute c with Equation 14.29 and finally the length of the part of the wheel sticking out the float, a, with Equation 14.30.

$$b = \tan(\phi) \cdot l_a \tag{14.27}$$

$$d = \frac{b}{\tan(\chi)} \tag{14.28}$$

$$c = l_a - d \tag{14.29}$$

$$a = c \cdot \sin(\phi) \tag{14.30}$$

In order to determine height of the part of the front wheel sticking out the floats the location

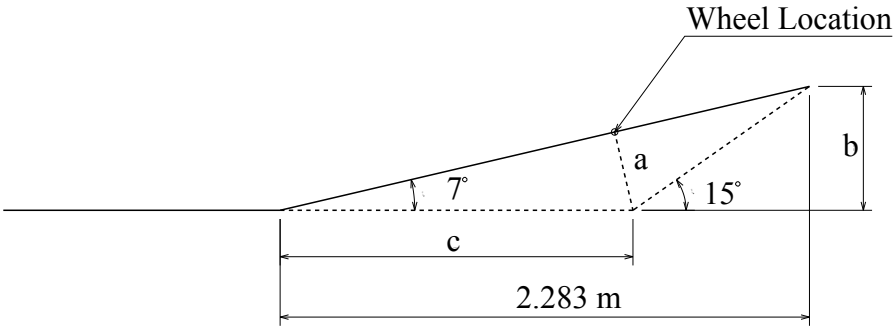

Figure 14.8: Dimensions and angles used to calculate the location of the back wheel.

of the front wheel is assumed to be 0.8 m (g). Also a minimum ground clearance for the floater is assumed to be 0.05 m (h). All dimensions used for this calculations are shown in Figure 14.9. First the angle σ between the front and back wheel needs to be computed using Equation 14.32. With this angle and the wheelbase (calculated with Equation 14.31) the height of the front wheels

sticking out the floats can be computed with Equation 14.33. A small summary of these values is shown in Table 14.9.

Table 14.8: Results for back wheel location calculations.

Back wheel		Front wheel	
Parameter	**Values**	**Parameter**	**Values**
b	0.28 m	Minimum ground clearance	0.05 m
d	1.05 m	Location front wheel	0.8 m
Back wheel location(c)	1.24 m	Wheelbase	2.49 m
a	0.15 m	σ	3.7 °
		f	0.1008 m

$$Wheelbase = c + l_f - g \tag{14.31}$$

$$\sigma = \arctan\left(\frac{h}{c}\right) \tag{14.32}$$

$$f = Wheelbase \cdot \tan(\sigma) \tag{14.33}$$

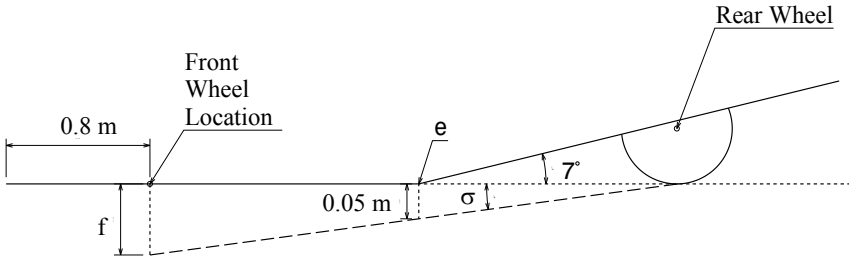

Figure 14.9: Dimensions and angles used to calculate the location of the back wheel.

Table 14.9: Results for front wheel height calculations.

Parameter	**Values**
Minimum ground clearance	0.05 m
Location front wheel	0.8 m
Wheelbase	2.49 m
σ	3.7 °
f	0.1008 m

With the wheel locations and dimensions known the frontal wheel area for both types of floats can be calculated. For the floats without sternpost angle is simply multiplying the minimum ground clearance by the width of the front and back wheels, which can be found in Table 14.7. For the floats with sternpost angle the wheel area under the floats increases, which causes an increase in drag. The wheel areas and drag increase are shown in Table 14.10. The wheel drag is calculated

with an assumed C_d of 0.18 [98]. This increase of drag due to the wheels is smaller than the increase of drag due to the reduced sternpost angle. For this reason it is decided to have a sternpost angle with the wheels sticking out of the floats. In the design a hydrodynamic shape is included around the wheels to further decrease the drag induced by the wheels.

Table 14.10: Wheel areas for the floats with and without a sternpost angle and the caused drag increase.

Parameters	Values
Wheel area without sternpost angle	0.0122 m^2
Wheel area with sternpost angle	0.0313 m^2
Drag increase due to wheels	84.6 N

14.3.6 Maintenance

The maintenance of the wheels could result in a problem because they are not very easy accessible. A solution for this, is to screw a pole in the main strut (as can be seen in Figure 14.7) under which a jack can be placed when the wheels must be replaced. The maximum force that will act on this strut will is half the total weight of the vehicle without the persons (1545 N), because the other half of the weight is acting on the other float. The aluminium closed cylindrical poles used for this will have the following characteristics. The front wheel will have a length of 34 cm (otherwise you are not able to attach it when Parashutle 2 stands on the ground) and requires a minimum radius of 9 mm (with safety factor) to account for the bending and normal forces. However, the maximum diameter that fits next to the wheel is just over 30 mm and because a pole with such a small diameter will easily get lost, the pole will have a outer radius of 15 mm. For the back wheel the same steps are done, these require a pole with a length of 28 cm and a minimum radius of 8.2 mm. But for the same reasons as for the front wheels pole, it will have an outer diameter of 25 mm.

The main struts in the floats are designed to easily carry the loads that are acting on the poles. These struts have an outer radius of 16 mm, a thickness of 5 mm and are able to hold more than two times the stress that the jack will create. The underside of the poles is a small flat plate that can be placed on a regular vehicle jack.

14.4 Water resistance

The water resistance of the undercarriage can be divided into two parts: the resistance due to the floats, presented in subsection 14.4.1, and resistance due to the wheels, detailed on in subsection 14.4.2.

14.4.1 Float resistance

The water resistance of the floats is calculated in Hullspeed for two cases, namely the two-person loading configuration (case 1) and the one-person configuration (case 2). Results are tabulated in Table 14.11. In Hullspeed one can import floats designed in Maxsurf and calculate the drag at different velocities. The different data points are extrapolated to be used in MATLAB for landing and take-off distance calculations. Hullspeed also takes into account the depth, hence the displacement. The depth of the floats should be changed in Maxsurf for the two cases and for different velocities because the lift produced by the kite will elevate the Parashuttle.

Different displacements of the float are made in Maxsurf, making it possible to compute the velocity the parafoil needs to elevate Parashuttle by a certain amount. This is done by calculating

the required lift for that displacement and then the required velocity for that lift. Finally water resistance is calculated in Hullspeed for a certain displacement and velocity.

Table 14.11: The water resistance predicted by Hullspeed for various velocities and related displacements.

Displacement [kg]	**Velocity case 1** [m/s]	**Velocity case 2** [m/s]	**Resistance case 1** [N]	**Resistance case 2** [N]
495	0	-	0	-
488	1.8	-	112	-
440	5.1	-	413	-
410	6.4	0	539	0
397	6.8	2.5	585	197
316	9.3	6.7	794	512
241	11.0	9.0	859	653
187	12.2	10.3	834	667
140	13.0	11.4	763	627
89	13.9	12.4	614	514
43	14.7	13.3	432	359
28	15.0	13.5	348	293
0	15.4	14.0	0	0

14.4.2 Wheel resistance

Next to the drag of the geometry of the floats the wheels (sticking out from the bottom) will create resistance as well. The drag of these is calculated as follows:

$$R_{wheels} = 2 \cdot \frac{1}{2}\rho V^2 A_{frontal,front} C_{d_{wheel}} + 2 \cdot \frac{1}{2}\rho V^2 A_{frontal,rear} C_{d_{wheel}} \tag{14.34}$$

The frontal area is the area of the wheel that can be 'seen' by the flow, i.e. the part that is not buried in the float. The drag coefficient of wheels is found to be 0.18 [98].

This will then be implemented in the model for landing and take-off.

14.5 Sensitivity analysis

The complete detailed design of the floats including the wheels and rudders has been established so far. Now a sensitivity analysis is performed to see whether the resulting design is sensitive to small changes. Having a stable design is of importance, because uncertainties can always cause something to change.

Two analyses will be performed. The first one will consider a change in slenderness ratio (SLR). In subsection 14.2.1 it was explained that assuming an SLR was one of the first steps in designing the floats. Case 1 will examine what would have been the result if a different SLR was assumed. The slenderness ratio will be decreased from 12 to 10 in order to test the sensitivity of the design. The second analysis will examine how an decrease in vehicle mass will affect the design. The mass of the complete vehicle excluding the floats was needed as an input for the float design calculations. This mass could change e.g. in an iteration. For the second case, the estimate of the mass of the vehicle excluding the floats (W_{rest}) will be changed from 420 kg to 390 kg.

Running the MATLAB-file again gives the geometry indicated in Table 14.12. The lower slenderness ratio logically implies a smaller length and a wider beam $\left(SLR = \frac{L}{b_{max}}\right)$. The beam changes by 12.7%.

Table 14.12: Sensitivity analysis of the floats, comparing the current design to designs with a lower slenderness ratio and lower vehicle mass.

Parameter	SLR=12	SLR=10	W_{rest}=390 kg	Difference case 1	Difference case 2
Geometry					
Length L [m]	4.34	4.08	4.24	5.77% ↓	2.08% ↓
Forebody length l_f [m]	2.06	1.94	2.01	5.82% ↓	2.43% ↓
Afterbody length l_a [m]	2.28	2.15	2.23	5.70% ↓	2.19% ↓
Max beam b_{max} [cm]	36.2	40.8	35.3	12.7% ↑	2.49% ↓
Mass [kg]					
W_1	7.21	7.05	6.34	2.23% ↓	12.07% ↓
W_2	15.24	14.92	12.94	2.10% ↓	15.09% ↓
W_3	11.03	10.53	9.66	4.53% ↓	12.42% ↓
Water resistance [N]					
v = 5 kts	77	79	77	2.53% ↑	0% =
v = 10 kts	247	252	246	1.98% ↑	0.40% ↓
v = 15 kts	548	548	539	0% =	1.64% ↓
v = 25 kts	1,167	1,170	1,149	0.25% ↑	1.54% ↓
v = 30 kts	1,559	1,568	1,535	0.57% ↑	1.54% ↓
Water stability					
Longitudinal range [cm]	75	50	75	33.3% ↓	0% =
Lateral range [cm]	70	70	70	0% =	0% =

The mass changes as well. If the thicknesses are optimised at every single point, i.e. the thickness changes continuously throughout the cross-section of the float (W_1 in Table 14.12), the mass for the new SLR is 2.23% lower that the one with $SLR = 12$. If the thickness is the same throughout the cross-section, i.e. there is one thickness for the complete float (W_2), the mass would decrease by 2.10%. When the thicknesses between two ribs are kept constant (W_3), the mass is decreased by 4.53%. See 14.2.3 for more information on the mass determination. One can see from the table that the mass decrease of the vehicle without floats has a relatively large impact on the mass of the floats (up to 15%) lighter.

Water resistance is also affected by altering the slenderness ratio or vehicle mass. The values are depicted in Table 14.12. For a lower slenderness ratio, the water resistance increases slightly due to the larger frontal area (the beam is larger). For a lower mass resistance decreases because of the smaller geometry.

The stability on water is determined for both cases. One can see that the lateral range of stability does not change with a change in SLR or vehicle mass. The Parashuttle will be stable if the centre of gravity (or the effective centre of gravity due to applied forces) is less than or equal to 35 cm from the middle. The longitudinal stability on the contrary does change if the slenderness ratio changes. It becomes smaller for lower SLR's, which is logical because of the decrease in length of the floats. A vehicle mass decrease does not change the stability in any way, since the floats get smaller but the centre of gravity location changes accordingly.

This sensitivity analysis has shown that the designed floats are well designed because:

- Decreasing the slenderness ratio would cause the Parashuttle to be less stable, although all other properties seem to improve. Since stability is a very important issue, decreasing the SLR is not an option. A higher SLR would make the floats too long to transport them on

a trailer.
- Vehicle mass cannot be decreased on command, so designing for less loads is not an option. If the vehicle mass happens to be smaller, this will be very beneficial for the floats.

14.6 Mass & material cost

The total material required for construction of the floats is estimated to be 12.8 kg of aluminium. This estimate is made by multiplying the float's skin area by the thickness of the skin and adding the mass of the ribs. There will always be scrap material during building of these floats. This scrap material is estimated to be 20% of total material, this brings the estimated material to 15.3 kg. The price of this material is estimated using CES EduPack 2012. Using a price of €22.40 per kilogram this result in a price per float of €35.80.

The total rim material mass was estimated to be 1.04 kg in section 14.3. The material cost of stainless steel is €3.88/kg (from CES EduPack, a program available on blackboard). Therefore the rims will have a material cost of €4. The rims will be around €200 a piece for the front wheels and €240 at the back. The front wheels, i.e. tire and rims, at the front will cost €331 a piece, and at the back they will cost €379. The front wheels will have a mass of approximately 1.6 kg, and the back wheels have an estimated mass of 2.6 kg.

In section 14.3 also the mass of the connection between wheels and floats is calculated to be 2.58 kg. With 2.45 €/kg, the material cost would be €6.32.

The rudder was designed in CATIA, its volume is estimated to be 11.74 cm^3. Most rudders are made of plywoods because this is a good material to produce rudders [99]. The density of this material, according to CES EduPack, is 800 kg/m^3, meaning the rudder will weigh approximately 0.94 kg. The material cost of plywood is 0.734 €/kg, so the material cost of a rudder would be €0.69, which is negligible compared to other costs.

The total mass of the two floats together will be 38.4 kg without rivets and production imperfections. Consulting Ir. Elham, who is experienced in the field of mass estimation, lead to the advice to add an extra 10% to the load carrying mass to account for riveting and welding. The load carrying mass is the total mass mentioned above except the rudder. This brings the total mass of the floats to 42 kg.

Table 14.13: Mass and cost breakdown of the complete undercarriage.

Part	**Mass**		**Cost**	
	Estimate [kg]	*Uncertainty [kg]*	*Estimate [€]*	*Uncertainty [€]*
Skin & ribs	25.6	± 0.6	71.66	± 3
Tires	7.26	Certain	620	± 30
Rims	1.0	± 0.5	880	± 50
Supporting struts	2.6	± 0.5	6.32	± 0.50
Rudder	1.9	± 0.2	Negligible	Negligible
Subtotal	38.4	± 1.8	1,577	± 95
Rivets & imperfections	10%	± 1%	Negligible	Negligible
Total	**42.0**	± 5.6	**1,577**	± 95

14.7 Technical drawing

Figure 14.10 presents a technical drawing of the floats. The two floats are separated by 2.3 m.

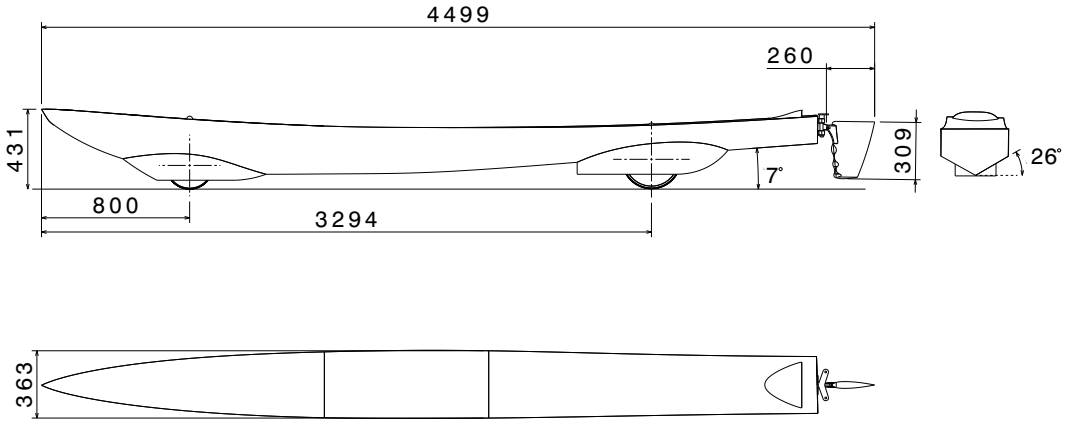

Figure 14.10: Technical drawing a float of Parashuttle 2

Chapter 15 | Parafoil connection system

The lift provided by Parashuttle's parafoil should be transferred to the fuselage through the kite connection system. Since this subsystem is independent of the parafoil used, this subsystem is designed before a parafoil is chosen. Requirements on the parafoil connection system are discussed in section 15.1, detailed design is performed in section 15.2.

15.1 Subsystem requirements

The main requirement on the parafoil connection system is its ability to transfer the lift force produced by the parafoil to the fuselage. Assuming that one line would transfer at most 70% of the maximum 2g lift force and applying a safety factor of 1.5 leads to the requirement that one side of the parafoil connection system should be able to handle a force of 10.2 kN.

Besides the parafoil connection system should allow for flight at a comfortable pitch angle for a range of centre of gravity locations. Through preliminary calculations the range of centre of gravity locations (including some margin) has been found to be between 2.2 and 2.5 m from the nose of the vehicle, meaning the kite connection system has to be able to deal with such a range.

15.2 Detailed design

To meet the second requirement a total of four U-bolts (type 6523) will be placed on the two top trusses of the fuselage on either side [100]. One pair of U-bolts will be placed right over the centre of gravity, one pair 10 cm in front of the centre of gravity and two pairs 10 and 20 cm behind the centre of gravity respectively. The kite should then be connected to either one of these bolts, depending on the centre of gravity location (which depends on the loading of the vehicle). Naturally the pilot should connect the pilot to the bolt located closest to the centre of gravity. Instructions on this procedure should be provided in Parashuttle's manual.

A Petzl AM'D carbine hook can connect the bolts on either side to the parafoil lines [101, 102]. Such a carabiner has a breaking load of 28 kN, the bolts have a working load of 12.5 kN and a breaking load of 29 kN. This means the parafoil connection system is overdesigned, however since failure of the system would be critical such overdesign is considered appropriate. The total mass of the components mentioned is 700g. Conservatively estimating the costs of the U-bolts to be €10 a piece, total costs are €100.

Chapter 16 | Cockpit

The pilot and passenger will spend their time operating the vehicle in the cockpit. Since the cockpit is influenced by many other subsystems and is not the most critical subsystem, this subsystem is designed as one of the last systems. For the design first the subsystem requirements are stated in section 16.1. The actual design is done in section 16.2 for the instruments, section 16.3 for the seats and section 16.4 for miscellaneous parts. In section 16.5 a summary of the cockpit design is shown.

16.1 Subsystem requirements

The cockpit should adhere to the following requirements:

1. The pilot shall be able to use all controls (including thrust) from within the cockpit as well as be able to start and shut down the engine.
2. The cockpit shall provide comfortable and safe seating for two persons.
3. The pilot shall be able to monitor airspeed, altitude, fuel remaining and engine RPM.
4. The cockpit shall provide a clearly recognisable audiovisual stall warning signal.
5. The cockpit shall provide the ability to communicate with ground authorities and air vehicles.

The cockpit was allocated a mass budget of 20 kg and a cost budget of €3,800.

16.2 Instruments

The cockpit houses all controls and tools the pilot uses during flight. These days there are many instruments that can help the pilot in many different ways. For example there are instruments for safety, communication, navigation, engine monitoring and so on. For Parashuttle 2 there are some mandatory instruments, which are derived from requirements [8].

Obligated instruments are an airspeed indicator, an altimeter, a fuel quantity indicator and pressure, temperature and RPM indicators for the engine. Another requirement is that Parashuttle 2 should be be able to communicate with the outside world, consisting of other aircraft and ground authorities. Hence Parashuttle 2 should also have a communication system.

Due to large differences in quality and price of instruments, the cockpit of Parashuttle 2 will be delivered in two versions. The standard version will house only obligated instruments, the more expensive deluxe version will include extra devices to provide the pilot with extra comfort. Appendix C shows the functions provided by the standard and deluxe version, estimating mass and cost at the bottom. The customer will choose between either of the two versions.

The Civil Aviation Authority [103] requires that the radio frequency recreational aviation uses ranges from 117.975 MHz to 137.000 MHz. Therefore a radio that is on that frequency must be integrated in the cockpit. The two versions house two different radios. The standard model houses a heavier but cheaper radio than the deluxe model, with both radios satisfying requirements.

In Appendix C the instruments are further described and it is listed what instruments are used in which version of the cockpit.

16.3 Seating

Parashuttle's two passengers will be seated in-line. Due to the relatively low mass budget of 10 kg for the seats [8], seat selection is based mainly on this. Since the seats are the main feature in ensuring a comfortable cockpit the seats also need to be comfortable. The seats of choice are

Black Max Comfortlite seats, truss-structured seats with a seating fabric made of nylon [104]. These seats can also be folded down to help getting in and out of the cockpit. Both seats will be fixed on the fuselage floor. The seats' properties are shown in Table 16.1.

Table 16.1: Properties of the Black Max Comfortlite seat.

Property	Value	Property	Value
Length	0.49 m	Price	€144
Width	0.46 m	Fabric material	Cordura Nylon
Height	0.66 m	Tubing material	6061T6 Aluminium
Mass	2.7 kg		

In order to ensure safe seating, both seats will be fitted with 4-point seatbelts, which are required by regulations [105]. However a 4-point seatbelt cannot be mounted with the aforementioned seats without an extra mounting point behind the seats to attach the shoulder belts to. This means that an extra structure must be made for the pilot seat, the passenger's seatbelt can be mounted to the engine compartment structure.

According to regulations the seatbelts should be able to sustain a 9 g forward inertia load factor, thus the mounting point should be able to sustain that as well. Assuming that 60% of a person's mass (min. 86 kg [105]) is carried by the shoulder straps in case of a crash, the maximum pulling force on the mounting point is 4.5 kN. The seat belt connection point will be discussed in chapter 18. The seat belts chosen will be Schroth 4-point push-button restraints. These restraints are certified for use in aircraft and weigh about 750 g. The cost of the restraints are not specified by the manufacturer, however they are estimated at €200 per restraint. In total the mass of the seats and restraints will then be 6.9 kg, with costs at €688.

16.4 Miscellaneous

With the instruments, seating and control having been discussed above, there are still features left to be integrated into the cockpit, such as heating (subsection 16.4.1), ventilation (subsection 16.4.2), upholstering (subsection 16.4.3) and the electrical system (subsection 16.4.4).

16.4.1 Heating

The heating in Parashuttle 2 will be done by using engine heat and re-routing it into the cockpit. Engine heat in the form of heated cooling fluid will be routed through a winding tube with radiator-like fins to increase surface area, a set-up similar to a car heater. The heated device will in turn heat the air surrounding it, which can be routed to the cockpit. The system's mass is estimated to be 10 kg, while costing €200.

16.4.2 Ventilation

For cockpit ventilation Parashuttle 2 will use small sliding windows in order to let outside air flow into the cockpit. A sliding window will be installed at both the pilot and passenger seat. The sliding windows will be part of the large cockpit windows and are thus incorporated in the fuselage.

16.4.3 Upholstering

The upholstering of the cockpit entails not only the upholstering itself, but also the engine compartment wall and insulation. For the engine compartment wall fire resistance is especially important. Therefore an aircraft certified soundproofing sheet will be applied between the engine and cockpit, together with a layer of plastic in order to have a nicer look in the cockpit. The soundproofing sheet will have a thickness of 1 cm as that is the most cost and mass effective. In total this will weigh

1.1 kg while costing (with the price from a reseller instead of a wholesaler) €28.6. The plastic layer attached to this will be made of polypropylene, a plastic commonly used in car dashboards. Using this material the plastic finish over the sound/firewall (being 1 mm thick) will weigh about 1.5 kg and will cost €2.2 (in pure material cost).

With the engine compartment separated from the cockpit only the fuselage upholstering needs to be done. On the floor a grip material will be used to ensure that the occupants can enter safely with wet feet. This anti-slip material is decided on in later stages of the project. For now the estimate of a mass of 5 kg and a cost of €80 will be used.

To ensure that water does not reach critical fuselage components such as the electrical system a sealant is applied in between the connections of different panels. Since it is unknown at this stage how much sealant will be needed, an estimate of 0.5 kg and €20 is decided on.

16.4.4 Electrical system

The lighting, the electric starter and all instruments described in section 16.2, require power in order to operate. This power will come from a battery [46, 106], the power for this battery will be drained from the engine. To drain power a regulator-rectifier is mounted near the engine [46]. This unit converts alternative current produced by the engine's generator into 12 Volt direct current, which is the input voltage required for all instruments. The cost for the battery and the regulator-rectifier are €92 and €88 respectively.

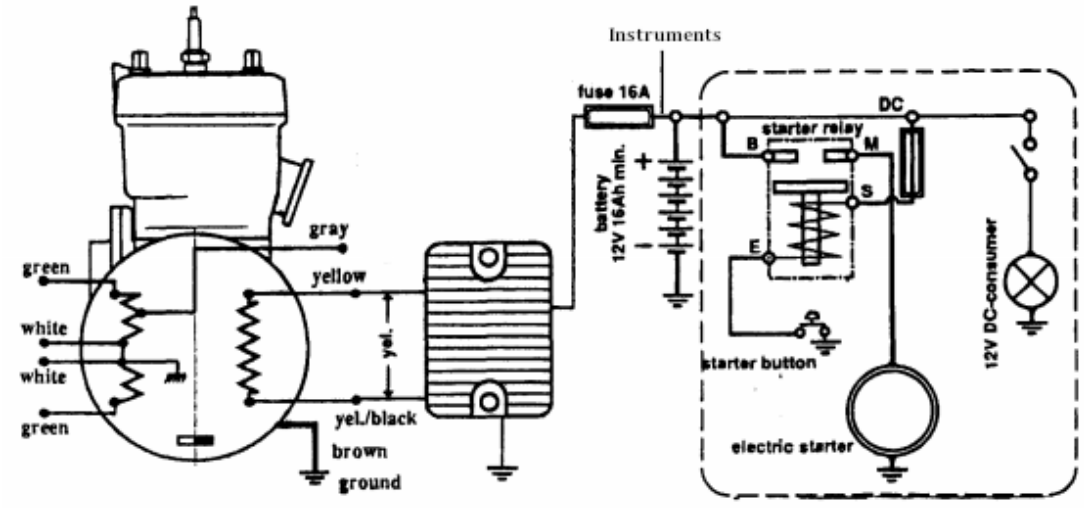

Figure 16.1: Wiring diagram for Parashuttle 2 [107].

In Figure 16.1 the wiring diagram for Parashuttle 2 can be seen. The engine is depicted on the left, the block to the right of the engine is the regulator-rectifier, which drains power from the engine and powers the 12V, 16Ah battery. The electric engine starter is illustrated in the right of the figure. The connection that leads power to the instruments is located between the battery and the regulator-rectifier.

In Figure 16.2 a block diagram of the electrical system is shown. It can be seen that all systems are connected parallel to each other, all having their own fuse. This way if there is a short circuit somewhere only that fuse has to be replaced, all other instruments will continue working. All fuses are located in a fusebox in the cockpit, which makes them easily accessible.

The current required to power all systems is relatively low. As stated in section 16.2 the instruments require 2 ampere at most and the lights (if embedded into the vehicle) inside and outside require additional current, in the order of 8 ampere [108, 109]. When charging a tablet, navigation system

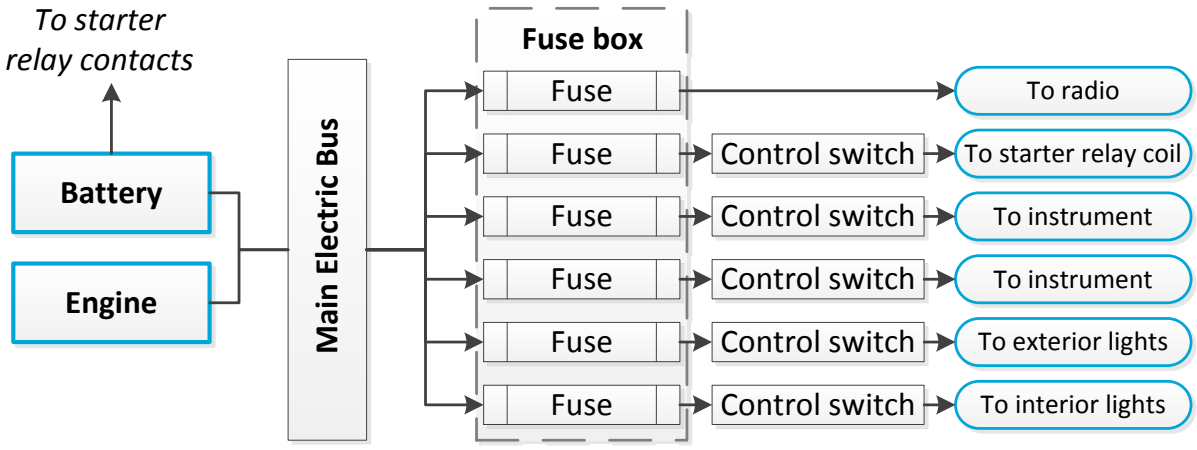

Figure 16.2: Basic block diagram of the electrical system of Parashuttle 2.

or something similar to the 12V charger from the cockpit another 3 ampere will be drained [110]. Parashuttle 2 is equipped with a 16 Ah battery, so powering all systems should not be a problem. The amount of power needed from the engine is the sum of the above, but also there is some power required to charge the battery. The chosen battery can achieve a 95% state of recharge in less than one hour [106], hence the current needed for this is in the order of 15 ampere. Using Equation 16.1 the amount of power to be drained from the engine can be derived.

$$P = V \cdot I \tag{16.1}$$

Using $V = 12V$ and $I = 28A$ (current required to charge the empty battery and power all instruments and lights) leads to an amount of power of 336W. This will be the maximum amount of power that is drained from the engine.

16.5 Summary

In Table 16.2 a final overview of the cost and mass of the cockpit parts can be seen.

Table 16.2: Cockpit cost and weight

Part	Cost	Mass
Instruments	€1,000	1.3 kg
Interior	€1,158	25 kg
Battery	€180	6.1 kg
Total:	€2,338	32.4 kg

Chapter 17 | Parafoil

The parafoil of Parashuttle 2 will provide it with the lift required to sustain flight. With little experience in parafoil design, the team has chosen to search for an available parafoil. An off-the-shelf parafoil will not only probably be less expensive than a custom made one, it also increases the desired plug-and-play abilities of Parashuttle 2. This chapter will discuss the requirements imposed on the parafoil in section 17.1 and will present a suitable parafoil in section 17.2. Parafoil properties (required for the models discussed in part II of this report) are dealt with in section 17.3.

17.1 Requirements

Of all requirements listed in appendix B only a limited number is applicable to the kite. Summarising one will find that the kite has to satisfy the requirements listed below. A kite fulfilling these requirements will be looked for in section 17.2.

1. The parafoil shall be able to lift a 495 kg structure at a cruise velocity of 45 km/h.
2. The parafoil shall be able to be stored within the cockpit.
3. The parafoil shall have a stall speed not exceeding 65 km/h.
4. The parafoil shall have a wing loading lower than 25 kg/m^2.
5. The parafoil shall be able to float and take off from (salt) water.
6. The parafoil shall allow for lateral control of Parashuttle 2.

During a preliminary mass and cost estimate a mass budget of 15 kg and a cost budget of €5,000 was allocated to the parafoil, these put additional requirements on the choice of parafoil.

17.2 Parafoil choice

Finding a kite capable of both floating on water and lifting roughly 500 kg proves a difficult challenge. Parafoils used by current paraplanes are self-inflating, only getting into shape when first dragged behind the vehicle. Such a procedure can not be followed in case Parashuttle 2 takes off from water, meaning a pre-inflated parafoil is to be used.

Taking inspiration from a visit to the maker of the original Parashuttle and the kite surfing community (where pre-inflated kites are launched from water before surfing) it was decided to use a Peter Lynn inflatable kite. His 50 m^2 Synergy kite [112] is big enough to lift Parashuttle 2, having a wing loading of just 10 kg/m^2 and (using basic lift theory) requiring a lift coefficient of about 0.6 in cruise. For now this parafoil will be chosen. Since little information is available on this experimental kite it has been decided to use reference data of a different parafoil to evaluate Parashuttle's flight performance. This data is shown Table 17.1.

Table 17.1: Specifications on a reference Parafoil, comparable to Peter Lynn's Synergy kite [111].

Parameter	Value
Wing area [m^2]	55.7
Chord length [m]	4.5
Actual span [m]	12.4
Aspect ratio [-]	2.7
Max. thickness [m]	0.675
Length of lines [m]	10
Effective span [m]	11.6
Arch height [m]	1.85

17.3 Parafoil properties

The flight performance model discussed in chapter 7 requires information on the aerodynamic characteristics and apparent mass and mass moment of inertia andof the parafoil. These are evaluated in the following. For light aerial vehicles the apparent mass, given by Equations 17.1 and 17.2, can have non-neglegible effects on flight performance [113]. In the analyses done in this

report apparent mass is only considered in longitudinal motion. Apparent mass models the effect of the mass of the air trapped in the parafoil on the motion of Parashuttle 2. Horizontal and vertical motion are distinguished when calculating it. Lissaman [113] derived the following equations for the apparent mass when moving in x- (horizontal) and z-direction (vertical) respectively:

$$m_{app_x} = 0.666(1+\frac{8}{3}a^2)bt^2\rho = 0.666\cdot(1+\frac{8}{3}\cdot\left(\frac{1.85}{11.6}\right)^2)\cdot 11.6\cdot 0.68^2\cdot 1.225 = 4.7kg \quad (17.1)$$

$$\begin{aligned} m_{app_z} &= 0.785\sqrt{1+2a^2(1-(t/c)^2)}\frac{AR}{1+AR}bc^2\rho \\ &= 0.785\cdot\sqrt{1+2\cdot(1.85/11.6)^2\cdot(1-0.15^2)}\frac{2.7}{3.7}\cdot 11.6\cdot 4.5^2\cdot 1.225 = 168.9kg \end{aligned} \quad (17.2)$$

Here, a is the arch of the parafoil divided by its span, b is the span, t is the thickness of the parafoil and ρ is the air density. The apparent masses are used in the force equations of motion, as implemented in the longitudinal control model described in chapter 7.

Besides the apparent masses, there is also an apparent mass moment of inertia. Since (again) it is only considered for longitudinal motion, only the mass moment of inertia for pitch motion is considered. Lissaman derived an equation for this, which is defined as:

$$I_{app} = \frac{\pi}{6}AR^2(t/c)^2c^3S = \frac{\pi}{6}\cdot 2.7^2\cdot 0.15^2\cdot 4.5^3\cdot 55.7 = 435.9kg\cdot m^2 \quad (17.3)$$

In this c is the chord length and AR is the aspect ratio of the parafoil. At this stage the parafoil aerodynamic characteristics still need to be defined. Research suggests that the angle of attack of a parafoil remains roughly constant during flight [114], meaning it is safe to assume that the lift coefficient of a parafoil is mostly constant (even if the angle of attack varies slightly) [115]. A reasonable lift coefficient of 0.6 is thus estimated [115, 116].

The drag coefficient of a parafoil is given by Equation 17.4 [32]. For an aspect ratio A of 2.7 the value of δ is known to be 0.017 [32]. The profile drag C_{D_0} consists of basic airfoil drag (0.015), surface irregularities (0.004), drag due to the open airfoil nose (usually 0.05 [117]) and line drag [32]. For the latter an estimated 200 lines of 1mm diameter and 10m length are assumed, resulting in a drag coefficient of 0.04. The parafoil's drag coefficient is thus given by:

$$\begin{aligned} C_D &= C_{D_0} + (1+\delta)\frac{C_L^2}{\pi A} \\ &= (0.015+0.004+0.05+0.04) + (1+0.017)\frac{C_L^2}{\pi\cdot 2.7} = 0.109+0.120C_L^2 \end{aligned} \quad (17.4)$$

This drag polar is plotted in Figure 17.1. For a lift coefficient of 0.6 (indicated by the dot in this figure) one observes that the lift to drag ratio of the parafoil is 4.0. This is slightly above but certainly not out of the range of common values, which are between 3.0 and 6.0 [115, 116, 118, 119]. This range has been indicated as well in Figure 17.1. One observes that the design point chosen is well within common ranges.

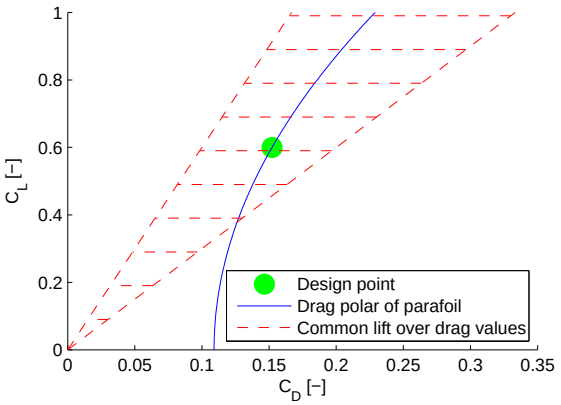

Figure 17.1: Comparison of the chosen design point to common lift over drag ratios.

Chapter 18 | Fuselage

The fuselage is the last major part of Parashuttle 2 to be designed, kept for last as the fuselage should house/integrate all other subsystems. With the detailed design of those now finished, the fuselage can be designed. The design methods will be discussed first in section 18.2. Thereafter, the design of the frame structure will be discussed in section 18.3. The polycarbonate windows will be discussed next in section 18.5, and the doors will be discussed afterwards in section 18.6. A first estimate of the fuselage drag will be given in section 18.7 and this chapter will conclude with a short summary in section 18.8.

18.1 Requirements

With the fuselage housing or supporting all other subsystems of Parashuttle 2, it is to be expected that the majority of requirements presented in appendix B influences fuselage design. In short, the fuselage has to fulfil the following requirements:

1. The fuselage shall be able to operate on both land and fresh and salt water.
2. The fuselage shall be able to transfer a 3g load originating from the undercarriage through the vehicle, as well as a 2g load originating from the kite.
3. The fuselage shall allow the crew to escape the vehicle safely without serious injury in case of an emergency.
4. The fuselage shall have low aerodynamic drag to improve performance and decrease emissions.
5. The fuselage shall provide access to the vehicle.

Additionally the fuselage shall mass less than 117 kg and cost less than €8,800 in order to confirm with the mass and cost budgets specified in earlier work [9].

18.2 Structural design methods

The fuselage will consist of two main parts, the load carrying frame structure and the fuselage skin. The skin's purpose is to provide passengers with comfort and additionally make the vehicle more aerodynamic, for enhanced looks and performance. The frame structure of the fuselage should carry all loads experienced in the load cases discussed in subsection 18.2.1.

18.2.1 Load cases

During regular and more extreme operations the fuselage structure has to carry all loads. The following load cases (deemed critical) were examined for the vehicle:

1. A turn with a load factor of 2 (times 1.5 due to ASTM regulations[120]) at full thrust with a fully loaded vehicle.
2. A load factor of -1 in flight at full thrust with a fully loaded vehicle.
3. A landing impact of 3 g, where the forces will act on the struts connecting to the floats.
4. Seatbelt forces of up to 9g forward, 3g upward and 1.5g sideways in a crash.

Flight loads

The extreme load factors in flight are -1 as a minimum and 2 as a maximum. Both can be experienced with the engine producing full thrust. The load case is depicted in Figure 18.1a. The mass mass of the fuselage itself is distributed along all members, where the thickness and radius of the members determine the distribution. The vertical loads in Figure 18.1a will be multiplied with the load factor n to get the actual loads.

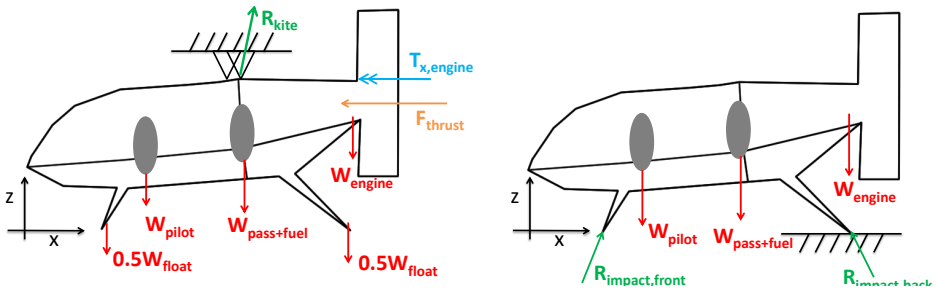

(a) Load case in flight. *(b) Load case in impact.*

Figure 18.1: Free body diagrams of load cases expected during operations.

Impact loads

The forces acting on the vehicle during landing impact are shown in Figure 18.1b. Here it is assumed that during touchdown thrust is set to zero. The reaction forces of the struts during a landing procedure were determined during the design of the undercarriage in chapter 14. For impact analysis the mass of the vehicle components are multiplied by the load factor of the impact, which was determined to be 3.0. These load cases would be used for the dimensioning of the struts connecting the floats to the fuselage.

Crash load case

This load case was added for the sizing of the rods around the attachments of the seatbelts. To analyse the fuselage structure's behaviour under the loads imposed to it by the seatbelts in case of impact the connection struts would be loaded in with their respective loads. The vehicle itself would still be under normal loads.

18.2.2 FEM representation and structural optimisation

For structural design the frame structure will be represented as a frame model in MATLAB. Analysis will be done by the FEM model described in chapter 8. A representation of this frame can be seen in Figure 18.2. The FEM program uses the properties of each individual beam to determine displacements and loads. The extensions mentioned in subsection 8.1.3 can be used to determine the internal moments and maximum stresses. It is possible to put the model under detailed three-dimensional loading.

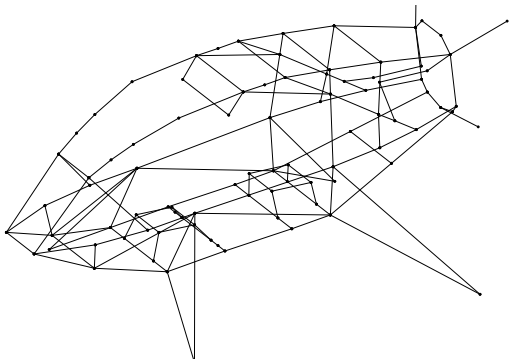

Figure 18.2: FEM representation of the fuselage.

Structural optimisation was done in MATLAB by determining which beams of the frame failed too early and which beams were overdesigned. A beam failing means that its Von Mises stress (given in Equation 18.1) times a safety factor of 1.5 was higher than the yield stress of the material used. A second failure mode is failure in buckling. This happens when a longitudinal force is applied that is higher than the critical force, given by Equation 18.2. A safety factor of 1.5 is applied to the buckling failure mode as well. The failure modes are depicted in Equations 18.3 and 18.4.

$$\sigma_{vm} = \sqrt{\sigma_x^2 + 3\tau^2} \tag{18.1}$$

$$P_{cr} = \frac{\pi^2 EI}{(kL)^2} \tag{18.2}$$

$$\sigma_y < 1.5\sigma_{vm} \tag{18.3}$$

$$P_{crit} < 1.5\sigma_x A_x \tag{18.4}$$

An overdesigned beam is a beam that carries too few loads. If a beam fails too early the program increases the inner and/or outer radius of a beam element, vice verse if a beam is overdesigned. Predefining a minimum thickness, minimum outer radius and a predefined number of iterations, the program should approach an ideal thickness distribution for each member. For manufacturability reasons, each element can only have a single value for its inner and outer radius.

Assumptions

The following assumptions have been made for this model:

1. The weight of skin panels is uniformly distributed along all members.
2. Curved beams can be represented as multiple consecutive straight beams.
3. Stress concentrations do not occur at connection points.
4. Connection points of beams are clamps. k in Equation 18.2 has a theoretical value of 0.5, however a conservative value of 0.65 has been chosen (see chapter 14).
5. The loads of the engine are equally divided over all four engine connection mounts.

18.2.3 Skin panel design and plate theory

To determine stresses in plates under out of plane loading (such as the floor skin) plate theory should be used since the skin is supported on all sides. Solutions for plate deflections under a point load are given in Equations 18.5, 18.9 and 18.10 [121–123], with the dimensions described in Figure 18.3a. However this theory only gives correct results when small deflections occur, implying $w < t$. Therefore it has been decided to compare the stress results with a thin beam, supported on both ends, as depicted in Figure 18.3b.

$$w(x,y) = \sum_m^\infty \sum_n^\infty w_{mn} \sin\left(\frac{m\pi x}{a}\right) \sin\left(\frac{n\pi y}{b}\right) \tag{18.5}$$

$$w_{mn} = \frac{1}{\pi^4 D} \frac{p_{mn}}{\left(\left(\frac{m}{a}\right)^2 + \left(\frac{n}{b}\right)^2\right)^2} \tag{18.6}$$

$$p_{mn} = \frac{4P}{ab} \sin\left(\frac{m\pi\epsilon}{a}\right) \sin\left(\frac{n\pi\eta}{b}\right) \tag{18.7}$$

$$D = \frac{Et^3}{12(1-\nu^2)} \tag{18.8}$$

$$M_x = -D\left(\frac{\delta^2 w}{\delta x^2} + \nu\frac{\delta^2 w}{\delta y^2}\right) \tag{18.9}$$

$$M_y = -D\left(\nu\frac{\delta^2 w}{\delta x^2} + \frac{\delta^2 w}{\delta y^2}\right) \tag{18.10}$$

Comparison is done using a place with a thickness of 2 mm and length and width of 0.5 m, on which a load of 10 N is applied at the centre. The Von Mises stress given by plate theory is 5.84 MPa, while the stress given by the beam is 7.5 MPa. The total deflection predicted by the plate theory method is 0.48 mm , compared to 1.1 mm for the beam method (Equation 18.11).

$$\delta_{max} = \frac{PL^3}{48EI} \tag{18.11}$$

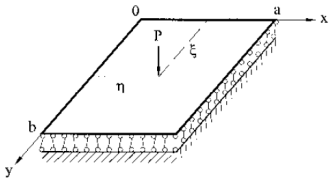

(a) Simply supported rectangular plate [123].

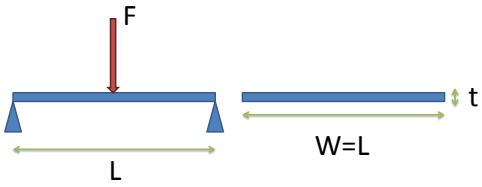

(b) Load case for comparison with plate theory.

Figure 18.3: Plate theory and a simplified load case

The real load case for such a plate would be a distributed force and not a point force. This leads to a slight reduction in loads as well.

18.2.4 Shallow shell theory

The polycarbonate windows used in the doors can be designed as thin shells. Shell theory [122, 124] is used to determine the stresses and displacements in the windows. A variant of classical shell theory is the shallow shell theory [123, 124]. Shells are stronger in carrying transverse loads than thin plates, with fewer displacements. The solution can be found by using equations 18.12, 18.13 and 18.14, in equation 18.5 and the moment equations in 18.2.3, where $f = f_1 + f_2$.

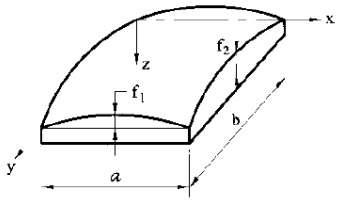

Figure 18.4: Supported shell [123].

$$w_{mn} = \left[\frac{\pi^4 n^4 t^4}{12(1-\nu^2)} A_{mn} + \frac{64 f^2 t^2}{A_{mn} a^4} \left(\frac{f_1}{f} + \frac{m^2 f_2}{n^2 f} \right)^2 \right]^{-1} \frac{p_{mn} t}{E} \tag{18.12}$$

$$p_{mn} = \frac{16 p_0}{\pi^2 mn} \tag{18.13}$$

$$A_{mn} = \left(\frac{m^2 b^2}{n^2 a^2} + 1 \right)^2 ; m, n = 1, 3, 5, \ldots \tag{18.14}$$

18.3 Design of the frame structure

The main load baring structure is a frame structure. The layout of the trusses has been chosen around the main load paths of the fuselage. All loads on the vehicle are transferred through this frame structure, and the structure provides adequate attachment points. The structure was optimised with respect to mass. Material selection will be discussed first, afterwards the design will be shown.

18.3.1 Material selection

The selection criteria for the trusses' material are:

1. Performance under all types of loading: tension, compression, shear and torque.
2. Cost and difficulty of joining two trusses under an angle.
3. Cost to produce the cylindrical rods.
4. Their performance with respect to mass and cost.

Fibre reinforced polymers were discarded because of the difficulty to join two of such beams at an angle. It is not possible to drill or weld FRP parts and joining results in relatively weak bonds. Steel was discarded because of its high density. Aluminium seems the most practical for the load carrying structure due to its widespread application in aircraft, relatively low masss and low cost.

Different aluminium and titanium alloys were used in the design program discussed in subsection 18.2.2. Finally, aluminium alloy Alu 8090 T851 was chosen for the frame structure and Alu 6061 T6 for the skins. The reasoning was that aluminium alloy 8090 was stronger and lighter than other alloys, albeit more expensive. Furthermore, the aluminium alloy used for the skin panels is typically used in yacht design and is thus resistant to salt water, as explained in subsection 14.2.2. Properties for the alloy used are depicted in Table 18.1.

Table 18.1: Properties of materials used in the fuselage design, found in CES Edupack.

Material	Density	Price	Yield strength	Modulus of elasticity
Aluminium 8090 T851	2570 kg/m^3	11.4 €/kg	440 MPa	82.0 GPa
Polycarbonate	1200 kg/m^3	4 €/kg	62.1 MPa	2.38 GPa
SPS (10% carbon fiber)	1090 kg/m^3	8 €/kg	78.0 MPa	7.40 GPa

18.3.2 Chairs and fuel tank attachments

Two chairs should transfer the passengers' loads to the rest of the fuselage structure. Below the passenger chair the fuel tank is located. These loads will be transferred to the fuselage using the construction depicted in Figure 18.5.

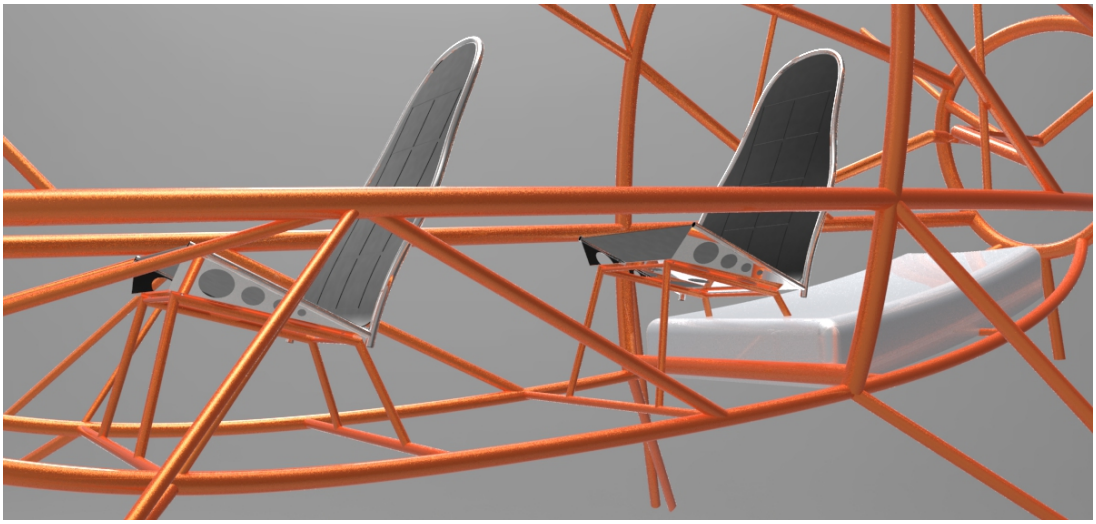

Figure 18.5: Design of chair truss structure and the fuel tank positioning.

18.3.3 Engine connections

The Rotax 582 engine has four attachment points, as depicted in Figure 18.6. There are three main loads introduced by the engine: thrust, weight and torque. The torque introduces shear on each of the attachment points, equal to the torque divided by half the width of the attachment points. The attachment plates themselves are along the thrust axis of the engine to carry the thrust loads, these loads are transferred vertically to the rest of the fuselage. Figure 18.9 shows the design of the engine attachment points.

18.3.4 Resulting design

The beams in this frame structure have circular cross-sections and differ in their inner and outer radii. Figure 18.7 displays the layout of the frame structure. The optimisation strategy described

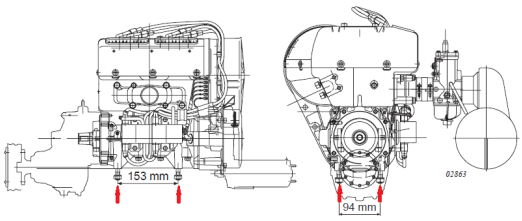

Figure 18.6: Mounting points of a Rotax 582 engine[107]. The schematic is of a Rotax 503, the attachment points are the same as a Rotax 582.

in subsection 18.2.2 resulted in an optimal thickness distribution along all the discretised elements. However the longer (curved) beams along the top, bottom and middle of the structure are easier to manufacture when being of constant thickness. Therefore, its has been decided to make these beams of constant dimensions, instead of applying the optimal thickness distribution. The mass of the frame structure will be 34 kg, and the cost is €390. Ten percent was added to accommodate for extra mass added during assembly, as is explained in section 14.6.

Comparison with CATIA

Using the dimensions found in the design of the fuselage in the CATIA design only resulted in a 1% difference in weight.

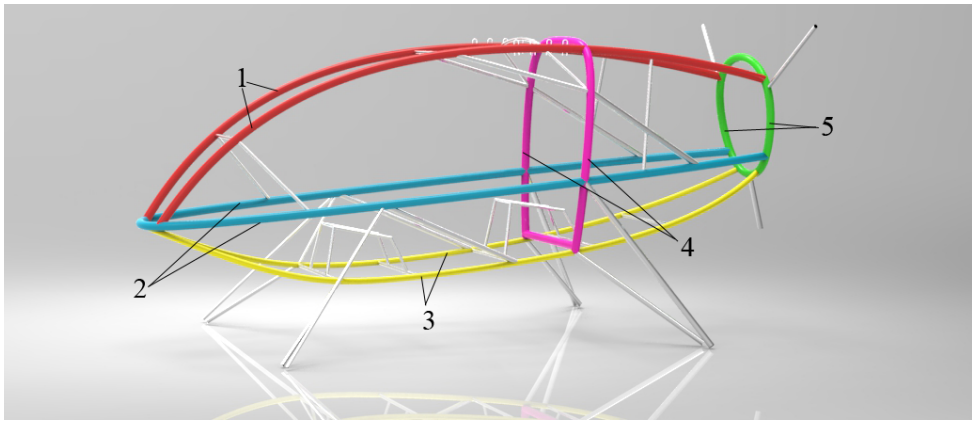

Figure 18.7: Frame structure of the fuselage. The trusses with a constant thickness are shown in distinguishing colors and numbers from the grey trusses

18.4 Skin and floor panels

There are two types of skins in the structure, floor skins and the panels around the engine. The floor skin should carry the loads of the passengers getting in the vehicle, this is its critical load case. The skin panels should be able to withstand someone leaning on it. Near the engine there will be air vents to supply fresh air to the engine. A schematic design of the floor skin is given in Figure 18.8. Aluminium 6061 T651 has been chosen as the material for the skin, its properties are shown in Table 14.3.

Figure 18.8: Cross section of the floor panel.

The load case for the floor panel was a concentrated load of 2000 N in the centre. The deflections

were kept at a minimum. Comparing results from plate theory and the simplified case (subsection 18.2.3), it was found that the deflections and stresses with a simplification of the loading case were higher than the ones predicted by plate theory. The material used was SPS (see Table 18.1 for the mechanical properties). because it was lightweight and strong. The dimensions for the floor panels are 1.4 m by 0.9 m, and 0.63 m by 0.52 m. The bigger plate has 5 stringers equally spaced along the shorter side and 12 stringers along the longer side. For the shorter plate, there are 5 in both directions. The thickness of the stringers is 1 mm and a height of 2.5 cm. The skin is 1 mm thick. This results in a total mass of 3.1 kg, and a material cost of €25.

The design of the outer skin panels is based on a force of 500 N in the centre. The thickness is 0.5 mm, and the stringer dimensions are 1.5 cm by 0.75 mm thick. Each skin panel has 3 stringers in each direction. The total mass of the skin panels is 16.5 kg, with a material cost of €37.

A remark to be made is that these skins are overdesigned, since the skins were modelled as beams simply supported at two ends. However as described in subsection 18.2.3 this is not the case. A plate supported on all sides experiences lower stresses and deforms less as is explained in subsection 18.2.3.

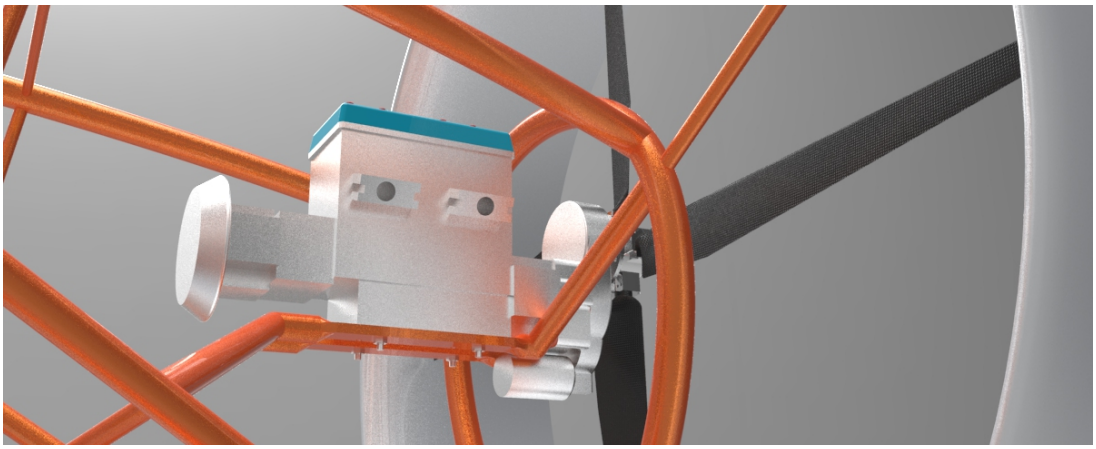

Figure 18.9: Design of the engine attachment points.

18.5 Polycarbonate windows

Three big windows, one of which is in the door frame, provide adequate view for the pilots. The design of the polycarbonate windows is based on the theory discussed in 18.2.4. Mechanical properties of polycarbonate can be found in Table 18.1. This material was chosen on the advise of Ir. Sinke, who suggested the windows can be produced a lot cheaper with this material. A thickness of 2 mm would suffice to keep all the displacements within 10 mm. The total area covered by the polycarbonate windows is 4.73 m^2. This results in 11.4 kg total and a price of €60.

18.6 Doors

In order to comply with the fifth requirement stated in section 18.1 a hinged door on the left side of the vehicle will be used. Due to the curved shape of Parashuttle's skin a hinge cannot be implemented everywhere, the straight truss connecting the top middle vertical truss does allow to do so. Hinging the door here ensures the door stays clear of the kite connection point, verified by using CATIA, as can be seen in Figure 18.10. The door can be hinged 110° to ensure the pilot and passenger can comfortably enter the vehicle.
In order to keep the door open an extending rod is used, indicated by (1) and (2). This rod will push the door open by itself once the door (3) is opened a certain amount. Not only the rod will carry the door, the hinges (4) will partly carry the door too. The aluminium frame around the door has been modelled similarly to the fuselage frame as explained 18.2.2. The design load is its own mass plus a window mass of 5 kg, times a load factor of 3 and a safety factor of 1.5. The load case was an opened door at an angle of 90 degrees. The mass of the frame is determined to be 1.6 kg while it costs €23. The frame has an outer diameter of 30 mm and a thickness of 1.2 mm.

Load calculations are done for the door being opened 90° since then its moment arm is largest, assuming that each of the two hinges carries half the load. In order to withstand this aluminium hinges of 0.13 kg in total, and €5 are needed. The rod will be attached to the main vertical bar of the fuselage, and will be 0.7 m long. In order to hold up the door automatically the rod needs a spring with a spring constant of 100 N/m, and weighs (when made from aluminium) 0.1 kg and costs €1. In order to open the door from the outside a door handle will be placed (5). This will most likely not result in a large drag increase due to the low speeds encountered by Parashuttle 2 and its small size. Once inside the cockpit the door has to be closed. Due to the large distance between the pilot chair and the end of the door a strap will be positioned between the underside of the frame and the cockpit. For both the handle and the strap a mass of 0.3 kg is estimated, costs are estimated at €10.

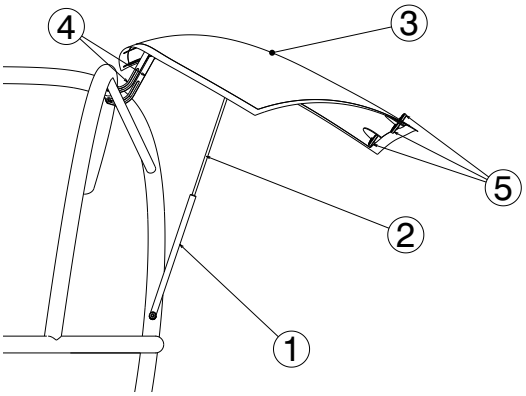

Figure 18.10: The door in opened position, showing the extending rod.

Summarising, the complete door system (without door panel) is estimated to weigh 3.7 kg with an uncertainty of ±0.2 kg. Costs are (without the door panel itself) are predicted to be €40 with an uncertainty range of −2 and +5 euro.

18.7 Fuselage drag characteristics

The flight performance model discussed in chapter 7 requires the fuselage drag as an input. It is assumed that the fuselage drag depends only on velocity and is given by Equation 18.15:

$$D = \frac{1}{2} C_D \rho S V^2 \tag{18.15}$$

In this equation the frontal area S is estimated to be 1.2 m^2 from preliminary CATIA drawings, with the air density being determined from the instantaneous altitude of the vehicle. All that remains is the fuselage drag coefficient C_D, for which an estimate is based on moderately streamlined bodies and helicopter fuselages [125, 126]. These sources predict a drag coefficient of roughly 0.04 for a smooth fuselage. Adding some margin for the landing gear and duct leads to an initial drag coefficient estimate of 0.06.

A more detailed drag estimate will be given in chapter 20.

18.8 Summary

The fuselage consist of 4 main components: the frame structure, skin and floor panels, the doors, and polycarbonate windows. The frame layout is based on loading points, load transfer and aerodynamic shape. The frame is designed for all maximum loads expected during flight with a safety factor of 1.5. The fuselage in its entirety is optimised for minimum mass. The mass of the fuselage is 67 kg, and material cost are estimated at €575.

Part IV - Design integration & analysis

Chapter 19 | Structural analysis

This chapter will discuss the structural integrity of the design of Parashuttle 2. Failure modes and loads of the fuselage structure and floats will be determined in sections 19.1 through 19.3 respectively. A sensitivity analysis will be performed in section 19.4.

19.1 Frame structure loading

To determine the failure modes of the fuselage structure and the accompanying loads the frame structure discussed in chapter 18 will be loaded with the load cases used to design it. It won't be loaded instantaneously, instead loads will be increased by small increments at a time. When a beam fails it is taken out and the complete design is then analysed again, starting at a low load factor. This gives the order of failure of the members together with the load at which they fail. The analysis program and failure criteria are explained in chapters 8 and 18 respectively.

During structural analysis of the frame it is assumed that the only failure modes are buckling and yield. A second assumption is that of a non load-carrying skin, implying the fuselage truss structure carries all loads. The skin's weight however does influence the loading of the design. As mentioned in chapter 18 three load cases are considered in the analysis:

1. Flight at full engine thrust with a load factor of 2.0 (excluding a safety factor).
2. Gliding flight (with zero thrust) at load factors of -1.0 and 2.0.
3. Impact on ground with 3g, and with multiple g forces acting on the pilot's seatbelt.

The vehicle should still be able to operate within the flight regime, while two beams are failed. For the first failure, it has been determined that it should not fail before the limit load is reached. The limit load is 1.5 times the maximum load expected during flight. For load case 1 and 2, the first failure should not occur before a load factor of 3.0, and for load case 3 the first yield failure should not occur before a load factor of 4.5g.

19.1.1 Results frame analysis

This section will discuss the results of the structural analysis. A preliminary analysis was done, the results of which were handled in the design. Afterwards, the new design was analysed and the failure modes were given.

Preliminary analysis and design changes

A preliminary structural analysis had some results that had to be incorporated into the design. Surprisingly, the first beams to fail are those connected to the engine duct. This could be because the simulation model treats the mass of the engine duct as point loads on the end of each beam. Therefore the program sees these as three independent beams under separate loading, whereas in reality loads get transferred through the duct's material to the frame. Additionally the load each truss carries depends on its stiffness and the total load may not be divided equally among all members. Failure of these three members is deemed critical or even catastrophic, due to the risk of the duct interfering with the propeller. This would damage the propeller and could even cause the pilot to lose complete control of the vehicle.

Furthermore, it was found that the struts connecting the fuselage to the floats failed too early during impact. The first failure occurred at an impact load of 4.3g.

These two failures resulted in an extra iteration.

Failure modes

Truss members will be referred to by their number, the location of all trusses is detailed on in figures D.1 and D.2 of appendix D.

The fuselage truss structure of Parashuttle 2 is designed to withstand a load factor of 3.0 in flight with a fully powered engine. Table 19.1 shows the order of failure expected during flight. The expected failure was around a load factor of 4.5, because on top of the load factor, safety factors were placed on stresses and buckling loads.

Table 19.1: Order of member failure, their load factors and failure mode during normal flight operations.

Failure	Element	Load factor	Failure mode
1st	5	4.4	Buckling
2nd	62	4.4	Buckling
3rd	61	2.5	Buckling
4th	63	3.1	Buckling
5th	68	3.1	Buckling
6th	40	2.7	Buckling
7th	111	3	Yield

Table 19.2 shows the order of failure expected during gliding flight. Failure load factors were expected to be higher than during full thrust flight (due to the absence of engine thrust), however one observes this is not the case. This could be due to the fact that thrust and other forces produced by the engine relieved stresses in some members, causing them to fail later in full thrust flight.

Table 19.2: Order of member failure, their load factors and failure mode during gliding flight

Failure	Element	Load factor	Failure mode
1st	62	4.1	Buckling
2nd	68	3.1	Buckling
3rd	4	4	Buckling
4th	5	4	Buckling
5th	60	2.1	Buckling
6th	61	2.2	Buckling
7th	111	2.7	Yield

In case of (hard) ground impact a failure load factor of around 4.5 is to be designed for. Table 19.3 shows the order of failure expected during this load case. It is observed that, after the additional safety factor imposed on the design, failure occurs after a load of 5.1 g. Multiple failures can occur before the structure completely failing.

19.1.2 Conclusion and discussion

In conclusion, the vehicle is suitable for flight, since the first failures occur after the limit loads are reached.

The effects of the engine are shown in Tables 19.1 and 19.2. In gliding flight, failure loads are slightly lower than during the full thrust flight. This can be explained by the fact that the engine thrust and shear forces due to torque might relieve certain forces in the beams.

Table 19.3: Order of member failure, their load factors and failure mode for the ground impact load case.

Failure	Element	Load factor	Failure mode
1st	61	5.1	Buckling
2nd	59	4.2	Buckling
3rd	60	4.9	Buckling
4th	3	5.2	Buckling
5th	63	5.2	Buckling
6th	66	5.2	Buckling

A load factor of 4.0 during gliding flight will not be experienced by the vehicle, during normal operations. It may be possible for the pilot to put the vehicle into a 75° roll using the emergency controls, however this will not happen by accident.

19.2 Analysis window panels

A stress analysis has been performed on the windows using shell theory explained in subsection 18.2.4. Figure 19.1 shows the stress distribution along the front window. The stress is a maximum of 20 MPa, when experiencing a uniformly distributed load of 5000 N/m^2. The yield of the polycarbonate is 76 MPa thus the window will not fail at this load.

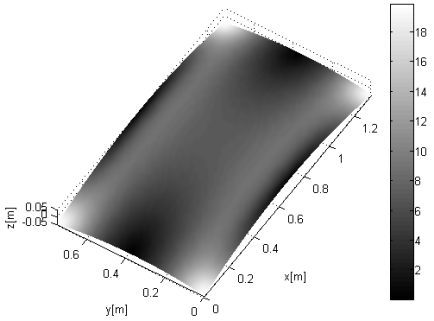

Figure 19.1: Von Mises stress distribution on the front window skin in MPa.

19.3 Floats loading

The structure of the floats has been designed in subsection 14.2.3, in this section the vertical impact velocity at which these floats would fail will be determined. This is done using the same model used in subsection 14.2.3. This time the thickness distribution is known and the vertical velocity is to be determined, rather than the other way around.

Setting an initial vertical impact velocity the model will be used to evaluate whether the floats will fail. In case they do not this procedure is repeated, using an impact speed of 0.05 m/s higher. First the optimal thickness structure for lowest mass was tested, showing that this skin thickness distribution would fail at a vertical velocity of 2.95 m/s. During such impact the von Mises stress was 233 MPa at the bottom plate at 0.24 meters from the nose, causing this to fail. The second structure was the design where the thickness is constant between adjacent ribs. Finally the design incorporating a constant thickness (equal to the maximum thickness required at any point on the float for that side) was analysed, results are shown in Table 19.4.

Failure of a side will lead to failure of the whole structure, as the forces can not be transversed any more. Vertical descent speed should never exceed the indicated failure velocity, else the floats'

structure should be redesigned.

Table 19.4: Results of structural analysis of the floats.

	Optimal thickness at each point	**Same thickness between ribs**	**Same thickness for each side**
Velocity [m/s]	2.95	3.35	3.4
Failure location	Bottom plate	Bottom plate	Bottom plate
x-coordinate of failure [m]	0.23	3.31	3.31
Stress at this point [MPa]	233	230	232

19.4 Sensitivity analysis

A sensitivity analysis has been performed for the elements in the frame structure. A sensitivity analysis for the floats has been done in section 14.5. For the frame structure a slightly different truss layout has been evaluated, as discussed in subsection 19.4.1. Results and conclusion of the sensitivity analysis are discussed in subsection 19.4.2.

19.4.1 Frame sensitivity

The sensitivity analysis of the frame structure consists of analysis of a slightly altered design. For the frame structure the locations of the trusses and their connections determine the loads they carry and thus their thickness. Therefore changing the layout of the trusses should give a different mass for the structure. By removing trusses at certain locations and placing others elsewhere, one can assess whether the structure can be further optimised for mass while still providing sufficient load-carrying capability.

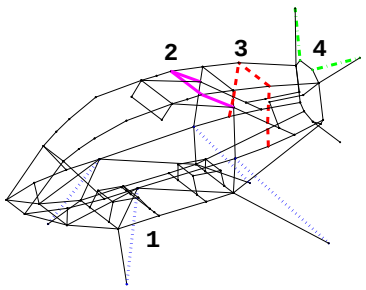

Figure 19.2: Changed layout of the sensitivity analysis.

The changes are depicted in Figure 19.2:

1. Only one beam per float attachment instead of two.
2. Extra support for the kite attachment.
3. Removal of the support between the back of the fuselage and the central ring.
4. Extra support for the duct, two extra beams for the top of the duct.
5. A combination of 3 and 4.
6. A combination of 2 and 4.

19.4.2 Results and conclusion

The results of the sensitivity analysis are shown in Table 19.5. It was decided to add the extra elements of layout number two. However, the extra supports for the duct were not added in to the design configuration. The extra beams only save an additional 0.5 kg, but add to production effort, lower the aesthetics , and give a slightly higher drag. The last two points are not applicable to the extra beams added to kite support, and they saved 2 kg.

Table 19.5: Difference in mass for each sensitivity analysis

Change	**1**	**2**	**3**	**4**	**5**	**6**
Δm	2.54	-2.06	1.03	-0.59	2.05	-2.57

Chapter 20 | Aerodynamic characteristics

The aerodynamic characteristics of Parashuttle 2 consist of both its parafoil, fuselage and float characteristics. Section 20.1 will detail on parafoil aerodynamics, while section 20.2 will give aerodynamic characteristics of the complete vehicle using the model explained in chapter 10.

20.1 Parafoil

Both a Computational Fluid Dynamics (CFD) analysis of the flexible parafoil and experimental testing are not feasible during the timespan of this project. Therefore an estimate of its aerodynamic characteristics will be made based on references, as already stated in chapter 17. The parafoil lift coefficient C_L is estimated as 0.6 [115, 116]. The drag of a parafoil is given by Equation 17.4, where C_{D_0} includes basic airfoil drag (0.015), surface irregularities (0.004), drag due to the open airfoil nose (0.05 [117]) and line drag (0.04). This leads to a L/D of 4.0 which is in the range of common values [115, 116, 118, 119].

For verification and validation of these values, CFD analysis and experimental testing of the actual kite should provide C_L-α, C_D-α and C_M-α curves, as well as the position of the aerodynamic centre for different angles of attack.

20.2 Vehicle

Aerodynamic forces (of which drag is of primary interest) acting on Parashuttle 2 should be analysed. Estimates of drag will be made in subsection 20.2.1, after which a CFD calculation will be performed in subsection 20.2.2. Finally results of both methods are elaborated on in subsection 20.2.3.

20.2.1 Drag estimate

Two estimates of the (zero lift) drag coefficient will be made. The first estimate is made using reference sources on drag of different shapes. In this case the fuselage will be approximated by an ellipsoid which, at the Reynolds numbers Parashuttle 2 operates in (10^6), yields a C_D of 0.3 in laminar flow and 0.1 in turbulent flow (based on frontal area) [125]. Parashuttle 2 will most likely encounter turbulent flow due to the somewhat sharp angles in the vehicle. Furthermore the shape of the fuselage resembles a combination between an ellipsoid and an airfoil (having a C_D of about 0.04 [125]). The floats are approximated as streamlined bodies, giving a C_D of 0.01 for each float based on the frontal area of the floats [127]. The total zero lift drag coefficient (based only on the frontal area of the fuselage), including an extra 'penalty' for struts and other irregularities, is now estimated to be 0.07 - 0.08.

The other estimate for the drag coefficient is based partly on the method specified by Torenbeek [128]. Since floats are not specified in Torenbeek they were added separately in the method. The float C_D was estimated from [129]. The C_D of the fuselage and C_D of the floats are then recalculated as a function of the fuselage frontal area. From this method the zero lift drag coefficient was estimated to be 0.05 - 0.06.

20.2.2 Computation Fluid Dynamics calculation

In order to analyse aerodynamic forces using CFD code, the three-dimensional CATIA model made is imported into the aerodynamic model (FLUENT). Subsequently this model is meshed in order to provide FLUENT with the solution space. Aerodynamic characteristics were found for three different speeds and five different angles of attack in order to see the effect of changing flight

conditions. The characteristics can be found in Table 20.1. The coefficients are based on a fuselage frontal area of 1.2 m^2.

Table 20.1: Lift (C_L), drag (C_D) and moment (C_M) coefficients (w.r.t. fuselage frontal area) for various speeds and angles of attack with a laminar solving model.

		Angle of attack [°]				
Coefficient	**Velocity [m/s]**	0	2	4	8	15
C_D	5	0.220	0.208	0.196	0.164	0.096
	10	0.213	0.201	0.189	0.157	0.090
	15	0.212	0.199	0.187	0.156	0.087
C_L	5	-0.291	-0.115	0.054	0.398	1.070
	10	-0.293	-0.116	0.053	0.397	1.069
	15	-0.292	-0.117	0.053	0.397	1.070
C_M	5	-0.118	-0.163	-0.203	-0.273	-0.343
	10	-0.115	-0.163	-0.203	-0.274	-0.343
	15	-0.116	-0.163	-0.203	- 0.274	-0.346

20.2.3 Results

As can be seen from Table 20.1 a higher angle of attack results in a larger lift coefficient and a smaller (total) drag coefficient. The moment coefficient is negative for each case, meaning Parashuttle 2 has a pitch down moment in all flying conditions. An explanation for the smaller drag at higher pitch angles is the fact that the fuselage is angled downwards, such that at higher angles it is more in line with the airflow. This can also be seen from Figure 20.1, which shows the pressure distribution around Parashuttle 2 for a angle of attack of 0° and 15°. It can be seen that at $\alpha = 0°$ the pressure concentration on the nose is larger than at $\alpha = 15°$. This will thus result in more drag than shown in Table 20.1.

One observes there is quite some discrepancy between the drag estimates from subsection 20.2.1 and the CFD calculation. The CFD result will naturally be somewhat higher since it takes into account drag due to lift, whereas estimates were made of only zero lift drag. However, since it was established that the CFD results should be taken with considerable uncertainty (as explained in chapter 10) one cannot say the CFD values are right. Therefore, using the three established estimates one can make a range of C_D values which should be taken into account in the performance analysis. This range is between 0.06 and 0.22. Prototype wind tunnel tests should be carried out in order to provide the actual aerodynamic characteristics of Parashuttle 2, such that the uncertainty associated with the CFD analysis and preliminary drag predictions can be taken away.

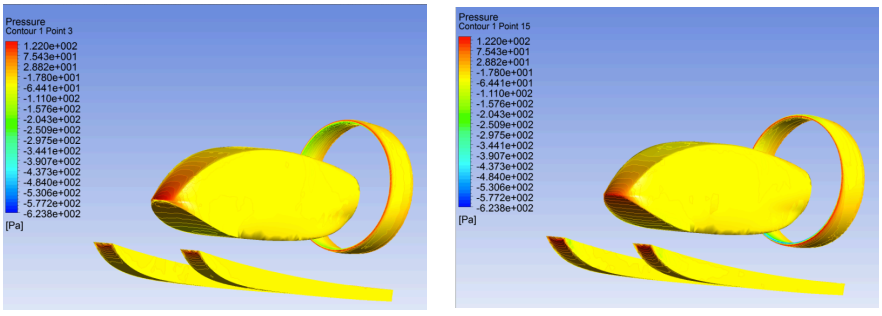

(a) $\alpha = 0°$ *(b)* $\alpha = 15°$

Figure 20.1: Pressure distributions over Parashuttle 2 at $V = 15$ m/s.

Chapter 21 | Performance

Being able to make Parashuttle 2 a marketable product which is able to compete with other paraplanes and microlight aircraft on the market requires it to at least offer performance similar to that of existing products. Standards to be met to do so have been identified in the requirements discussed in section 4.2. This chapter will analyse the flight performance of Parashuttle 2 in section 21.1, its noise characteristics in section 21.2 and its emissions in section 21.3.

21.1 Flight performance

To assess longitudinal and lateral flight performance in sections 21.1.1 and 21.1.2 respectively requires a prediction of the total moment of inertia around the vehicle's centre of gravity. Using data on the major components of Parashuttle 2 and its preliminary centre of gravity location, estimates of the moment of inertia around the vehicle's y- and z-axis were made: $4.0 \cdot 10^2 kgm^2$ and $3.3 \cdot 10^2 kgm^2$ respectively. Performance analysis was done using these values and a total vehicle mass of 495 kg (or 405 kg in case of only one passenger).

A human's mass moment of inertia was estimated using [130]. The fuel tank, engine and floats were modelled as homogeneous rectangular boxes (for which $I = \frac{1}{12}m(l^2 + w^2)$, the propeller as a slender rod (for which $I = \frac{1}{12}ml^2$) and the duct as a thin ring (for which $I = \frac{1}{2}mr^2$) [131].

21.1.1 Longitudinal flight performance

As shown in the flow diagram in Figure 7.1 of chapter 7 range, endurance, take-off and landing performance and control system response of Parashuttle 2 will be assessed in this section. As an indication a typical flight profile of Parashuttle 2 is shown in Figure 21.1, showing take-off, climb, level flight, descent and landing (a low altitude is used to make the entire flight profile clearly visible).

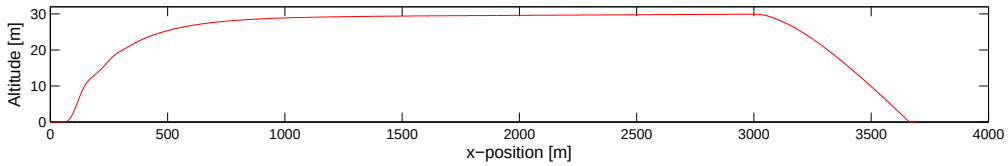

Figure 21.1: Typical Parashuttle flight profile: take-off, climb, level flight, descent and landing.

One of the major uncertainties in the flight performance models is the lift and drag behaviour of the parafoil during flight. A constant C_L of 0.6 has been assumed, together with a drag polar from scientific research. These together resulted in a reasonable parafoil lift over drag ratio of 4.0. Scientific literature suggests the lift over drag ratio of a kite can be as low as 3.0 and as high as 6.0 [115, 116, 118, 119]. To assess the sensitivity of the design to such fluctuations, range and endurance have been evaluated for this range of values. Additionally both have been computed for flights with either one or two passengers. Results of these computations are shown in Table 21.1. As can be seen the range requirement (100 km) is met. The endurance requirement is not met; the model predicted 147 minutes instead of 150 minutes. Since endurance is not a driving requirement and the difference is only a few minutes, this is not an issue.

The results were verified the range equations provided in [27]. The specific fuel consumption was based on the fuel consumption of the Rotax 582[51] and power required for certain lift over drag estimates. The order of error was within the range of 10%.

Table 21.1: Range (left, in kilometres) and endurance (right, in minutes) for various lift over drag ratios and loadings.

Passen-gers	Lift over drag 3.0	4.0	5.0	6.0
1	111km	137km	160km	200km
2	106km	130km	153km	173km

Passen-gers	Lift over drag 3.0	4.0	5.0	6.0
1	141min	172min	199min	248min
2	122min	147min	173min	194min

The procedure for determining take-off and landing distance was discussed in chapter 7. One of the uncertainties in this procedure was the rolling friction coefficient, originally taken at 0.04 but known to range between 0.02 and 0.1 [74][132, p. 212]. Additionally there is uncertainty in the thrust force, with the validation of the propeller model in chapter 6 showing thrust can be overestimated by a factor two. The longitudinal model used to obtain performance figures in this chapter suggests take-off is not possible with a 50% decreased thrust and a roll friction coefficient of 0.10. The critical thrust force for that roll friction coefficient was 55% of original thrust. It was assumed that the braking coefficient was 0.6, though it can be as high as 0.7 and as low as 0.4 [74][132, p. 213].

In case of take-off and landing on water the water drag is included, which was based on computer predictions. These feature an uncertainty of roughly 20%, therefore these are varied in case of water performance. Take-off and landing performance taking into account these uncertainties is shown in tables 21.2 and 21.3.

Table 21.2: Take-off distance (left) and landing (right) distance (in metres) on land for a variety of friction coefficients, thrust levels and braking forces.

Thrust force	μ_{roll} 0.02	0.04	0.06	0.10
Original	36 m	37 m	38 m	41 m
-25%	59 m	60 m	63 m	68 m
-45%	147 m	156 m	166 m	193 m

Braking force	μ_{brake} 0.4	0.5	0.6	0.7
Original	40 m	36 m	32 m	30 m
-25%	46 m	41 m	38 m	35 m
-50%	54 m	49 m	46 m	43 m

Table 21.3: Take-off distance (left) and landing (right) distance (in metres) on water for a various levels of water drag and thrust levels.

	Water drag		
Thrust force	-20%	Original	+20%
Original	52 m	59 m	69 m
-10%	66 m	79 m	102 m
-20%	95 m	128 m	219 m

Water drag		
-20%	Original	+20%
81 m	70 m	61 m

A final parameter defining the performance of Parashuttle 2 in longitudinal flight is its ability to climb. Table 21.4 shows the computed climb rate of Parashuttle 2 for its two loading cases and the different values of lift over drag mentioned previously.

Table 21.4: Maximum climb rate (in m/s) for various values of L/D and number of passengers.

	Lift over drag			
Passengers	3.0	4.0	5.0	6.0
1	4.8 m/s	5.7 m/s	6.3 m/s	6.7 m/s
2	3.6 m/s	4.7 m/s	5.4 m/s	5.9 m/s

21.1.2 Lateral flight performance

As explained in chapter 7 the primary goal of the lateral flight model built is to assess the turning performance of Parashuttle 2. Aspects defining this performance are the vehicle's turn radius and maximum rotational acceleration (which is limited by the pilot's maximum stick deflection). Factors influencing these parameters are the vehicle's moment of inertia and kite response to a deflection. Both could vary by as much as 20%, hence the sensitivity of the design to such changes has been investigated. A typical flight profile in turn is shown in Figure 21.2, together with turn radii and rotational accelerations for varying kite response.

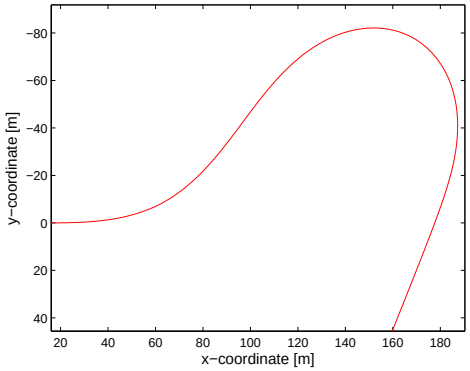

	Kite responsiveness		
	-20%	Original	+20%
Turn radius	46.5 m	41 m	36.5 m
Turning acceleration	2.5 °/s^2	3.3 °/s^2	4.2 °/s^2

Figure 21.2: Turning flight profile of Parashuttle 2 (left) and turning performance analysis (right).

21.2 Noise

One of the regulations Parashuttle 2 must comply with is that it may not produce too much noise, with regulations stating that a microlight vehicle shall not produce noise levels exceeding 60 dB at 150 metres distance with full engine power and engine RPM.

Because of the low flight speeds aerodynamic noise of the fuselage will be low. At maximum power the engine will rotate at 6500 RPM which (with a gear providing a reduction ratio of 2.62) results in a maximum blade tip speed of 171 m/s. This gives a tip Mach number M_t of approximately 0.6. For a tip Mach number of this order vortex noise is relatively low [133], hence the main sources of noise will be the propeller and the engine itself.

Calculating noise levels is complicated and it will not be fully done in this report. Instead a simple model for propeller noise will be explained. This model is derived from Equation 21.1 [133]:

$$p_m = \frac{169.3mBRM_t}{SA}\left[\frac{0.76P_h}{M_t^2} - T\cos(\theta)\right]J_{mB}(x) \tag{21.1}$$

Here p_m is the sound pressure level (SPL, in dynes/cm^2), m is the order of the harmonic, B is the number of blades, R is the propeller radius (in ft), M_t is the tip Mach number, S is the distance between the propeller hub and the observer (in ft), A is the propeller disc area (in ft^2), P_h is the power (in hp), T is thrust (in lbs), θ is the angle between the forward propeller axis and the line to observer and J_{mB} is the Bessel function of order mB. The latter is a function of x, which is equal to $0.8M_t$mB$sin(\theta)$.

To get noise on a decibel scale, the sound pressure level is implemented in Equation 21.2:

$$SPL = 20\log\left(\frac{p_m}{p_{ref}}\right) \tag{21.2}$$

Where p_{ref} is commonly taken as 0.0002 $dynes/cm^2$ [133]. Using the functions above a noise of approximately 52 dB is estimated. This noise level is estimated with Parashuttle 2 flying directly

above the observer, hence at an angle θ of 90°. Another method to estimate propeller noise is by using Equation 21.3 [134]:

$$SPL_{max} = 83.4 + 15.3log(P_{br}) - 20log(D) + 38.5M_t - 3(B-2) + 10log(N_p) - 20log(r) \quad (21.3)$$

Here P_{br} is the power (in kW), D is the diameter (in m), M_t is the tip Mach number, B is the number of blades, N_p is the number of propellers and r is the distance from the propeller (in m). For Parashuttle 2 this results in a propeller noise of approximately 51dB.

Both methods stated above result in a noise estimate of approximately 51 dB. This is well beneath the 60 dB requirement. However when validating these noise levels with reference microlight aircraft the values are too low. For example the Voyageur II produces 69 dB [135], but the methods used above predict noises of 23 dB and 44 dB respectively for such setting. It is concluded that the models used to estimate the noise of Parashuttle 2 are not reliable, hence measurements on a working prototype should be executed.

21.3 Emissions

The Rotax 582 engine runs on automotive fuel with an octane rating of at least 87 by Canadian standards (corresponding to Euro 95 fuel, which has a slightly higher octane rating) [45]. Biofuel is also supported [136], hence the emissions of both these types of fuels will be analysed.

For this analysis ideal combustion is considered, meaning fuel and air react in such a way that only water and carbon-dioxide are left. To estimate the emissions associated with burning fuel the chemical formulas of both fuels are needed. As there are different compounds of fuels 2,2,4-trimethylpentane is taken as a basis for calculation [137]. Its combustion reaction is:

$$2C_8H_{18} + 25O_2 \rightarrow 16CO_2 + 18H_2O \quad (21.4)$$

Using the molecular masses of all components one finds that during combustion of 1 kg of C_8H_{18} 3.08 kg of CO_2 and 1.42 kg of H_2O are produced. Biofuel's chemical reaction is as follows:

$$C_{20}H_{40} + 29O_2 \rightarrow 20CO_2 + 20H_2O \quad (21.5)$$

For each kg of biofuel burnt, 2.82 kg of CO_2 and 1.15 kg of H_2O are produced. Biofuel has a lower specific energy than gasoline meaning that one cannot say right away that biofuel results in lower CO_2 emissions [138]. In order to give an estimate of the amount of Parashuttle's emissions the amount of fuel used during a normal mission profile needs to be known. Assuming that most fuel is used during a normal flight, about 40 litres or 28 kg of gasoline is used during a flight of 120 km. This flight would require 32.4 kg of biofuel, since this has a lower energy density.

Calculating the amount of CO_2 produced for both fuels it is found that gasoline yields 86.2 kg of CO_2 and biofuel 91.3 kg. CO_2 emissions per kg are shown in Table 21.5. In reality these numbers will be slightly lower due to non-ideal combustion. Normally there will be some production of soot and nitrogen oxide as well.

Compared to a modern car Parashuttle 2 will emit about seven times as much carbon-dioxide, however for 100 km of travel distance it also uses about seven times as much fuel. Assuming similar engine efficiency this verifies the calculated emissions.

Table 21.5: CO_2 emissions in g/km for different fuels.

Fuel type	Gasoline	Biofuel
Emissions	700	750

Chapter 22 | Stability & Control

In the previous chapter the performance characteristics of the final design of Parashuttle 2 have been analysed. These give an indication of the flight performance which could be achieved by this product. This chapter will examine the ease of control of the vehicle, investigating its stability characteristics in section 22.1 and control input response in section 22.2.

22.1 Stability characteristics

To allow for comfortable flight Parashuttle 2 should be stable in an equilibrium position close to horizontal. To determine stability characteristics the dynamic response of the vehicle to a change in climb rate was examined. Damped oscillatory behaviour of the vehicle's velocity and climb angle was observed after such a change, indicating Parashuttle 2 is longitudinally stable in flight.

The pitch angle has a constant equilibrium value of 7.7° but shows undamped motion, which can be explained due to the fact that the moment equation discussed in chapter 7 did not take into account damping of this motion.

The most worrying aspect of the plots of pitch is the oscillatory motion right after take-off. A plot of such behaviour is shown in Figure 22.1, where artificial damping has been implemented. One observes an unpleasant motion with a period of 0.75 s. Research into the damping coefficient of this behaviour (not included in the current model) is therefore a necessity.

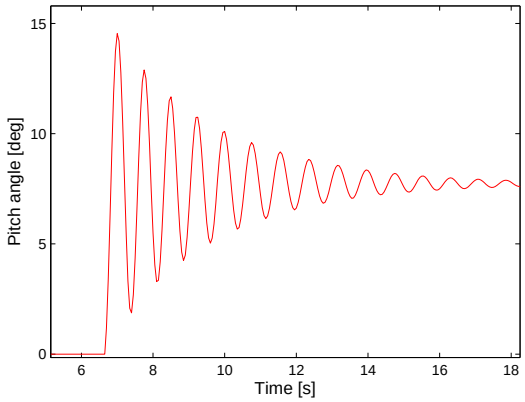

Figure 22.1: Typical pitch behaviour after take-off (artificial damping applied).

22.2 Control response characteristics

As mentioned in chapter 7 a control system has been built into the simulation to determine the vehicle's response to a control input. To tune and investigate this control system the gain factor k_1 has been adjusted, after which a plot showing the desired and actual response for various values of k_1 has been made. This plot is shown in Figure 22.2. Additionally the rise time t_{rise} (time to rise from 10% to 90% of final value), overshoot and settling time (time after which the response remains within 5% of the final value) are given in Figure 22.2. From these figures it can be seen that a gain factor of 3 results in aircraft behaviour being closest to its intended behaviour.

Additionally the vehicle's response to a step input in desired rotational rate has been investigated. As explained in chapter 7 a proportional control system has been implemented for turning flight as well, using a gain k_2. Again this gain has been adjusted to find the value of k_2 giving desirable control characteristics. Control responses and control characteristics are again shown in Figure 22.3.

One observes that, due to the limited control stick displacement and corresponding maximum turn acceleration, overshoot does not occur. Such properties are desirable in case of a turn. One would prefer fast response to a control behaviour, therefore a value of $k_2 = 20$ is chosen to model vehicle behaviour in turns.

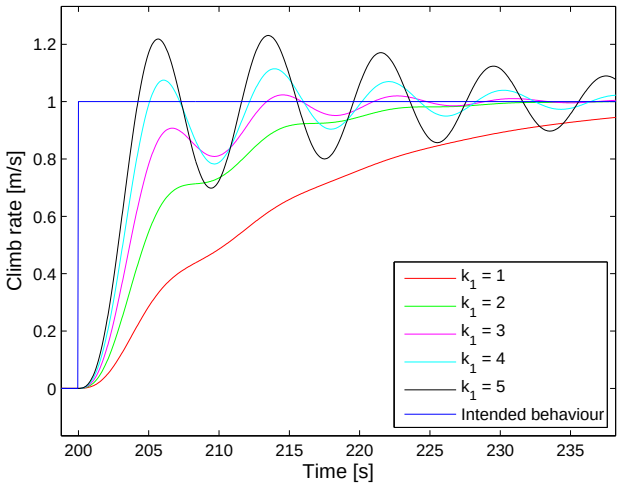

Value of k_1	Rise time	Overshoot	Settling time
1	28.2s	0%	39.4s
2	12.0s	0%	20.3s
3	4.5s	2%	12.5s
4	3.0s	11%	23.2s
5	2.5s	23%	50s

Figure 22.2: Comparison of desired and obtained control response for various values of the gain k_1 (left) and control characteristics for these values (right).

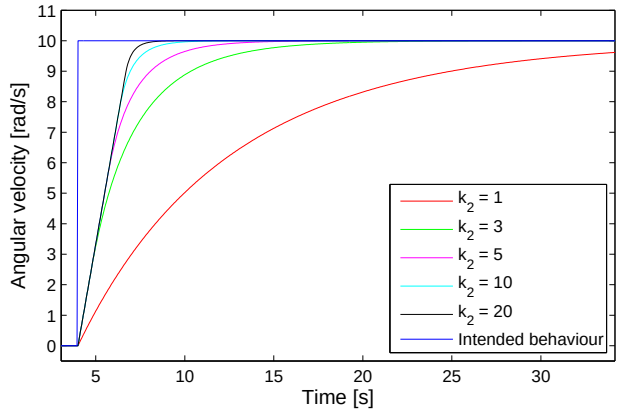

Value of k_2	Rise time	Overshoot	Settling time
1	20s	0%	27.6s
3	6s	0%	8.5s
5	4.3s	0%	5.3s
10	2.6s	0%	3.5s
20	2.4s	0%	3.0s

Figure 22.3: Comparison of desired and obtained control response for various values of the gain k_2 (left) and control characteristics for these values (right).

Chapter 23 | Sustainability strategy

Sustainability considerations are considered more and more important by customers, meaning that Parashuttle's sustainability should be considered. Private flying is per definition not sustainable (emissions of CO_2 could have been prevented by simply not flying), however care has been taken to ensure Parashuttle 2 is as sustainable as possible. This is done through the aspects explained in this chapter.

Use of biofuel - Parashuttle's engine is able to operate on biofuel and automotive fuel, for now the team's intention is to run the engine using biofuel. Even though in section 21.3 it was stated that biofuel has higher CO_2 emissions, this CO_2 is already in the carbon cycle [139]. Using biofuel hence adds no extra CO_2 to the carbon cycle and thus makes Parashuttle 2 flying on biofuel a more sustainable design compared to one flying on gasoline.

Electric engine - A second aspect is that during design it was taken into account that the combustion engine should be replaceable by an electric engine, once in the future batteries are more efficient in power to weight ratio. Replacing the gasoline engine with an electric engine would allow Parashuttle 2 to be recharged using renewable energy sources and would result in zero greenhouse gas emissions.

Aerodynamic shape - Another way of keeping greenhouse gas emissions as low as possible is by ensuring that during operation there is a low amount of drag. This is ensured by designing an aerodynamic shape for Parashuttle 2 such that drag is minimised.

Recyclability - Finally Parashuttle 2 is mostly made of recyclable materials such as aluminium. In this way the end-of-life impact of Parashuttle 2 is kept as low as possible, since most of Parashuttle 2 can be reused in other products.

These aspects ensure that Parashuttle 2 will be a sustainable way of flying for pleasure.

Chapter 24 | RAMS characteristics

Throughout the design of Parashuttle 2 Reliability, Availability, Maintainability and Safety (RAMS) considerations have been taken into account. This chapter describes the final design's characteristics with regard to RAMS. Reliability is described in section 24.1, availability will be elaborated on in section 24.2. In section 24.3 the maintainability of the final design is described and finally safety considerations are explained in section 24.4.

24.1 Reliability

In defining reliability of the design, risks and uncertainties associated with components of Parashuttle 2 have to be evaluated. To do so a risk map is made, in which uncertainties in the design's components and consequences associated with their failure are depicted using cardinal scales. Uncertainty in design is classified by the level of development of components, ranging from 'feasible in theory' to 'proven in flight'. Consequence of failure is classified ranging from 'negligible' to 'catastrophic'. The following components have been included in the risk map:

1. Engine
2. Propeller
3. Duct
4. Fuel tank
5. Electric starter
6. Float stability
7. Float capacity
8. Front wheels
9. Rear wheels
10. Brakes
11. Rudders
12. Parafoil
13. Parafoil attachment
14. Parafoil control
15. Brake control
16. Rudder control
17. Thrust control
18. Instruments
19. Radio
20. Seats & Seatbelts
21. Fuselage frame structure
22. Float structure
23. Doors
24. Emergency control lines
25. Electrical system

Table 24.1: Technical Risk Map for Parashuttle 2.

Parashuttle 2		**Consequence**			
		Negligible	Marginal	Critical	Catastrophic
Probability	Feasible in theory				12
	Working laboratory model				
	Based on existing non-flight engineering		11, 23	4, 8, 10	6, 7, 13
	Extrapolated from existing flight design	3	14, 16	2, 9, 15, 25	21, 22
	Proven in flight		18, 19, 20	1, 5, 17, 24	

The items most towards the upper right corner in Table 24.1 are the those giving highest risk, these should be (thoroughly) investigated before manufacture. The seven risks located in the six boxes of the upper right corner are briefly discussed below.

12 Parafoil: If Parashuttle 2 doesn't have a properly designed parafoil it will not be able to fly. Little information is available on parafoils meeting requirements. Because of the limited time and resources available to the team, it is assumed that there is a parafoil that does meet

requirements. This should still be designed (hence is feasible in theory), failure would be catastrophic,

6 **Float stability:** If the floats do not provide enough stability, Parashuttle 2 is at risk of capsizing. Stability on water was determined using the program Hydromax, hence it is a working laboratory model.

7 **Float capacity:** If the floats do not provide enough floating capacity Parashuttle 2 will sink. Floating capacity is calculated using the software program Maxsurf, hence it is a working laboratory model.

13 **Parafoil attachment:** The way in which the parafoil is attached to the fuselage is based on an existing mechanism that has not yet been used in flight, but that has worked in other engineering fields. The consequences of a failing connection system would be disastrous, however the probability of failure is low.

4 **Fuel tank:** The fuel tank has been designed based on the fuel tanks of cars. When the fuel tank leaks the engine will at some point stop running and Parashuttle should be landed where possible. Since the vehicle is not capable of fulfilling its mission, a fuel tank failure is considered a critical risk. One could argue that the fuel can explode, which would be catastrophic. However a fuel tank only explodes due to fire or other external causes. This failure does not have to do with the fuel tank.

8 **Front wheels:** Failing front wheels would be critical, because when landing on water no problem arises and when landing on land the vehicle can still slide over the ground. It is based on existing non-flight engineering because of the rotational springs used to keep the wheels aligned.

10 **Brakes:** The brakes have been designed taking motorcycle brakes as a reference, they are therefore based on non-flight engineering. Because the brakes serve as a steering mechanism, brake failure is a critical risk. Besides Parashuttle might not be able to come to a standstill in time without brakes.

For the reliability of Parashuttle 2 this risk map means the following. Failure of the parafoil (12) has been deemed to be catastrophic, while its design feasible in theory. This means that at this stage the reliability of Parashuttle 2 is decreased by the parafoil due to the lack of knowledge on the use or design of (floating) parafoils. The control forces required in the control system were based on parafoil dynamics and were highly uncertain, meaning that (although safety factors have been applied) thorough investigation into parafoil design and dynamics is required to increase the reliability of Parashuttle 2.

All other components introduce risk and thus a decline of reliability, however this decrease is very small compared with the one induced by the parafoil.

24.2 Availability

Availability concerns aspects that prevent Parashuttle 2 from being used continuously, these aspects will be gone through in this section. Many availability characteristics are related to the operations and logistics of Parashuttle 2, established in chapter 2.

Maintenance - The first event that could prevent Parashuttle 2 from operating is required maintenance. Maintenance characteristics are discussed in section 24.3. Maintenance could be periodic or 'on the spot' (in case of urgent repair following a failure).

Operations and logistics - Parashuttle 2 can not easily be taken for a flight. Extensive preparation is required before take-off is possible. Parashuttle 2 should be retrieved from its storage space, be loaded onto a trailer, be brought to the take-off site and be unloaded from the trailer. Protective covers should be removed, after which the pre-flight checks, preparation and loading can be executed. During all these activities Parashuttle 2 cannot be used to fly. Not only is preparation involved, there are some activities that have to be done after flight

as well. In fact this is almost the inverse of preparation (post-flight checks, load onto trailer, transport to storage etc.).

Fuel shortage - Parashuttle's endurance limits its airborne time, roughly every 2.5 hours the vehicle should be refuelled at either a petrol station or an airport.

Weather - Weather is an uncontrollable factor that influences the possibility of flying. Though Parashuttle 2 is comfortable to operate in a larger variety of weather conditions than regular paraplanes, the vehicle can not be flown when conditions are too severe. Moreover Parashuttle 2 cannot be flown during IFR conditions due to regulations [105, 140].

24.3 Maintainability

The maintainability of the final design consists of an outline of scheduled and non-scheduled maintenance activities and the ease of performing these activities. This section describes activities that have to be undertaken for maintenance of different subsystems and the final design as a whole.

The first and easiest activity of maintenance is visually checking the vehicle before and after each flight, as already described in chapter 2. Finding damage or other irregularities during one of these inspections will lead to non-scheduled maintenance. Damage or irregularities could vary from cracks or scratches in a subsystem to engine problems. The latter can usually be avoided by scheduled preventive maintenance and checks of the engine. Every part of the engine needs maintenance after using the engine a certain number of hours as described in the maintenance manual of the Rotax 582 [141]. This also describes that general engine maintenance needs to be conducted after every 300 hours of engine use. Rubber parts in the engine need replacement every five years or as required by condition. To be able to conduct engine maintenance easily two hatches are included in the skin at the engine location, one on each side of the vehicle.

Another subsystem needing regular maintenance is the undercarriage, since this is in contact with (salt) water. An activities to be conducted after every contact with salt water is washing salt residue off, especially for the wheels (which are buried in holes in the floats and could contain a lot of salt residue). Bolts in contact with salt water should be removed once a year and waterproof grease needs to be applied over the surface of the undercarriage [142].

The control system requires regular scheduled maintenance since it is a crucial part of Parashuttle 2. Besides normal inspections the control system and the rest of the cockpit need overhaul once every half year to avoid damage or (even worse) failing in flight. During this overhaul the control lines could be re-lubricated or the instruments could be gauged again. Since the control lines are made of stainless steel it is important to monitor control line wear at the clamping system and pulleys. To increase maintainability a hatch is included in front of the pilot seat. The parafoil (connected to the trusses and control lines) needs regular maintenance besides the visual inspection before and after every flight. A complete inspection, with predefined maintenance checks, is necessary after each 100 hours of flight or each year [143]. In case the parafoil has been in contact with water it needs to be dried and cleaned after the flight.

The maintainability of the fuselage as a whole is very good, since the trusses can be reached easily and the skin is made of panels. These skin panels can be interchanged individually in case of damage or other irregularities, which should be noticed in pre- and post-flight checks.

24.4 Safety

Safety is an important aspect of Parashuttle's design, therefore it has been kept in mind during the design process. Features contributing to safety are discussed in this section.

Reserve control handles - The direct control system could fail, either due to mechanical failure of the steering mechanism or snapping of the control cables. In case of such failure the vehicle should still be controllable, this is ensured by implementing a reserve pair of control cables. These cables are attached to two handles located at the roof of the cockpit. In case the pilot loses control over his regular steering mechanism he can pull these handles and still control both sides of the parafoil independently.

Life vests - Life vests are important in case the aircraft crashes on water. Two life vests are included in Parashuttle's design. These are located underneath the seats and are easy to detach and put on. The specifications of these life vests can be seen in Table 24.2.

Table 24.2: Life vest specifications per piece.

Type	EAM - GA12 [144]
Mass	0.27 kg
Dimensions	18.1cm × 8.9cm × 5.1cm
Price	€30,00

Seat belts - Seat belts are of major importance for passenger safety. They are able to withstand impacts of 9g, the load experienced in a crash. Seat belts are also useful during normal flight, particularly during manoeuvres as they keep the occupants in their seats.

Impact and safety factors - The whole structure is designed in such a way that it can withstand a landing impact of 3g, which is a very rough landing. On top of this safety factors on the applied loads are incorporated. For the landing gear this safety factor is 1.5, implying that the structure is actually able to bear loads up to 4.5g.

Floats safety - The buoyancy of the floats is 180% of required buoyancy, a requirement imposed by the FAA [96]. The floats have five different watertight compartments, hence if there is a leak only one compartment of the float floods.

Visibility - Visibility from the inside is high due to the use of large transparent panels. This ensures the pilot can have a good impression of the vehicle's attitude while landing and taking off. It also ensures obstacles at the take-off site are easily noticed by the pilot. Furthermore the pilot can easily spot other aircraft and make sure he does not come too close to them. Finally the pilot is able to look up, giving a view of the parafoil hanging above.

Communications - Contact with the ground is established using a radio. Control towers and ground crew can give advice or orders on what route the pilot should take in order to avoid mid-air collisions or collisions on the runway/water. A transponder is included in order to provide the location of Parashuttle 2 to others.

Chapter 25 | Production plan

In part III of this report all subsystems of Parashuttle 2 have been designed and integrated. This process of integration, in which Parashuttle 2 is built up from its constituent parts into a final product is gone through when producing it. This chapter will elaborate on the process to be gone through during production, showing the logical order of steps. This order is depicted in Figure 25.1. First all phases will be explained in section 25.1, then an estimate of the time required for the production of one Parashuttle 2 is elaborated on in section 25.2.

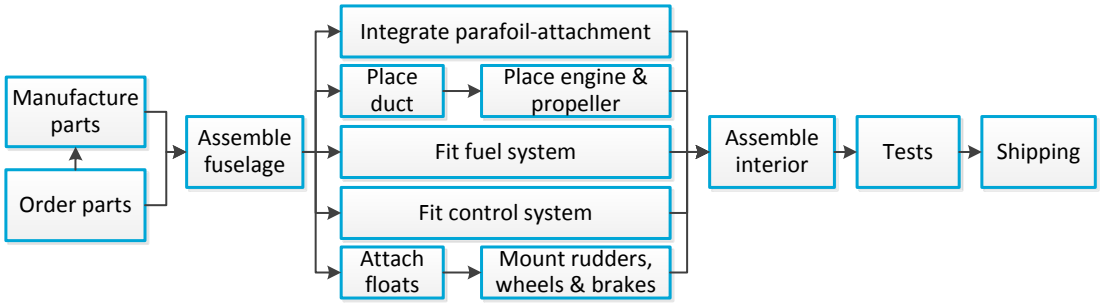

Figure 25.1: The flow of activities to be gone through during production of Parashuttle 2.

25.1 Production process

The production steps of Parashuttle 2 (shown in Figure 25.1) are the following:

Manufacture parts - Some major parts of Parashuttle 2 (the floats, aluminium skin, duct and transparent skin of the cockpit) are newly designed, hence they can not be ordered anywhere. All these parts will be manufactured by the Parashuttle 2 crew.

The floats and fuselage skin plates are made of aluminium. For both aluminium sheets will be ordered and cut to the right size. After that they must be bent accordingly, the plates of the floats will then be riveted to each other. The polycarbonate skin will also be processed by the Parashuttle 2 crew. Polycarbonate plates will be ordered after which they will be thermoformed [145] into shape. This process is as follows: polycarbonate sheets are heated, the heated sheets then indexes into a form station where a mating mould and pressure-box close on the sheet. A vacuum will be applied to remove the trapped air and to pull the material into or onto the mould. This pressurised air is used to form the material to the mould's shape. Because of the large parts plug-assists are used in addition to vacuum in order to provide the needed material distribution and thicknesses in the finished parts. Three different polycarbonate surfaces are required for Parashuttle 2, so three different moulds are needed.

The duct, consisting of a foam core with a glass fibre skin, is to be manufactured. First solid foam blocks are ordered, from these solid blocks the duct pieces are cut out (For example a quarter of the duct is cut at a time to save material). These duct pieces are glued together to obtain the duct shape. The outer surface should be prepared accordingly to allow for addition of fibreglass, done by a lay-up procedure [146].

The fuel tank is manufactured by cutting polyethylene and ethylene vinyl alcohol sheets. These are then welded into the right shape with a plastic welding kit [147].

Order parts - The materials for the parts mentioned above and other parts of Parashuttle 2 (such

as its floats, fuselage bars, instruments, engine, propeller, etc.) will be bought of the shelf. Before actual production of Parashuttle 2 can start these items should be ordered. Previously the demand for Parashuttle 2 was estimated to be around a thousand, meaning it will most likely be manufactured on a production line. Therefore it should be ensured that sufficient stock is available at all times. This requires keeping in mind delivery times of up to a month for more complex parts such as the engine or the propeller.

Assemble frame - The trusses of Parashuttle's fuselage will be ordered, meaning assembly still needs to be done. Two people should weld tubes in a correct manner. Once the fuselage structure is completed, all other components can be fitted in a concurrent manner.

Integrate parafoil attachment - The U-bolts of the parafoil connection system can be bolted into place once the structure of the fuselage has been assembled. The two carbine hooks should be attached to the main parafoil lines, such that it can be hooked into place once needed.

Place duct, engine & propeller - Parashuttle's duct should be mounted to the back of the fuselage using the connective rods designed for this purpose. Once the duct is in place the engine can be installed into the fuselage, after which the propeller can be attached to it.

Fit fuel system - With the engine now in place its fuel line can be attached. The fuel tank should be mounted in the bottom of the fuselage, with the fuel line attached to it. The fuel hose and filler cap required for refuelling can then be incorporated in the side of the fuselage.

Fit control system - The control system of Parashuttle 2 is an intricate system consisting of levers, pulleys and wires, which is to be mounted in the cockpit. When fitting the interior of the cockpit this system should thus be in place already. Parts of the control system should be connected to the fuselage trusses and wires should be run already.

Attach skin - Now that most parts are integrated in the vehicle the skin can be attached to the frame.

Attach floats and mount rudders, wheels and brakes - As a final step of producing the bare fuselage, the prefabricated floats should be attached using its designated struts. At this stage the wheels should be incorporated in the floats already. Once the floats have been attached the brakes and rudders (which together form the control system on land and water) can be mounted. The connections from the fuselage to these systems can be put in place now.

Assemble interior - At this stage of production the full fuselage has been assembled, with all hardware in place. Before fitting the fuselage interior (seats, covers, etc.) one should first put in place the electrical system of Parashuttle 2, placing the sensors and running the wires required. Once all wires and instruments are in place the seats can be mounted and covers can be applied in the cockpit for aesthetic purposes.

Testing - With the production of Parashuttle 2 now done the final product should be tested. A ground and flight test should be executed to determine whether the product is worthy of delivery to the customer.

Shipping - Once the product has been fully assembled and tested it can either be picked up by the customer (and be taken home on a trailer) or it can be transported to the customer. This should be done either by truck or (in case of an overseas delivery) by ship. The latter form requires Parashuttle 2 to be first loaded into a container.

25.2 Labour hours

To make an estimate of the costs associated with the production of Parashuttle 2 labour costs should be investigated. This required an indication of labour time required. As mentioned above

at least two persons are needed for manufacture. Based on the fact that Parashuttle 2 will be sold assembled, it is assumed that manufacturing is done by skilled and experienced workers.

Manufactured parts - As described in section 25.1 several parts are to be manufactured by the Parashuttle 2 crew. For all these parts labour hours are required. For the aluminium skin there are several sheets that should be bent into the right shape. Bending machines can do this at a speed of $6.7 m/min$ [148]. Including the whole process of preparing the machine, cutting and bending it will take approximately 30 minutes to manufacture a plate. Parashuttle 2 is composed of 16 different aluminium skin parts, hence it will take approximately 8 labour hours to process all aluminium skin of a vehicle.

The transparent polycarbonate skin is thermoformed, a process mainly done by machines and not requiring a lot of attention (one person should monitor the process). The most time-consuming part of thermoforming is the curing of the polycarbonate, which takes around 15 hours per mm thickness of the material [149]. The polycarbonate skin will be approximately 2 mm thick, hence 30 hours of time is estimated for this. With some additional time to prepare and run the thermoforming machine, 35 hours are estimated for the manufacturing of each part of the skin. Parashuttle 2 contains three of these skin parts. However during the curing of one plate the machine can already begin with the next skin plate and the worker can also work on other parts during the curing of all parts (he has to check the curing parts once every few hours), so 25 labour hours are estimated for the total processing time of the polycarbonate skin.

Constructing the floats is a big part of the total work to be done. The sheets have to be cut using an aluminium laser cutting machine, which will take approximately 4 hours [150]. Then the sheets have to be bent to the form of the ribs and skin, which takes approximately 2 hours [148]. Drilling, riveting and welding requires a lot of time, 80 hours are estimated for this based on experience [151]. For the rudder plywood must be shaped, which for an experienced woodworker would take around 3 hours. Thereafter fibreglass and epoxy will be applied on the rudder and then it must cure. This takes some time because the worker can only do one side at a time. Finally the rudder will be scoured to make it smooth. This process takes about 5 hours per rudder. The total time for a set of rudders is 16 hours. A total of 96 labour hours for the floats including the rudders is then required.

Cutting the duct's foam using a foam cutting machine (cutting at a rate of $1 m/min$ [152]) will take around 2 labour hours. The entire glass fibre lay-up process will take approximately 15 labour hours [153].

Finally for the fuel tank little time is required. For cutting, welding and curing 3 hours are estimated.

This gives a total of 147 labour hours for manufacturing the parts.

Assembly - When all required parts are gathered (all ordered parts are in and all manufactured parts are finished) the assembly of Parashuttle 2 can be started. It is complex to estimate the exact number of hours spent on assembly. For reference aircraft assembly time ranges from 40 hours to over 600 hours (see Table 25.1), depending on the complexity of the aircraft.

Compared to the reference aircraft of Table 25.1 Parashuttle's complexity is graded around 7. From the table it then follows that assembly time is roughly 300 hours.

However when production is done in line the same crew performs the same tasks on subsequent products over and over again, leading to them developing a routine. This routine results in cost-reduction once the program is in full production. The ever decreasing number of hours required to perform a certain work package in a station is described by a so-called learning curve [159]. This curve presents the hours required to perform the work package as

Table 25.1: Number of labour hours and complexity of reference aircraft

Paraplane	Labour hours	Complexity
Lightning Experimental kit [154]	500	9
Steel Breeze 2-place [155]	40	2
Zenith CH 750 Cruzer [156]	400	8
Sky Raider [157]	300	7
X-Air [158]	150	5

a function of the aircraft serial number. The learning curve is given by Equation 25.1:

$$E_N = K \cdot N^s \tag{25.1}$$

where E_N is the required effort for the N^{th} aircraft, K is the effort for the first aircraft and s is the slope constant. In Figure 25.2 the learning curve of Parashuttle 2 is shown. An initial value of 600 hours is estimated. Usually a reduction factor of 80% is used in the airframe industry sector [160], however to be conservative a reduction factor of 90% is assumed.

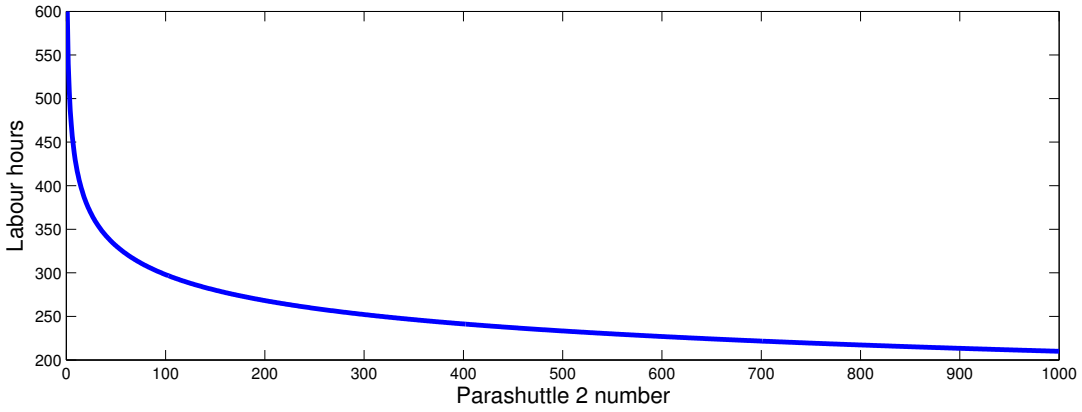

Figure 25.2: Learning curve of the production of Parashuttle 2

From Figure 25.2 the average labour time for a Parashuttle 2 when producing 1000 units is 250 hours, decreasing as more units are produced. For the production plan 250 hours of labour are estimated for the assembly of Parashuttle 2.

The total number of labour hours is the sum of manufacturing and assembly. This results in 397 labour hours needed to produce one Parashuttle 2.

Chapter 26 | Future activities

With detailed design including an iteration finished, the final steps to a real product can be taken. Before Parashuttle 2 is able to be built and flown several actions still have to be performed. This project design and development diagram is shown, in their respective order, in Figure 26.1.

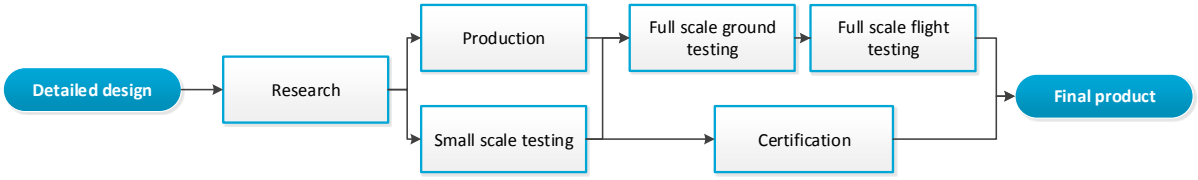

Figure 26.1: Steps to be taken for a finished product.

The following sections will elaborate on each element of the logic shown in Figure 26.1.

26.1 Research

During the Design Synthesis Exercise not all aspects of Parashuttle 2 could be researched fully. One of these aspects is the parafoil, for which aerodynamic and dynamic properties need to be researched as well as the kite specifications. Aerodynamic characteristics include its lift and drag polar, dynamics properties to be investigated are the orientation of the parafoil with respect to the paraplane during flight and the forces and moments created by the parafoil due to control lines deflections. The latter is especially important for accurate simulation of turning and rolling flight.

Another aspect to be investigated is the loads of the skin, for example due to a person leaning on a side panel. The deformations and loads associated with this should be researched more. Moreover the pitch response of the vehicle should be investigated further, as well as the vehicle response in case of a bird strike (on the parafoil, fuselage and propeller). Also the ability to withstand gusts during flight should be looked at in more detail. Furthermore small parts of the design (such as hinges) which were not completely designed during the Design Synthesis Exercise and should be considered in more detail before production.

26.2 Production

At this stage of the project Parashuttle 2 only exists as a 3D computer model. Although the production process has been thought through in chapter 25 it is not yet proven whether it can actually be produced as specified. Also, the detail of the design is not yet accurate enough for production. An example is the specifications of bolts. During implementation of the production process issues in production will undoubtedly arise. These will be treated accordingly. Alterations to the production process can be made in order to make the process as efficient as possible. Furthermore, the exact production steps have to be specified in more detail, to simplify the production for the manufacturer.

After this research in the detailed production steps, the prototypes have to be manufactured. These vehicles will be used to perform the tests which are done during and after this manufacturing.

26.3 Small scale testing

Concurrently with production, small scale testing needs be done in order to validate parts of the design. The components of Parashuttle 2 to be tested individually are listed below:

Engine - The engine should be tested for its range of rotational speeds, monitoring the fuel consumption at the same time. In this way the fuel consumption given by the manufacturer can be verified. Besides engine noise should be tested.

Propeller and duct - Making use of a wind tunnel, the thrust produced by the propellers at various rotational speeds can be measured. Using such test the thrust predictions can be validated.

Cockpit instruments - All instruments should be tested before their integration in the cockpit, in order to verify their correct functioning. At this stage the circuitry can be checked as well.

Floats - After construction the floats should be tested for their provision of floating capacity. Additionally the drag in water should be tested to validate the models used. The floating capacity in case of a leak in one of the float components should be tested as well.

Door - As the door is integrated with the fuselage, one should ensure that the door is able to open and close properly and does not interfere with the fuselage.

Control system - When building the fuselage, the control system must be tested. This entails test of control forces and friction.

Structure failure - Each structural component must be testing on failure. This way, the expected loading location and moment can be validated using the test.

26.4 Full scale ground testing

During full scale ground tests the completely assembled vehicle should be tested for its land and water performance. The order of tests to be executed is as follows:

Load cases - Through the static application of forces that can be experienced in flight as well the prototype will be tested for its ability to handle all intended loads.

Engine - The engine (now assembled in the vehicle) will be started up from within the cockpit. Its thrust will be varied to confirm proper functioning of the thrust lever. Furthermore the vibrations caused by the engine can be observed by applying maximum thrust (without the propeller attached).

Inertia testing - The moment of inertia of Parashuttle 2 needs to be determined by using an inertia swing. This inertia swing works by measuring pendulum motion from which the inertia can be deduced [30].

Pitch response testing - In order to verify the pitch response of the vehicle it should be hung from the attachment point with a variety of payloads (to change the centre of gravity) from which the pitch equilibrium of the vehicle can be found.

Land handling - Initially Parashuttle 2 will only be driven over land, first accelerating and braking in a straight line and then turning as well. All this is done without the kite attached.

Land-water transfer - With the vehicle being able to operate, it is now time to transfer it into water. Its ability to float and stability characteristics should be tested.

Water handling - Similarly to the test on land, Parashuttle 2 will first be moved in a straight line, after which turning manoeuvres are done. Again this is done without the kite attached.

Water-land transfer - Like the transfer from land to water, Parashuttle's ability to drive from water onto land should be tested. Test ability to taxi from water onto land.

Handling with kite - At this stage the kite can be attached to the vehicle, allowing for its land and water handling to be tested in the presence of the kite.

Failure test - The vehicle should be tested on ultimate loading, to get an idea of failing moment and location.

26.5 Full scale flight testing

Following all ground tests mentioned above, Parashuttle 2 should be tested in flight conditions. The flight tests should be performed with a specially equipped version of Parashuttle 2, namely one with a ballistic recovery parachute. With this parachute the complete flight envelope can be tested while having a back-up in case a test does not go as expected. This way it can be proved that Parashuttle 2 is safe to operate without a safety parachute. The safety parachute is one from BRS aerospace [161] and is mounted at the left underside of the vehicle, just below the engine. This is quite close to the fuel tank and thus extra reinforcement is needed to protect the fuel tank from the explosives used in the recovery parachute. This will introduce extra mass (just like the recovery parachute) and this has to be accounted for in the flight testing. The exact way this reinforcement should be applied has to be investigated in later stages of the development. For the operation of the recovery parachute, it will deploy on the left side of Parashuttle 2 such that it stays clear of the main parafoil (the lines of the safety parachute are also much longer than those of the parafoil). When landed the vehicle lies on its right side thus making sure that the door (on the left side) can still be opened.

The following tests should be executed:

Parafoil raising - Since it is essential that Parashuttle's parafoil lifts itself prior to take-off, it is required to confirm the correct functioning of this system before an actual take-off.

Take-off - Once the previous step has been taken, Parashuttle 2 can be accelerated even further until it lifts off. Once it clears the ground, throttle should immediately be decreased to touch down again. This procedure should be gone through on both land and water.

Landing Extending the flight tests a bit (still keeping them in a straight line) allows for testing the landing procedure of Parashuttle 2. Again this should be done on both land and water.

Flight manoeuvres - Once Parashuttle 2 is able to safely take off and land, its flight manoeuvres can be executed one by one. This starts with first climbing and descending, following by gentle steady (and increasingly sharp) turns.

Different take-off and landing surface - Once Parashuttle 2 can be controlled in the air one can test its ability to take off and land on different surfaces.

Flight performance - At this stage engineers can validate the flight performance of Parashuttle 2, testing it for parameters like range, endurance, turn radius and climb rate.

Different environmental conditions - After the previous steps (which should be performed in clear conditions, with low wind speeds) the flight tests can be performed in different weather and environment conditions. This must be tested up to the specified capability of the vehicle.

RAMS testing - After the flight envelope has been fully explored Parashuttle 2 has to be flown for many hours to get an idea of the reliability, availability, maintenance and safety.

26.6 Certification

Certification procedures will run in parallel with full scale ground and flight testing. This way certain tests may be combined for cost savings. To certify the vehicle all requirements as stated in [18, 105, 162] should be met and verified in the way specified by those same sources. When elements fail the certification, iterations should be done in steps shown earlier in Figure 26.1.

Chapter 27 | Cost breakdown

With the detailed design finished and the production plan and future activities for the development of Parashuttle 2 having been specified in chapters 25 and 26 a detailed cost breakdown can be made. This chapter will cover this in two parts. A cost structure for the product is in section 27.1, so a sales and profit prediction can be made in chapter 28. section 27.2 shows a cost breakdown structure presenting an estimate of cost required for further stages of the design process. The latter section is based on information of the previous chapter.

27.1 Product cost breakdown

This section presents costs related to final product, distinguishing material cost, manufacturing cost and fixed costs. These are presented in subsections 27.1.1 through 27.1.3 respectively.

27.1.1 Material cost

Material cost considers the cost of the parts of Parashuttle 2. This variable cost depends on the volume of production. Material costs of all parts were each researched and specified in their respective chapters. These were based on market prices of single products. Since the sales estimate is around a thousand (as will be elaborated on in chapter 28), an estimate will be made for the cost based on an economy of scale.

Each cost is investigated in as much detail as possible. Still uncertainties remain in subsystem costs, an attempt has been made to express these in order to get a more realistic representation of costs. In appendix chapter E component costs of Parashuttle 2 with their uncertainties are shown. Uncertainties should decrease in the final stages of design, as described in chapter 26.

27.1.2 Manufacturing cost

The costs specified in the previous subsection only consider the materials used in and components bought for Parashuttle 2. Since manufacturing is an elaborate process it contributes a significant part of total costs.

Previously an rough estimate of 800 labour hours (based on vehicle complexity) was made [9]. Based on the production plan given in chapter 25 a more accurate estimate can now be given. The total number of labour hours is the sum of the hours required to manufacture the different parts for a single vehicle and to assemble all these parts. Approximately 397 labour hours are needed for producing one Parashuttle 2. It is found that the average hourly labour cost in Europe was €28/h in 2012.[163–165]. The total labour cost is then estimated to be €11,116.

27.1.3 Fixed costs

There are a number of fixed costs which should be included for the production of Parashuttle 2. This concerns for instance facilities, moulds and machinery. Manufacturing the transparent polycarbonate skin requires three moulds, these moulds are estimated to cost €30,000 each [166]. Also a thermoforming machine is needed in the thermoforming process, this unit is estimated to cost €10,000 [167]. Tools are needed for bending, forming and cutting of aluminium sheets for the skin and floats, for these tools €12,500 is estimated [148, 150]. Hand lay-up tools for manufacturing the glass fibre duct are estimated to cost €9,000 [168], tools for cutting the foam will cost around €5,000 [152]. Furthermore rivet and welding tools required for the floats and assembly cost approximately €600 and €800 respectively [169, 170]. The production of rudders needs a good woodworker and woodworking tools that will cost approximately €1,200 [171]. For the

fuel tank the earlier mentioned cutting machine is used, but a plastic welding kit must be purchased too, which will cost €150 [147]. Furthermore €30,000 is kept apart for additional tooling such as drilling machines, painting tools, a hoisting crane and other tools.

Another part of fixed costs is the premises in which all parts are stored, the machines are located and Parashuttle 2 will be produced. Current rental rates in Holland are approximately €48 per m^2 per year [172]. Assuming the required space is 500 m^2, annual costs will be €24,000. This space is required for an assumed period of time of ten years. The "building" cost will add up to €240,000.

Other fixed costs include marketing, administrative and unforeseen costs. These are estimated at €100,000, €50,000 and €50,000 respectively. Summing all up the total fixed cost for the first year will be around €600,000. Fixed costs will decrease for later years because the machines are already purchased (only rent for the premises and machine maintenance must be paid). An overview of all costs can be found in appendix chapter E.

27.2 Project development cost

In Figure 26.1 of chapter 26 future design and development activities were shown. In this section an estimate will be made of the costs involved with each activity.

The first activity is the extra research to be conducted. For this personnel is needed as well as facilities (wind tunnels, computers etc.). The second activity is production, done concurrently with small scale testing. The production cost of the first prototypes will be higher than those of the products to be sold. The production cost at this stage are the production costs as specified earlier, with an added amount since it is the first time and not all the kinks in the production plan are ironed out. This extra cost is estimated to be 20% of the total production cost for a normal Parashuttle 2 meaning that a prototype of Parashuttle 2 will cost 1.2 times as much as a normal version.

The small scale testing carried out concurrently is another cost driver for the project development cost. For testing several facilities are required, such as a wind tunnel, a body of water, a structural failure test rig and measurement equipment. Furthermore personnel is needed to carry out testing. This all leads to considerable costs associated with small scale testing.

For the full scale ground testing a swing capable of carrying Parashuttle 2 is needed as well as one completely assembled vehicle for failure testing. Besides a testing area is needed where ground handling capabilities (both on land and water) can be assessed. For that of course fuel is needed as well as personnel carrying out the tests. For full scale flight testing, a first cost inducer is the flying prototype of Parashuttle 2. As explained this prototype will be fitted with an extra safety parachute, costing between €2,250 and €9,350 [161]. Not only this parachute needs to be paid for, but also the extra reinforcement needed for the ballistic system included with the safety parachute. Furthermore this safety parachute needs to be included in the vehicle, leading to extra manufacturing costs.

Total project development cost, excluding the research still needed, is estimated to be between 5-25% of the total project cost[173]. In a worst case scenario one multiplies 25% of the 4000 design hours with the average hourly rate of €28 and adds to this the cost of five prototype Parashuttles with an additional €5,000 to account for the safety kite. Summing all project development costs leads to a total cost for project development of €231,000.

Chapter 28 | Final market analysis

In chapter 3 the list price for Parashuttle 2 was established at €35,000, with demand expected to be in the order of thousands. Now knowing the expected costs of production from the previous chapter allows for the exact determination of the market price of Parashuttle 2 and an estimation of the achievable market volume and share at this price. These aspects are discussed in section 28.1. The profit and return on investment following from this are treated in section 28.2.

28.1 Final market price and volume

In section 3.1 the market volume was estimated to be in the order of thousands. Based on this number it is decided to have a production volume of a thousand Parashuttles. To determine the market price of one single product first the total production cost needs to be computed. A margin is included to have a marginal profit, which is needed to return investments and to eventually make profit. The total product cost is based on the material cost and manufacturing cost, as mentioned in section 27.1. Here the total product cost is determined to be €29,690. With an assumed profit margin of 10% of the total production cost this brings the product market price to €32,660. It has to be said that this market price is excluding VAT, however all parts bought off the shelf have VAT already included in the price, so product costs might have been overestimated.

28.2 Return on investment

In Figure 28.1 the total cost, total revenue and profit are plotted for the number of Parashuttles sold. The break-even point is indicated, located at the 281th Parashuttle 2. The total cost is computed by first computing the total investment, which are the fixed cost and the project development cost added up(€830,000). This number is added to the total product cost multiplied by the number of products sold. The total revenue is calculated by multiplying the product market price by the number of products sold. Profit is computed by subtracting the total cost from the total revenue. The break-even point is determined to be at the location where the loss turns into profit, hence where the loss/profit line crosses the zero-profit line.

Total profit after selling a thousand Parashuttles is calculated to be €2.15 million. To compute the return on investment the total profit is divided by the initial investment (the fixed cost). The return on investment was determined to be approximately 2.6. However, it has to be said that additional research into exact fixed and variable costs is required when the first Parashuttle 2 is actually built.

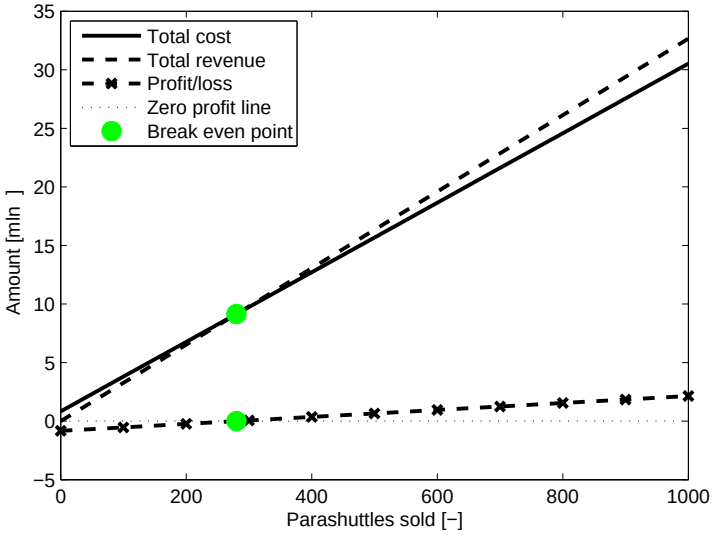

Figure 28.1: Plot of the total revenue, total cost, profit and break-even point as a function of Parashuttles sold.

Chapter 29 | Final design & validation

In previous parts of the report all subsystems of Parashuttle 2 have been designed and integrated, part IV of this report detailed on the functioning and performance of this full system. The degree up to which the final product complies with customer wishes is to be assessed at this stage. Before this is done the current design will be optimised in section 29.1, after which the final design's specifications will be given in section 29.2 and design validation is done in section 29.3.

29.1 Design iteration

As stated in parts III and IV of this report the current design includes uncertainties regarding its mass and cost. In appendix E the final cost breakdown of the vehicle including uncertainties is given. One observes that in the worst-case scenario the maximum take-off mass of 495 kg is just met, but that the vehicle could be up to 39 kg under its specified mass in a best-case scenario.

At this stage of design the team has two options: redesign the vehicle for a lower intended mass or optimise the vehicle for other purposes. In chapter 3 it was discussed that to be used by governmental and commercial agencies Parashuttle 2 should have a range and endurance significantly higher than 100 km and 2.5 hours. Since Parashuttle 2 already offers the required operating costs (a fuel consumption of 40 litres in 2.5 hours leads to operating costs of €30/h) and meets take-off and landing criteria, it has been decided to allocate the left-over mass budget to additional fuel, thus optimising the vehicle for range and endurance. Using this modification the estimated demand of a thousand is reasonable. The fuel tank will thus be increased to a capacity of 46 kg (66 litres of fuel), increasing range and endurance to 198 km and 3.7 hours. The redesign causes the structure to fail under 3.7g loads in flight and 4.9g loads upon impact, this is still within requirements.

29.2 Final design

The final design made during this project is shown in the pictures below, the design's three-view drawing in shown in appendix F. Specifications of the final design can be found in Table 29.1. The final design is rendered in Figure 29.1 and Figure 29.2.

Table 29.1: Specifications of the final Parashuttle 2 design.

Specification	Value
List price	€32,660
OEW	265 kg
Fuel capacity	66 L / 46 kg
MTOW	495 kg
Parafoil	Inflated, model TBD
Cruise speed	15.3 m/s
Range	198 km
Endurance	3.7 h
Engine type	Rotax 582
Engine power	48 kW
Propeller type	4 bladed
Propeller diameter	1.65 m
Emissions (CO_2)	700 g/km
Fuel type	Gasoline/biofuel
Dimensions	4.6m(l) x 2.3m(w) x 2.65m(h)
Fuselage dimensions	3.77m(l) x 1.02m(w) x 1.25m(h)

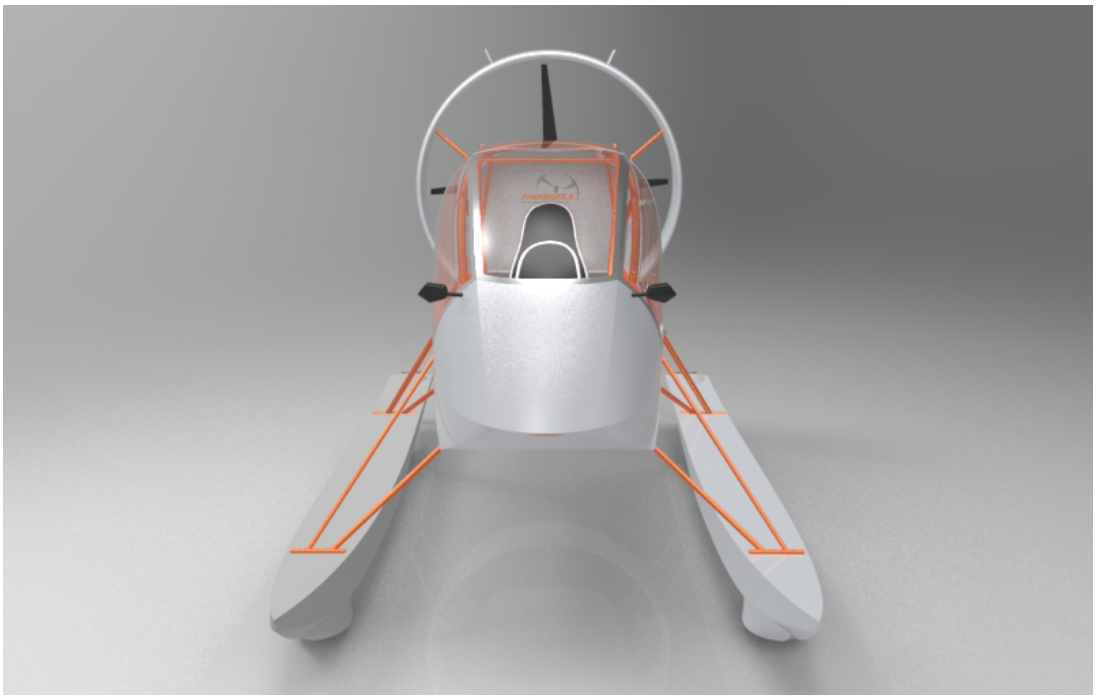

Figure 29.1: Front view of the Parashuttle 2.

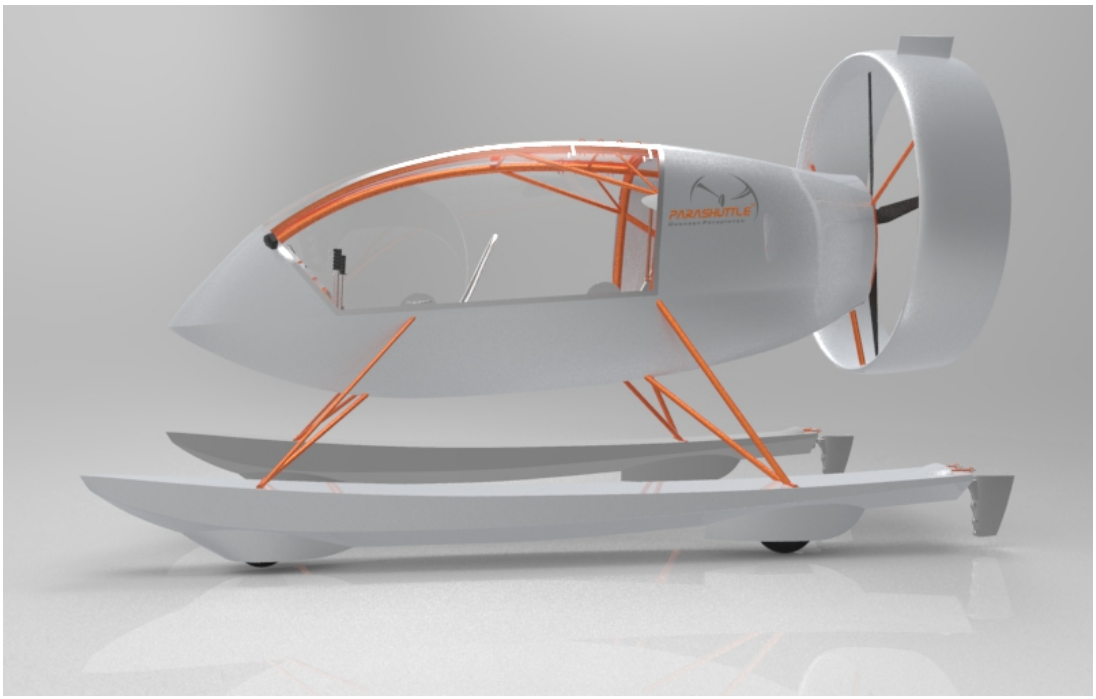

Figure 29.2: Side view of the Parashuttle 2.

29.3 Design compliance

Since the customer demands were fully reflected in the list of requirements presented in section 4.2, this list of requirements will be run through to see whether Parashuttle 2 meets all requirements. The compliance matrix obtained after this process is shown in appendix B. In this appendix the requirements met are indicated with ✓ , the requirements not met with ✗ and requirements which were not researched during this project (but are expected to be met) with -. As can be seen from this appendix not all requirements are met. An overview of requirements not met is presented in the following. All of these were no critical or driving requirements for the project, making it acceptable that the design does not meet these.

1. Parashuttle 2 is too high to fit in a normal container (P2-Mar-1-3), however this can be dealt with by using available higher containers [174].
2. Parashuttle's operational empty weight is also higher than that of its predecessor (P2-Sus-1-1) and its emissions are higher (P2-Sus-1-4). These requirements were striving values at the start of the design but proved to be not feasible.
3. Parashuttle 2 is also not able to come to a standstill from 2 m/s within 5 m on water (P2-Mis-2-3-2). As it is expected that operators of Parashuttle 2 carefully operate the vehicle on water this is not a problem.
4. Three performance requirements having to do with flight path angles are not met (P2-Mis-4-2-1-2, P2-Mis-4-2-2-1, P2-Mis-4-2-2-2). Values associated with these requirements proved to be infeasible, however these were striving values at the start of the project so underperformance is accepted.
5. The design does not meet safety requirement P2-Saf-1-2: landing safely in case of parafoil failure. During testing it should thus be shown that parafoil failure will not occur during use within the flight envelope, such that not meeting this requirement has no critical effect on the design.
6. The same holds for landing safely in case one of the parafoil attachment lines fails (P2-Mis-4-3-3). Due to this requirement and the fact that not all disturbance requirements were researched, the requirement on handling disturbances is also not met (P2-Mis-4-3). It is however expected that these non-researched requirements will be met and as explained previously parafoil line failure is not critical, thus making sure that not meeting the disturbance requirement is a non-critical part of the compliance matrix.

Assessing the complete compliance matrix in appendix B leads to the conclusion that, keeping in mind the points mentioned above, Parashuttle 2 adequately fulfils all requirements imposed on it. The product is able to fulfil the need statement expressed in the introduction and does so at a reasonable price.

Chapter 30 | Design evaluation

With the final design of Parashuttle 2, the result of 10 weeks of work by the groups' ten members, having been presented in the previous chapter a reflection can be done on the design process followed. This project was the first complete design project for all team-members and has proved a real learning experience for all.

An initial design strategy was given in Figure 11.1 in chapter 11, this was a first idea of how the group would tackle the problems the design of such a complex product posed. Looking back at the design process this scheme has been adhered to well. Allocating different group members to the design of specific subsystems while keeping in mind the interrelations between the components has worked well, though it has been found that extensive communication was required to prevent design errors. Good communication was ensured through regular meetings and shared documents.

Deviations from the initial planning were also encountered, the iteration specified in Figure 11.1 was not followed as such. At the start of the project the team had not anticipated the uncertainties faced, instead thinking that at some stage a design mass would be obtained which could be iterated. In reality uncertainties made it hard to perform such an iteration and it proved more beneficial to optimise the design for range and endurance. This iteration did lead to a redesign of the fuel tank, therefore the iteration arrow of Figure 11.1 was partly followed.

This does not mean that iterations were not gone through during this project however, instead multiple iterations were gone through on a subsystem level. These iterations are presented in Table 30.1 below. It should be noted that in this report only final values have been given, so values before these iterations are not mentioned.

Table 30.1: The iterations performed in this design process, with their causes and effects.

Iteration	Reason	Change
Wheels	The wheels chosen initially were too large for them to rotate within the floats during turning. Additionally mounting the big wheels would provide major challenges.	Decreased the size of the tires.
Wheel fairing	The initial wheel fairings did not allow the vehicle to drive up a 15° ramp. Instead the fairings would bump into the ramp.	The wheel fairings were remodelled for land clearance.
Float positioning	Analysis showed the vehicle was close to toppling over when in crosswind with a person on the float.	The floats have been moved further apart for additional lateral stability.
Fuselage impact load case	Analysis showed the initial fuselage structure would fail during impact.	The cross-sectional dimensions of trusses have been increased.
Fuselage skin	The main stakeholder expressed his desire for a more aesthetic design	The fuselage skin was moved to the outside of the truss structure, rather than the inside.
Door	Due to the change in the positioning of the fuselage skin, the previously chosen hinge line could not be used anymore.	A new hinge line for the door was chosen and an accompanying mechanism was designed.

Continued on next page.

Table 30.1 – continued from previous page.

Iteration	Reason	Change
Pilot controls	In the initial system the application of feet controls induced unwanted forces on the arm controls.	The mechanism behind the feet control system was changed.
Fuel system	It was decided to use left-over mass to increase range and endurance.	The fuel tank was increased in size to accomodate extra fuel.

Not only has the team learnt to come up with a technical design during this project, the team has also gained experience in managing such a project. Organisational roles have been assigned to all team members, who have taken up and executed these roles well. Besides the team has experienced the involvement of a stakeholder in such a project. Initially it was thought that communication between the stakeholder and a design team would mostly be initiated by the latter, however during this project the stakeholder has often brought in novel concepts and ideas. Though due to technical reasons not all of these suggestions could be implemented in the design, all input was greatly appreciated.

A final learning point of this project has been the dealing with unexpected twists and turns in the design process. Though careful planning was done before the start of the project, work was done according to predefined schemes and active communication was practised, minor setbacks (miscommunication, required redesigns etc.) were still encountered. Dealing with such issues required the ability to improvise or change existing plans and the team has been able to do so.

In the end the team has foremost enjoyed working on this design of Parashuttle 2 and is satisfied with the product come up with. All major requirements have been met whilst making a product which is only slightly over the intended production price. When one day Parashuttle 2 is in full production, the team would love to take it for a ride.

References

[1] F. Cohen et al. "Finding everland: Flight fantasies and the desire to transcend mortality". In: *Journal of Experimental Social Psychology* 47.1 (2011), pp. 88 –102. ISSN: 0022-1031. DOI: 10.1016/j.jesp.2010.08.013.

[2] S. Garth et al. *Ovid's Metamorphoses in fifteen books - Volume 2*. Printed for J. Tonson, 1717, pp. 262–266.

[3] J. L. Heilbron and W. F. Bynum. "1903 and all that". In: *Nature* 6918 (2003), 15–18. DOI: 10.1038/421015a.

[4] L.K. Loftin. *Quest for performance: The evolution of modern aircraft*. 468. Scientific and Technical Information Branch, National Aeronautics and Space Administration, 1985.

[5] International Air Transport Association. "2012 Annual Review". In: *68th Annual General Meeting*. International Air Traffic Association. June 2012.

[6] L.T. Tan and K.H. Tan. "Alternative air vehicles for sterile insect technique aerial release". In: *Journal of Applied Entomology* (2011), pp. 7–11. ISSN: 1439-0418. DOI: 10.1111/j.1439-0418.2011.01649.x.

[8] D.M. Atherstone et al. *DSE Parashuttle 2 - Baseline Report*. Tech. rep. Internal Document. Delft University of Technology, May 2013.

[9] D.M. Atherstone et al. *DSE Parashuttle 2 - Mid-Term Report*. Tech. rep. Internal Document. Delft University of Technology, May 2013.

[16] *FAA Data and Statistics*. Federal Aviation Administration. 2011. URL: http://www.faa.gov/data_research/aviation_data_statistics/civil_airmen_statistics/2011/ (Retrieved 04/26/2013).

[17] *FAA Sports Licenses*. Federal Aviation Administration. 2012. URL: http://www.faa.gov/licenses_certificates/airmen_certification/sport_pilot/ (Retrieved 04/26/2013).

[18] *Micro Light Aeroplanes (Regeling MLA's)*. Anonymous. 2013. URL: http://wetten.overheid.nl/BWBR0015237/geldigheidsdatum_21-01-2013 (Retrieved 04/26/2013).

[19] Dr. ir. Mark Voskuijl. "Project Guide Design Synthesis Exercise". TU Delft Internal document. Apr. 2013.

[20] T.I. Hailey. "The powered parachute as an archaeological aerial reconnaissance vehicle". In: *Archaeological Prospection* 12.2 (2005), pp. 69–78. ISSN: 1099-0763. DOI: 10.1002/arp.247.

[21] R.W. Graham, R.E. Read, and J. Kure. "Small format microlight surveys". In: *ITC Journal* 1 (1985), pp. 14–20.

[22] S. Shafiee and E. Topal. "When will fossil fuel reserves be diminished?" In: *Energy Policy* 37.1 (2009), pp. 181 –189. ISSN: 0301-4215.

[23] J. Noguera. "Oil prices: Breaks and trends". In: *Energy Economics* 37.0 (2013), pp. 60 –67. ISSN: 0140-9883. DOI: 10.1016/j.eneco.2012.12.008.

[24] Y. Yang et al. "New Nanostructured Li2S/Silicon Rechargeable Battery with High Specific Energy". In: *Nano Letters* 10.4 (2010), pp. 1486–1491. DOI: 10.1021/nl100504q.

[25] J.L. Pereira. "Hover and wind-tunnel testing of shrouded rotors for improved micro air vehicle design". MA thesis. University of Maryland, 2008.

[26] H. Ginsberg. "Development of aircraft with parachute, parafoil, or flexible wings". In: *13th AIAA Aerodynamic Deecelerator Systems Technology Conference*. 95-1577. American Institute of Aeronautics and Astronautics. 1995, p. 242.

[27] G.J.J. Ruijgrok. *Elements of airplane performance*. VSSD, 2009.

[28] W. Dobrzynski et al. *Propeller Noise Tests in the German-Dutch Wind Tunnel DNW*. Tech. rep. Federal Aviation Administration and Deutschen Zentrums für Luft- und Raumfahrt, Dec. 1986.

[29] C.A. Lyon et al. *Summary of Low-Speed Airfoil Data - Volume 3*. SoarTech Publications, 1997.
[30] J.R. Chambers. "Longitudinal dynamic modelling and control of Powered Parachute Aircraft". MA thesis. Rochester University of Technology, Apr. 2007.
[32] J.S. Lingard. "The aerodynamics of gliding parachutes". In: *AIAA Paper* 2427 (1986).
[34] L. Larsson and R.E. Eliasson. *Principles of Yacht Design*. 2nd ed. McGraw-Hill, 2000.
[36] A.L. Canamar. "Seaplane conceptual design and sizing". MA thesis. University of Glasgow, 2012.
[38] Anonymous. *Hullspeed Windows version 15 user manual*. Formation Design Systems Pty Ltd. 2009.
[39] R. López I. Ortigosa and J. García. "Prediction of total resistance coefficients using neural networks". English. In: *Journal of Maritime Research* 6.3 (2009), pp. 15–26. ISSN: 1697-4840.
[40] Brett Murie Michel de Vos and Viliami Siale. *A critical analysis of resistance prediction using regression methods for high speed hull forms*. Tech. rep. Australian Maritime Engineering CRC Ltd, 2005.
[41] *FluentCFDGuide*. Ansys. 2010.
[42] H.H.K. Versteeg and W. Malalasekera. *An Introduction to Computational Fluid Dynamics: The Finite Volume Method*. Pearson Education Limited, 2007. ISBN: 9780131274983.
[43] J.D. Anderson. *Fundamentals of Aerodynamics*. 4th. McGraw-Hill New York, 2007. ISBN: 007-125408-0.
[44] I.H.A. Abbott and A.E. Von Doenhoff. *Theory of Wing Sections: Including a Summary of Airfoil Data*. Dover Books on Aeronautical Engineering Series. Dover publications Incorporated, 1959. ISBN: 9780486605869.
[47] J. Roskam. *Airplane Design part II: Preliminary Sizing of Airplanes*. Airplane design. Darcorporation, 1989. ISBN: 9781884885426.
[48] T.A. Ward. *Aerospace Propulsion Systems*. John Wiley & Sons, 2010. ISBN: 9780470824979.
[49] J. Stack. *Tests of airfoils designed to delay the compressibility burble*. Tech. rep. National Advisory Committee for Aeronautics, 1939.
[50] A. Brocklehurst and G.N. Barakos. "A review of helicopter rotor blade tip shapes". In: *Progress in Aerospace Sciences* 56.0 (2013), pp. 35 –74. ISSN: 0376-0421. DOI: 10.1016/j.paerosci.2012.06.003.
[51] Anonymous. *Operations manual for engine types Rotax 447, 503 and 582*. Rotax aircraft engines. 1999. URL: http://www.rotaxservice.com/documents/582perf.pdf.
[52] P.A. Smith. "2.04 - Carbon Fiber Reinforced Plastics—Properties". In: *Comprehensive Composite Materials*. Ed. by A. Kelly and C. Zweben. Oxford: Pergamon, 2000, pp. 107 –150. ISBN: 978-0-08-042993-9. DOI: 10.1016/B0-08-042993-9/00072-3.
[53] R.F.J. McCarthy, G.H. Haines, and R.A. Newley. "Polymer composite applications to aerospace equipment". In: *Composites Manufacturing* 5.2 (1994), pp. 83 –93. ISSN: 0956-7143. DOI: 10.1016/0956-7143(94)90059-0.
[55] F.M. de Piolenc and G.E. Vright Jr. *Ducted Fan Desing, Volume 1 (Revised)*. Marc de Piolenc, 2001, p. 170.
[56] H.H. Hubbard and United States National Advisory Committee for Aeronautics. *Sound Measurements for Five Shrouded Propellers at Static Conditions*. Technical note. National Advisory Committee for Aeronautics, 1950.
[57] S. Yilmaz, D. Erdem, and M. Kavsaogly. "Effects of Duct Shape on a Ducted Propeller Performance". In: *51st AIAA Aerospace sciences meeting including the new horizons forum and aerospace exposition*. AIAA. 2013.
[58] W.J. McCroskey. *A critical assessment of wind tunnel results for the NACA 0012 airfoil*. Tech. rep. DTIC Document, 1987.
[59] G.A. Keoleian et al. "Application of life cycle inventory analysis to fuel tank system design". English. In: *The International Journal of Life Cycle Assessment* 3.1 (1998), pp. 18–28.

ISSN: 0948-3349. DOI: 10.1007/BF02978446. URL: http://dx.doi.org/10.1007/BF02978446.

[60] P.J. Alvarado. "Steel vs. plastics: the competition for light-vehicle fuel tanks". In: *JOM Journal of the Minerals, Metals and Materials Society* 48.7 (1996), pp. 22–25.

[61] L. Cheng et al. "Simulation and Analysis of Crashworthiness of Fuel Tank for Helicoptersx". In: *Chinese Journal of Aeronautics* 20.3 (2007), pp. 230 –235. ISSN: 1000-9361. DOI: 10.1016/S1000-9361(07)60037-5. URL: http://www.sciencedirect.com/science/article/pii/S1000936107600375.

[62] J.A. Brydson. *Plastics Materials*. 7th. Butterworth-Heinemann, 1999. ISBN: 978-0-7506-4132-6.

[63] M. Ward, S. Culpepper, and M. Costello. "Parafoil Control Using Payload Weight Shift". In: (2012). DOI: 10.2514/6.2012-4738.

[64] L. Veldhuis and B.W. van Oudheusden. *Aerodynamics I - AE2102*. University Lecture. 2010.

[65] M.P. Potjer. *DAR exercise: Parashuttle Performance*. Tech. rep. Delft University of Technology, 2010.

[66] J.A. Mulder et al. "Flight Dynamics: Lecture notes". TU Delft Internal document. Mar. 2013.

[67] R.C. Hibbeler. *Mechanics of Materials*. Prentice Hall, 2010. ISBN: 9810685092.

[73] D. Karnopp. *Vehicle Stability*. Dekker Mechanical Engineering, 2004. ISBN: ISBN 0-8247-5711-4.

[74] J. Roskam. *Airplane design part IV: Layout of landing gear and systems*. DARcorporation, 2002, p. 31. ISBN: 1-884885-53-5.

[75] TNC-CDAAR. *Hand Grip Strength*. Sept. 2003. URL: http://cdaar.tufts.edu/protocols/Handgrip.pdf (Retrieved 06/11/2013).

[76] C. Bertorello et al. *Trimaran Model Test Results and Comparison with Different High Speed Craft*. Tech. rep. Cooperation of Università di Napoli Federico II, Università di Genova and Università di Trieste, 2001.

[77] K. Potgieter. "Understanding Design and Performance of Stepped Hulls". retrieved from (http://www.navaldesign.co.za/articles.html) on 31-05-2013 and recommended by Prof. Ir. Hopman (Maritime Engineering).

[78] D.P. Raymer. *Aircraft Design, A Conceptual Approach*. AIAA Education Series. American Institute of Aeronautics and Astronautics, Inc., 1992.

[79] M. Langley. *Seaplane float and hull design*. London, United Kingdom: Sir Isaac Pitman & Sons, LTD., 1935, p. 65.

[80] K.M. Tomaszewski. *Hydrodynamic Design of Seaplanes Floats*. Tech. rep. Ministry of Supply. Aeronautical Research Council, 1950.

[81] I. Dathe and M. de Leo. "Hydrodynamic Characteristics of Seaplanes as Affected by Hull Shape Parameters". In: *A.I.A.A. Advance Marine Vehicles Journal* (1989).

[82] F. Vargas. *Concept Design of Seaplane Floats*. Tech. rep. Department of Aerospace Engineering, University of Glasgow, 2011.

[83] D.J Brimm. *Seaplanes: Maneuvering, Maintaining, Operating*. Pitman Publishing Corporation, 1937, p. 173.

[84] T.H. van Karman. *The impact on seaplane floats during landing*. Tech. rep. NACA-TN-321. Aerodynamical Institute of the Technical high school, Aachen, Oct. 1929.

[85] W.C. Hugli Jr. and W.C. Axt. *Hydrodynamic Investigation of a Series of Hull Models Suitable for Small Flying Boats and Amphibians*. Tech. rep. Stevens Institute of Technology.

[91] *Non-Circular Pressure Vessels*. Tech. rep. 1981. URL: http://www.gowelding.com/pv/square.pdf.

[92] Prof. G. Kempf. *Manoeuvrability*. 1960. URL: http://ittc.sname.org/proc9/Manoeuvrability.pdf (Retrieved 06/18/2013).

[93] L. Larsson and R.E. Eliasson. *Principles of yacht design*. second. International Marine, 1994, pp. 96–130.

[94] D.S. Miklosovic et al. "Leading-edge tubercles delay stall on humpback whale (Megaptera novaeangliae) flippers". In: *Physics of Fluids* 16.5 (2004).
[95] H. Johari et al. "Effects of Leading-Edge Protuberances on Airfoil Performance". In: *AIAA Journal* 45.11 (2007). DOI: 10.2514/1.28497.
[96] Federal Aviation Administration. *Seaplane, Skiplane and Float/Ski Equipped Helicopter Operations Handbook*. 2004.
[97] T. H. G. Megson. *Aircraft Structures for engineering students*. fourth. Elsevier Ltd., 2009.
[98] J. Roskam. *Airplane Design: Preliminary Calculations of Aerodynamic, Thrust and Power Characteristics*. Airplane Design. Darcorporation, 2000. ISBN: 9781884885525.
[99] J.R. Watson and J. Derck. *Rudder blades and centerboards*. Tech. rep. Gougeon Brothers, inc, 2002. URL: http://www.jamestowndistributors.com/userportal/pdfs/WestSystem/Rudder_Blades_and_Centerboards_000_448.pdf (Retrieved 06/19/2013).
[105] *EASA CS-VLA*. European Aviation Safety Agency. 2009. URL: http://www.easa.europa.eu/agency-measures/docs/certification-specifications/CS-VLA/CS-VLA%20%20Amdt%201%20combined.pdf (Retrieved 05/01/2013).
[111] G.J. Brown. "Parafoil steady turn response to control input". In: *12th RAeS/AIAA Aerodynamic Decelerator Systems Technology Conference and Seminar*. London, United Kingdom, 1993, pp. 248–254.
[113] P.B.S. Lissaman and G.J. Brown. "Apparent mass effects on parafoil dynamics". In: *RAeS/AIAA Aerodynamic Decelerator Systems Technology Conference and Seminar, 12 th, London, United Kingdom*. 1993, pp. 233–239.
[114] O. Prakash, A. Daftary, and N. Ananthkrishnan. "Trim and Stability Analysis of Parafoil/Payload System using Bifurcation Methods". In: *AIAA 18th Aerodynamic Decelerator Systems Technology Conference and Seminar, AIAA*. Vol. 1666. 2005.
[115] C. Matos et al. "Wind tunnel measurements of Parafoil Geometry and Aerodynamics". In: *AIAA Paper* (1998), pp. 98–0606.
[116] V. Kalro et al. "Parallel finite element simulation of large ram-air parachutes". In: *International journal for numerical methods in fluids* 24.12 (1997), pp. 1353–1369.
[117] J.S. Lingard. "Ram-air parachute design". In: *Precision Aerial Delivery Seminar, 13th AIAA Aerodynamic Decelerator Systems Technology Conference*. 1995.
[118] C.M. Madsen and C.J. Cerimele. "Flight performance, aerodynamics, and simulation development for the X-38 parafoil test program". In: *AIAA Paper* 2108 (2003), pp. 19–22.
[119] J. Kim and C. Park. "Wind power generation with a parawing on ships, a proposal". In: *Energy* 35.3 (2010), pp. 1425 –1432. ISSN: 0360-5442. DOI: 10.1016/j.energy.2009.11.027. URL: http://www.sciencedirect.com/science/article/pii/S0360544209005167.
[120] Anonymous. *Standard Specification for Design and Performance Requirements for Powered Parachute Aircraft*. Tech. rep. F2244 – 10. ASTM International, 2010.
[121] O.A. Bauchau and J.I. Craig. *Structural Analysis: With Applications to Aerospace Structures*. Springer, 2009.
[122] S. Timoshenko, S. Woinowsky-Krieger, and S. Woinowsky. *Theory of plates and shells*. Vol. 2. McGraw-hill New York, 1959.
[123] Eduard Ventsel and Theodor Krauthammer. *Thin Plates and Shells Theory, Analysis, and Applications*. Marcel Dekker, Inc, 2001.
[124] Vasilij Zacharovič Vlasov. *General theory of shells and its applications in engineering*. National Aeronautics and Space Administration, 1964.
[125] Y.A. Çengel and J.M. Cimbala. *Fluid mechanics: fundamentals and applications*. McGraw-Hill Series in Mechanical Engineering. McGraw-Hill Higher Education, 2006. ISBN: 9780072472363.
[126] C.P. van Dam. "Recent experience with different methods of drag prediction". In: *Progress in Aerospace Sciences* 35.8 (1999), pp. 751 –798. ISSN: 0376-0421. DOI: 10.1016/S0376-0421(99)00009-3.
[127] S.F. Hoerner. *Fluid-dynamic drag: practical information on aerodynamic drag and hydrodynamic resistance*. Hoerner Fluid Dynamics, 1965.

[128] E. Torenbeek. *Synthesis of Subsonic Airplane Design: An Introduction to the Preliminary Design of Subsonic General Aviation and Transport Aircraft, with Emphasis on Layout, Aerodynamic Design, Propulsion and Performance*. Springer, 1982. ISBN: 9789024727247.
[129] W.S. Diehl. *Tests on Airplane Fuselages, Floats and Hulls*. Tech. rep. Bureau of Aeronautics, 1926.
[130] W.R. Santschi, J. DuBois, and C. Omoto. *Moments of Inertia and Centres of Gravity of the Living Human Body*. Tech. rep. AD0410451. May 1963.
[131] R.C. Hibbeler. *Engineering Mechanics: Statics*. Engineering Mechanics. Prentice Hall, 2010. ISBN: 9810681348.
[132] A.K. Kundu. *Aircraft Design*. Cambridge University Press, 2010. ISBN: 9781139487450.
[133] J.E. Made and D.W. Kurtz. "A Review of Aerodynamic Noise From Propellers, Rofors, and Liff Fans". In: (1970).
[134] Prof. dr. D.G. Simons. *Elements of aviation acoustics - Airplane Noise Sources*. University Lecture. 2013.
[137] W. Dabelstein et al. *Automotive Fuels*. Wiley-VCH Verlag GmbH & Co. KGaA, 2000. ISBN: 9783527306732. DOI: 10.1002/14356007.a16_719.pub2.
[138] Ir. J.A. Melkert. *AE1105 Sustainable Development - Alternative Aviation Fuels*. University Lecture. 2010.
[139] Charles L. Peterson and Todd Hustrulid. "{CARBON} {CYCLE} {FOR} {RAPESEED} {OIL} {BIODIESEL} {FUELS}". In: *Biomass and Bioenergy* 14.2 (1998), pp. 91 –101. DOI: http://dx.doi.org/10.1016/S0961-9534(97)10028-9.
[140] Anonymous. *EASA CS-LSA*. EASA. 2011. (Retrieved 05/01/2013).
[145] P. Schwarzmann and A. Illing. *Thermoforming: A Practical Guide*. Hanser Gardner Publications, 2001. ISBN: 9781569902752.
[146] J. Owen et al. *Integrated Design and Manufacture Using Fibre-Reinforced Polymeric Composites*. Integrated Design and Manufacture Using Fibre-reinforced Polymeric Composites. Woodhead, 2000. ISBN: 9781855734531.
[149] *Introduction to thermoforming*. crclarke. 2013. URL: http://www.crclarke.co.uk/products/PDF/data/1plastic.pdf (Retrieved 06/19/2013).
[151] V.P. Brugemann. *Design and Construction*. University Reading. 2013.
[153] S. Mazumdar. *Composites Manufacturing: Materials, Product, and Process Engineering*. Mechanical engineering: Materials science. Taylor & Francis, 2001. ISBN: 9780849305856.
[159] J. Sinke. *Organisation of the production process*. University Reading. 2013.
[160] K. Hartley. "The Learning Curve and Its Application to the Aircraft Industry". English. In: *The Journal of Industrial Economics* 13.2 (1965), pp. 122–128. ISSN: 00221821. URL: http://www.jstor.org/stable/2097667.
[161] *Experimental Aircraft*. BRS Aerospace. URL: http://www.brsparachutes.com/experimental_aircraft.aspx (Retrieved 06/18/2013).
[162] Anonymous. *British Civil Airworthiness Requirements Section S - Small Light Aeroplanes*. Tech. rep. Civil Aviation Authority, 2009.
[168] G. Schuh, R. Neugebauer, and E. Uhlmann. *Future Trends in Production Engineering: Proceedings of the First Conference of the German Academic Society for Production Engineering (WGP), Berlin, Germany, 8th-9th June 2011*. Springer, 2013. ISBN: 9783642244919.
[171] *Woodworking Plans & Tools*. Woodcraft. 2013. URL: http://www.woodcraft.com/ (Retrieved 06/20/2013).
[173] B. Fox et al. *Test and evaluation trends and costs for aircraft and guided weapons*. Tech. rep. DTIC Document, 2004.
[174] Eurostat. *Illustrated Glossary for Transport Statistics*. Publication Office of the European Union, 2009. ISBN: 978-92-79-17082-9.
[175] *Indices & Data | Human Development Index*. United Nations Development Programme. 2012. URL: http://hdr.undp.org/en/statistics/ (Retrieved 05/01/2013).
[176] *Regeling Voertuigen*. Anonymous. 2013. URL: http://wetten.overheid.nl/BWBR0025798/geldigheidsdatum_01-05-2013 (Retrieved 05/01/2013).

[177] *Dimensions of road-legal trailers in the U.S.* American Automobile Association. 2012. URL: http://drivinglaws.aaa.com/laws/trailer-dimensions/ (Retrieved 05/01/2013).

[178] *Towing with a car - GOV.UK*. Anonymous. 2013. URL: https://www.gov.uk/towing-with-car/driving-licence-rules-and-what-you-can-tow (Retrieved 05/01/2013).

[179] *NTTA - Trailer Law - Trailer Maximum Dimension*. NTTA. 2013. URL: http://www.ntta.co.uk/law/law/dimensions.aspx (Retrieved 05/01/2013).

[180] D.L. Johnson and W.W. Vaughan. "Terrestrial environment (climatic) criteria handbook for use in aerospace vehicle development". In: *11th AMS Conference on Aviation, Range, and Aerospace Meteorology*. NASA. Oct. 2000.

[181] K.B. Pandoff, R.E. Burr, and United States. Dept. of the Army. Office of the Surgeon General. *Medical aspects of harsh environments*. Medical Aspects of Harsh Environments Volume 2. Office of the Surgeon General, United States Army, 2002, p. 1012. ISBN: 9780160511844.

Other sources

[7] L.J. Doensen. *Parashuttle website*. 2013. URL: http://www.parashuttle.nl/Welcome.html (Retrieved 05/22/2013).

[10] *How many pilots worldwide?* Paragliding Forum. 2011. URL: http://www.paraglidingforum.com/viewtopic.php?p=p14428 (Retrieved 04/25/2013).

[11] *La fédération Française de Vol Libre*. La fédération Française de Vol Libre. 2003. URL: http://federation.ffvl.fr/ (Retrieved 04/26/2013).

[12] *Xtreme BigAir community forum*. Xtreme BigAir. 2012. URL: http://xtremebigair.com/ (Retrieved 04/26/2013).

[13] *Deutscher Hängegleiterverband e.V.* Deutscher Hängegleiterverband e.V. 2003. URL: http://www.dhv.de/web/ (Retrieved 04/26/2013).

[14] *U.S. Hang Gliding and Paragliding Association*. The United States Hang Gliding and Paragliding Association. 2004. URL: http://www.ushpa.aero/default.asp (Retrieved 04/26/2013).

[15] *Hang Gliding and Paragliding Association of Canada*. Hang Gliding and Paragliding Association of Canada. 2004. URL: http://www.hpac.ca/pub/ (Retrieved 04/26/2013).

[31] Anonymous. *Rotax 582 Engine Specifications*. Rotax aircraft engines. 1999.

[33] *Frame3DD - Static and dynamic structural analysis of 2D and 3D frames*. URL: http://frame3dd.sourceforge.net/ (Retrieved 06/04/2013).

[35] *Hydromax FAQ*. Formation Design Systems Pty Ltd. URL: http://www.floats.cz/english/prices/prices.htm (Retrieved 06/19/2013).

[37] Anonymous. "Resistance of ships". Lecture from Técnico Lisboa. URL: https://dspace.ist.utl.pt/bitstream/2295/1015486/1/RP_Lecture6and7.pdf.

[45] Anonymous. *Power drive system specification*. Rotax engines. 2013. URL: http://www.rotaxservice.com/ (Retrieved 05/02/2013).

[46] *Rotax 582 UL DCDI 65HP - Power drive system specification*. Rotax. 2013. URL: http://www.rotaxservice.com/rotax_engines/rotax_582UL.htm (Retrieved 06/07/2013).

[54] *POWERFIN Home*. Powerfin Propellers. 2011. URL: http://powerfin.com/home.html (Retrieved 06/04/2013).

[68] *Cessna 120 prices*. Sky-craft limited. URL: http://www.sky-craft.co.uk/acatalog/Skycraft_Parts_For_Cessna_Aircraft.html (Retrieved 06/17/2013).

[69] *Products*. McFarlane Aviation. URL: http://www.mcfarlane-aviation.com/Products/?CategoryID=47 (Retrieved 06/10/2013).

[70] *Friction coefficients*. Anonymous. URL: http://buildingcriteria2.tpub.com/ufc_4_152_01/ufc_4_152_010141.htm (Retrieved 06/10/2013).

[71] *Material properties*. AK steel. URL: http://www.aksteel.com/pdf/markets_products/stainless/austenitic/304_304L_Data_Sheet.pdf (Retrieved 06/16/2013).

[72] *Control cable prices*. Sky-craft limited. URL: http://www.sky-craft.co.uk/acatalog/Skycraft_Home_Builder_Permit_Aircraft_Control_Cable.html (Retrieved 06/17/2013).

[86] Inc. Aerocet. *Maintenance manual and instructions for continued airworthiness for Aerocet model 2200 twin seaplane floats installed on a super cub airplane*. Apr. 2009. URL: http://www.aerocet.com/files/A-10035_Rev03_110513.pdf (Retrieved 06/16/2013).

[87] Mead floats Inc. *MEAD M-1430 Amphibious Float*. URL: http://meadfloats.com/wp-content/uploads/1430A-Spec-Sheet-2012.pdf (Retrieved 06/16/2013).

[88] *STOL CH 701 performance*. Zenith air. URL: http://www.zenithair.com/stolch701/7-perf.html (Retrieved 06/19/2013).

[89] *Aqua Floats for LSA*. Aqua float. 2005. URL: http://www.aquafloat.com/kitaqua.html (Retrieved 06/04/2013).

[90] *2200 Amphibious*. Clamar Floats. 2013. URL: http://www.clamarfloats.com/2200a.htm (Retrieved 06/04/2013).
[100] *Wichard 2013 Catalogue - English*. Wichard. 2013. URL: http://www.wichard.com/images/info_pages/catalogue-eng-light-124.pdf (Retrieved 06/11/2013).
[101] *Petzl AM'D Carabiner*. Petzl. 2013. URL: http://www.petzl.com/en/outdoor/locking-carabiners/amd (Retrieved 06/11/2013).
[102] *Petzl AM'D Locking Carabiner*. Backcountry. 2013. URL: http://www.backcountry.com/petzl-amd-triact-locking-carabiner (Retrieved 06/11/2013).
[103] *Aeronautical Radio Station Operator's Guide*. Civil Aviation Authority. 2012. URL: http://www.caa.co.uk/docs/33/CAP452.PDF (Retrieved 06/06/2013).
[104] *Black Max - Comfortlite Seats*. Black Max. 2003. URL: http://www.blackmaxbrakes.com/comfortlite-seat (Retrieved 06/06/2013).
[106] *Genesis selection guide*. Genesis. 2013. URL: http://www.enersysreservepower.com/documents/US-GPL-SG-002_0706.pdf (Retrieved 06/21/2013).
[107] *Rotax - Installation Manual*. Rotax. 1999. URL: http://www.rotax-aircraft-engines.com/portaldata/5/dokus/d00287.pdf (Retrieved 06/24/2013).
[108] *Electrical interior lighting*. Aircraft Spruce. 2013. URL: http://www.aircraft-spruce.com/menus/el/interiolighting.html (Retrieved 06/21/2013).
[109] *Electrical exterior lighting*. Aircraft Spruce. 2013. URL: http://www.aircraft-spruce.com/menus/el/whelen_exteriorlighting.html (Retrieved 06/21/2013).
[110] *Car chargers 12V*. Ebay. 2013. URL: http://www.ebay.com/bhp/car-charger-12v-2a (Retrieved 06/21/2013).
[112] S. Vellekoop. *Groene kite energie*. http://www.vliegerop.com/UserFiles/File/Peter%20Lynn%2050%20meter%20kite.pdf. Published in Kitesurf Magazine.
[135] *Instruction Manual - Dynamic Voyageur II*. Delta Trikes Aviation. URL: http://www.ul-bolaget.se/english/instructionvoy.pdf (Retrieved 06/14/2013).
[136] *Bad-Ass Biofuel Snow Speeder Headed to Antarctica*. 2010. URL: http://www.wired.com/autopia/2010/08/bio-inspired-ice-vehicle/ (Retrieved 05/22/2013).
[141] *Maintenance manual Rotax engine*. Rotax. URL: http://www.rotax-aircraft-engines.com/portaldata/5/dokus/d00288.pdf (Retrieved 06/11/2013).
[142] *Service manual for wipline model 4000 amphibious and seaplane floats*. Wipaire. URL: http://www.wipaire.com/pdf/service_manuals/1002552.pdf (Retrieved 06/11/2013).
[143] *Maintenance*. Mac Para Technology. URL: http://www.macpara.com/en/maintenance.html (Retrieved 06/19/2013).
[144] *GA-12*. EAM Aviation. 2013. URL: http://www.theraft.com/vest-general/ga-12 (Retrieved 06/07/2013).
[147] *Plastic welding | Welding | Northern tools + equitment*. Northerntools. 2013. URL: http://www.northerntool.com/shop/tools/category_welding+plastic-welding (Retrieved 06/20/2013).
[148] *Pkate Bending Rolss, Sheet Metal Slip Rolling Machines*. American machine tools. 2012. URL: http://www.americanmachinetools.com/bending_rolls.htm (Retrieved 06/20/2013).
[150] *Aluminium sheet cutting machine*. Alibaba. 2013. URL: http://www.alibaba.com/product-gs/902013220/Large_format_laser_1325_cheap_laser.html (Retrieved 06/20/2013).
[152] *High speed Full automatic foam cutting machine*. Alibaba. 2013. URL: http://www.alibaba.com/product-gs/676354460/High_speed_Full_automatic_foam_cutting.html (Retrieved 06/20/2013).
[154] *Lightning Experimental kit*. Arion Aircraft. URL: http://www.flylightning.net/lightning-esp.html (Retrieved 06/18/2013).
[155] *Easy does it*. Paraplanes. URL: http://www.flying-directory.com/0809/images/e-wdla0809-paraplane.pdf (Retrieved 06/18/2013).

[156] *Zenith CH 750 Cruzer*. Zenith. URL: http://www.zenithair.com/stolch750/index-cruzer.html (Retrieved 06/18/2013).
[157] *Sky Raider LLC*. Sky Raider. URL: http://skyraiderllc.com/main.htm (Retrieved 06/18/2013).
[158] *X-air ultralight aircraft kit*. Aurstralian flying. URL: http://www.australianflying.com.au/classifieds/x-air-ultralight-aircraft-kit (Retrieved 06/18/2013).
[163] *Labour costs EU*. Eurostat. URL: http://epp.eurostat.ec.europa.eu/cache/ITY_PUBLIC/3-10042013-AP/EN/3-10042013-AP-EN.PDF (Retrieved 06/19/2013).
[164] *Lasser vacatures*. Indeed. 2013. URL: http://www.indeed.nl/vacature-bekijken?jk=7ec24565762055f4&q=Lasser&tk=17tiu61m214517h6&from=web (Retrieved 06/21/2013).
[165] *Loonkosten voor de werkgever*. berekenhet. 2013. URL: http://www.berekenhet.nl/ondernemen/loonkosten-werkgever.html (Retrieved 06/21/2013).
[166] *The Thermoforming Process Compared with Injection Molding*. Productive plastics. 2013. URL: http://www.productiveplastics.com/processes.asp (Retrieved 06/19/2013).
[167] *Price thermoforming machines*. Alibaba. 2013. URL: http://www.alibaba.com/products/F0/price_thermoforming_machines/CID147111----------1239-6927,1213-2468,1238-5430.html (Retrieved 06/19/2013).
[169] *Rivets from Northern tools + equitment*. Northerntools. 2013. URL: http://www.northerntool.com/shop/tools/NTESearch?storeId=6970&ipp=24&Ntt=rivets (Retrieved 06/20/2013).
[170] *Multiprocess welders|Welding|Northern tools + equitment*. Northerntools. 2013. URL: http://www.northerntool.com/shop/tools/NTESearch?storeId=6970&ipp=24&Ntt=rivets (Retrieved 06/20/2013).
[172] *Huurprijzen bedrijfsruimte*. Casadata. Mar. 15, 2013. URL: http://www.casadata.nl/Default.aspx?wtId=5927 (Retrieved 06/19/2013).
[182] *Alinco DR-635 Mobilogoon*. Portoshop. 2013. URL: http://www.portoshop.nl/alinco-mobilofoon-p-413.html (Retrieved 06/06/2013).
[183] *MGL Avionics V10 VHF Aviation Radio Transceiver*. MGL Avionics. 2001. URL: http://www.mglavionics.com/html/radios.html (Retrieved 06/06/2013).
[184] *Singels*. MGL Avionics. 2001. URL: http://www.mglavionics.com/html/singles.html (Retrieved 06/06/2013).
[185] *Stratomaster Instrument Price List*. Heavenbound Aviation. 2008. URL: http://www.heavenboundaviation.com/andystratomaster1PRICES.htm (Retrieved 06/06/2013).
[186] *Xtreme EFIS*. MGL Avionics. 2001. URL: http://www.mglavionics.com/html/xtreme_efis.html (Retrieved 06/06/2013).

Appendix A | Functionality diagrams

In this appendix the functional breakdown structure and functional flow diagrams, as referred to in chapter 4, are shown. The functional breakdown structure is shown in Figure A.1, the functional flow diagrams are shown in figures A.2 through A.7.

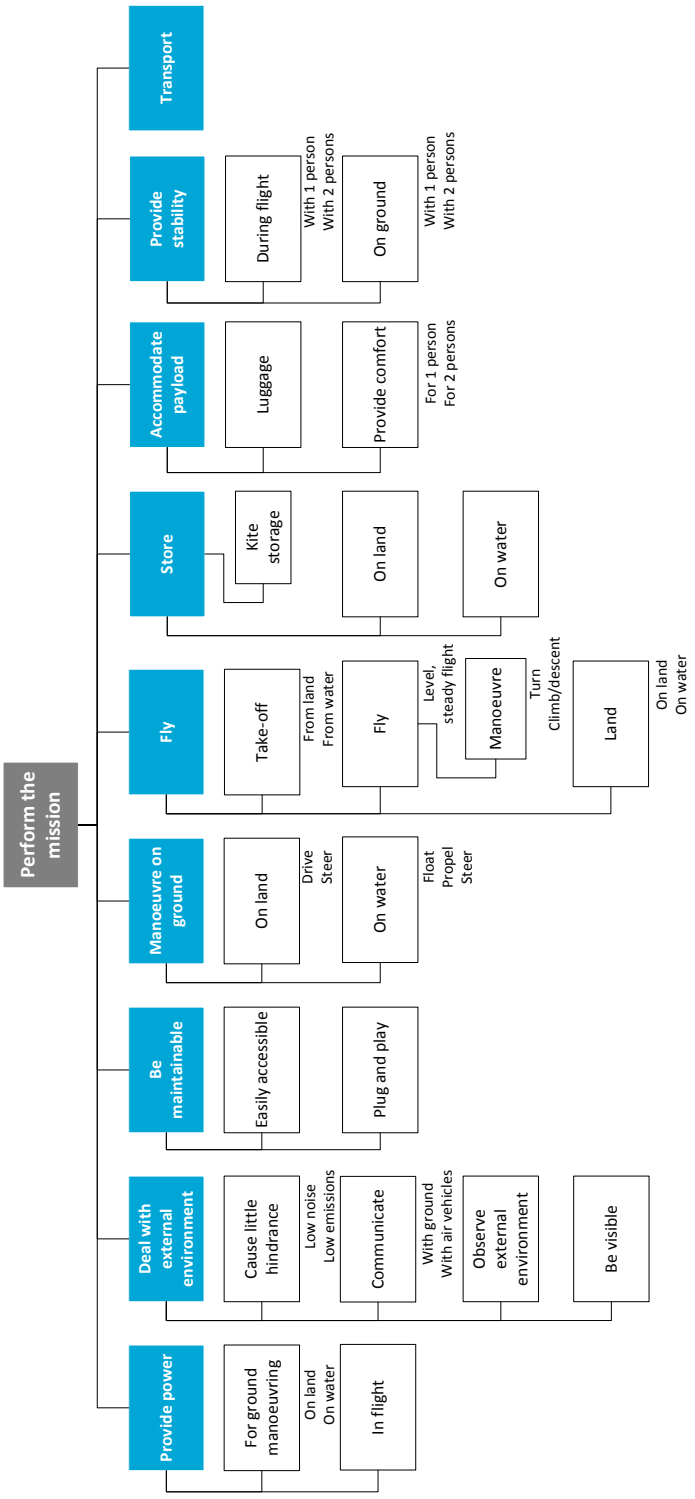

Figure A.1: Functional Breakdown Structure of Parashuttle 2, as referred to in chapter 4.

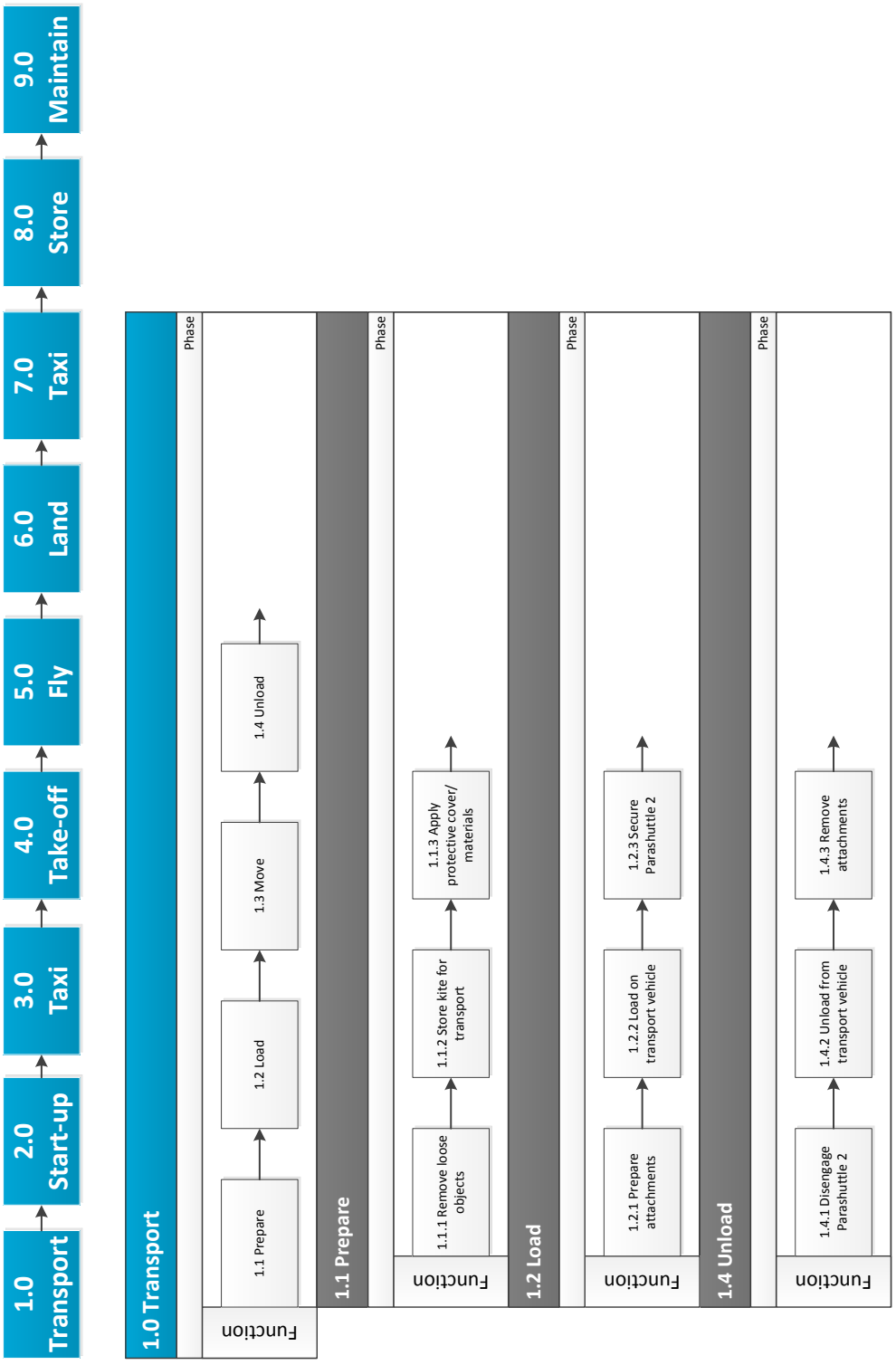

Figure A.2: Functional Flow Diagram (part 1) of Parashuttle 2, as referred to in chapter 4.

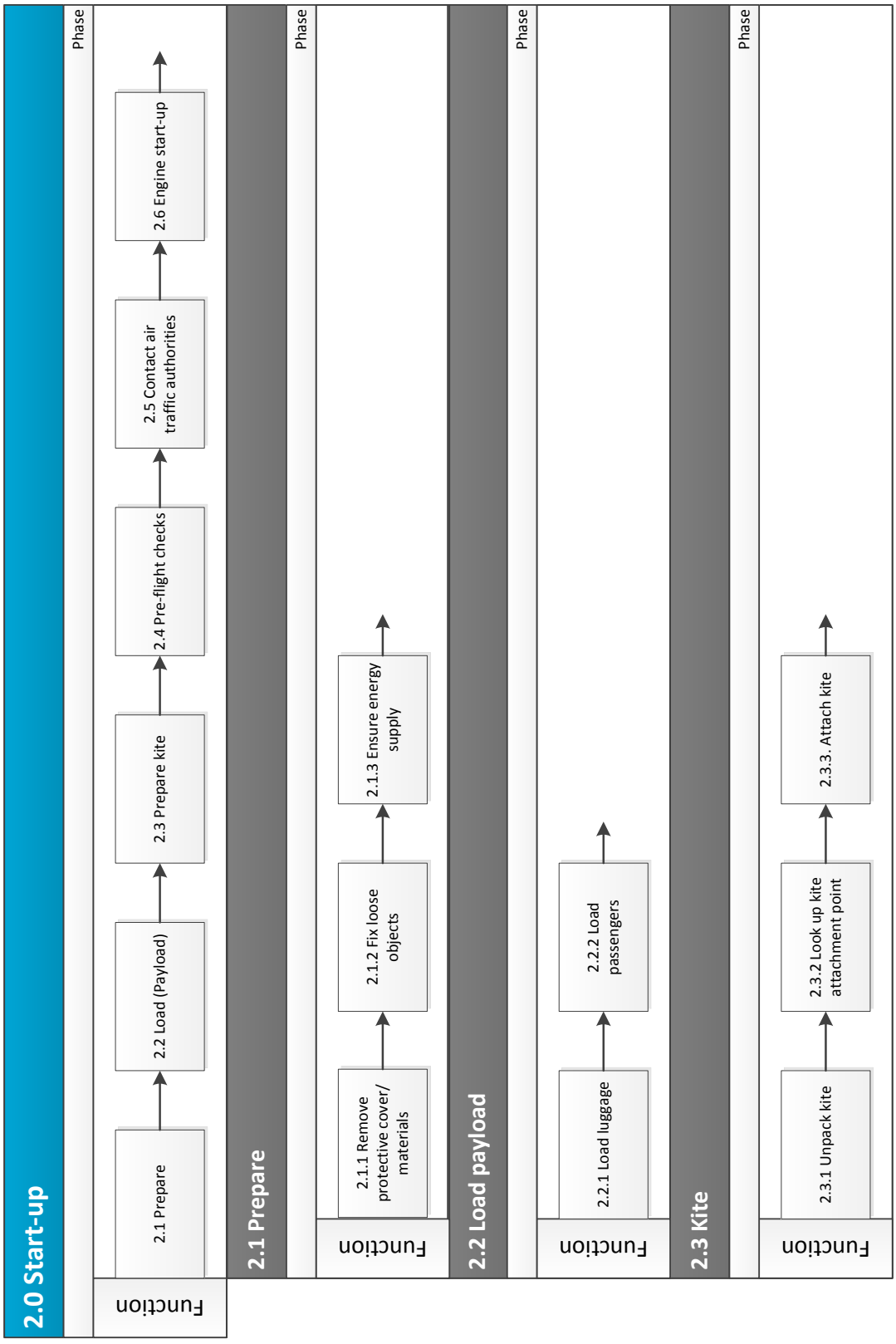

Figure A.3: Functional Flow Diagram (part 2) of Parashuttle 2, as referred to in chapter 4.

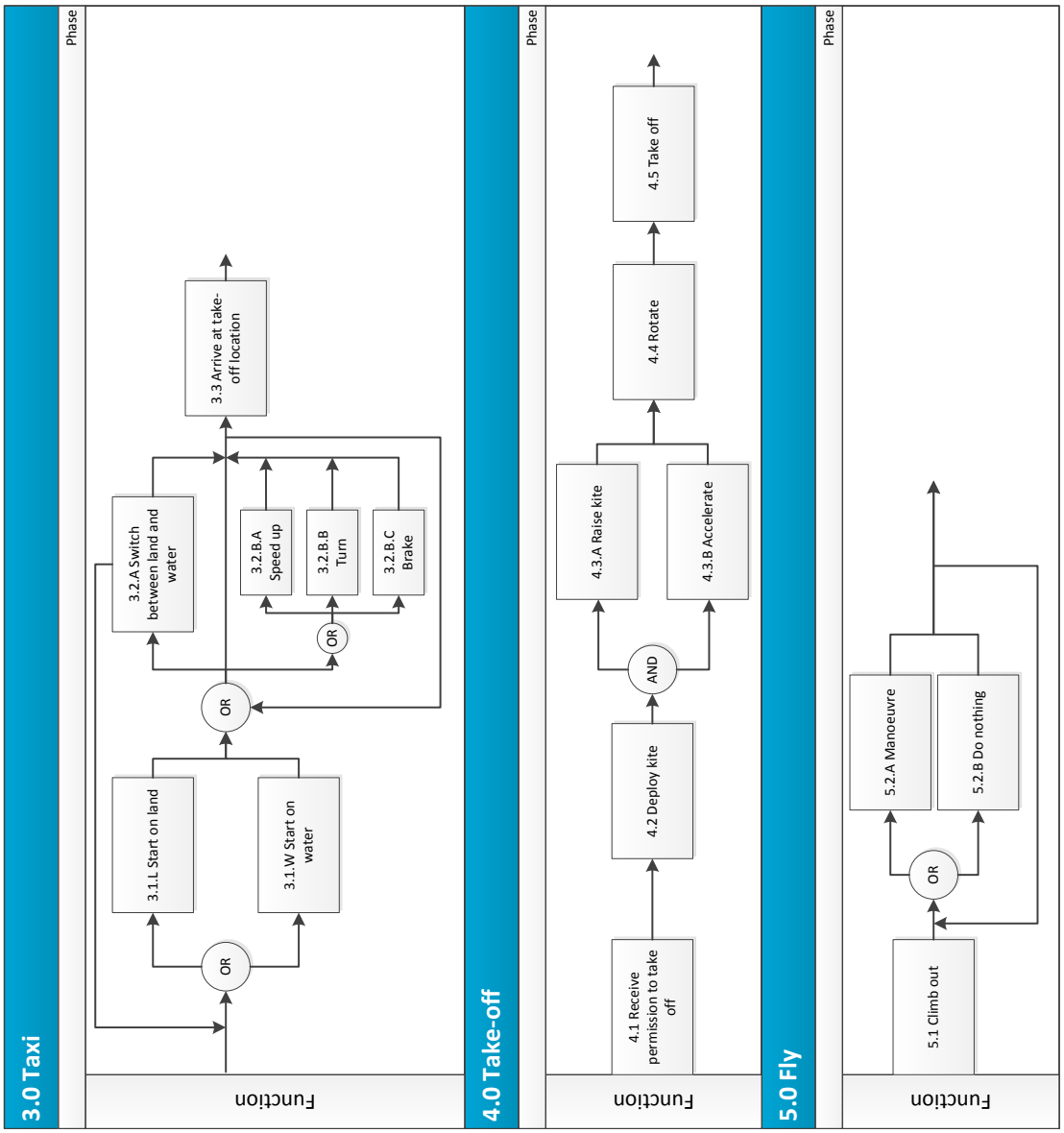

Figure A.4: Functional Flow Diagram (part 3) of Parashuttle 2, as referred to in chapter 4.

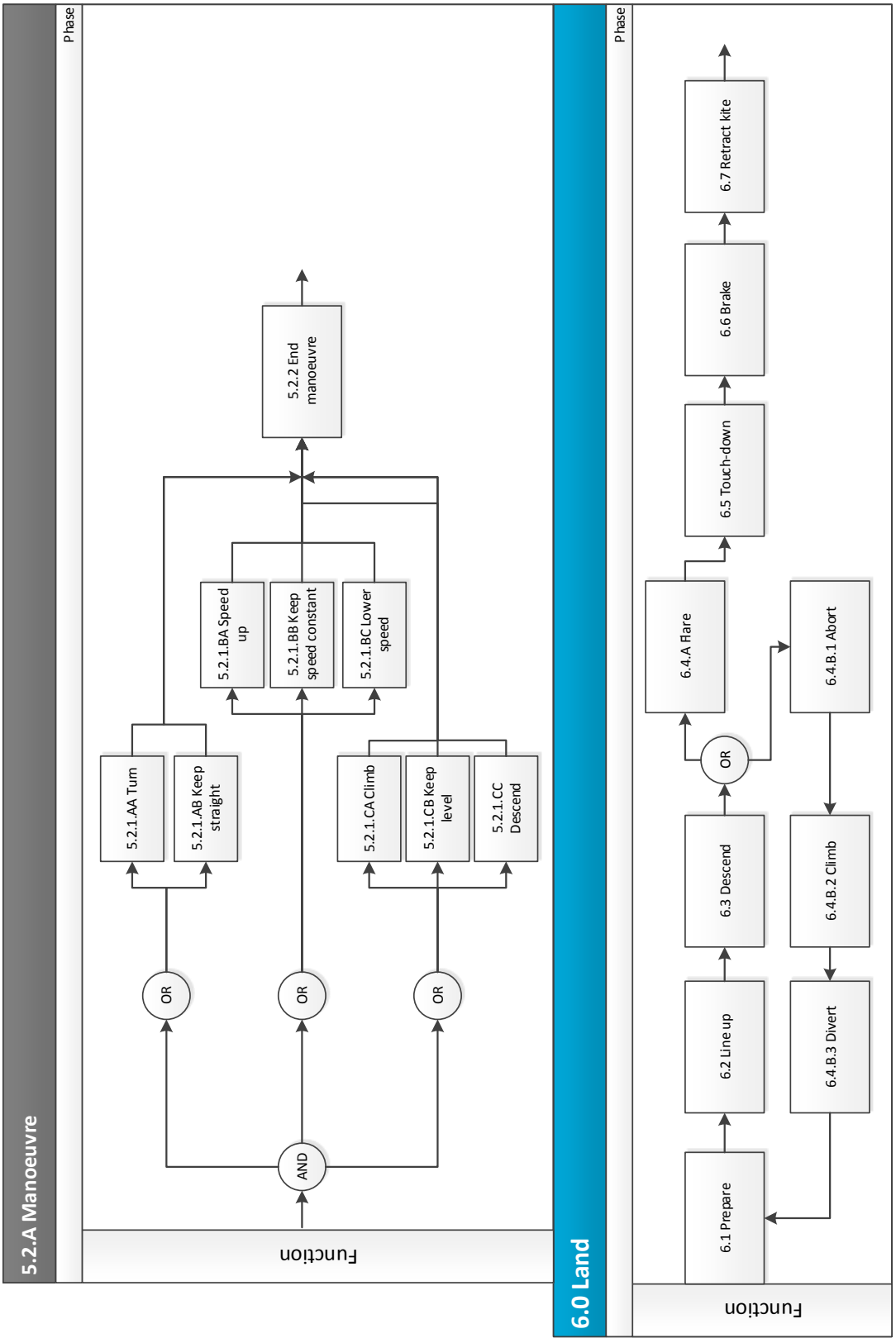

Figure A.5: Functional Flow Diagram (part 4) of Parashuttle 2, as referred to in chapter 4.

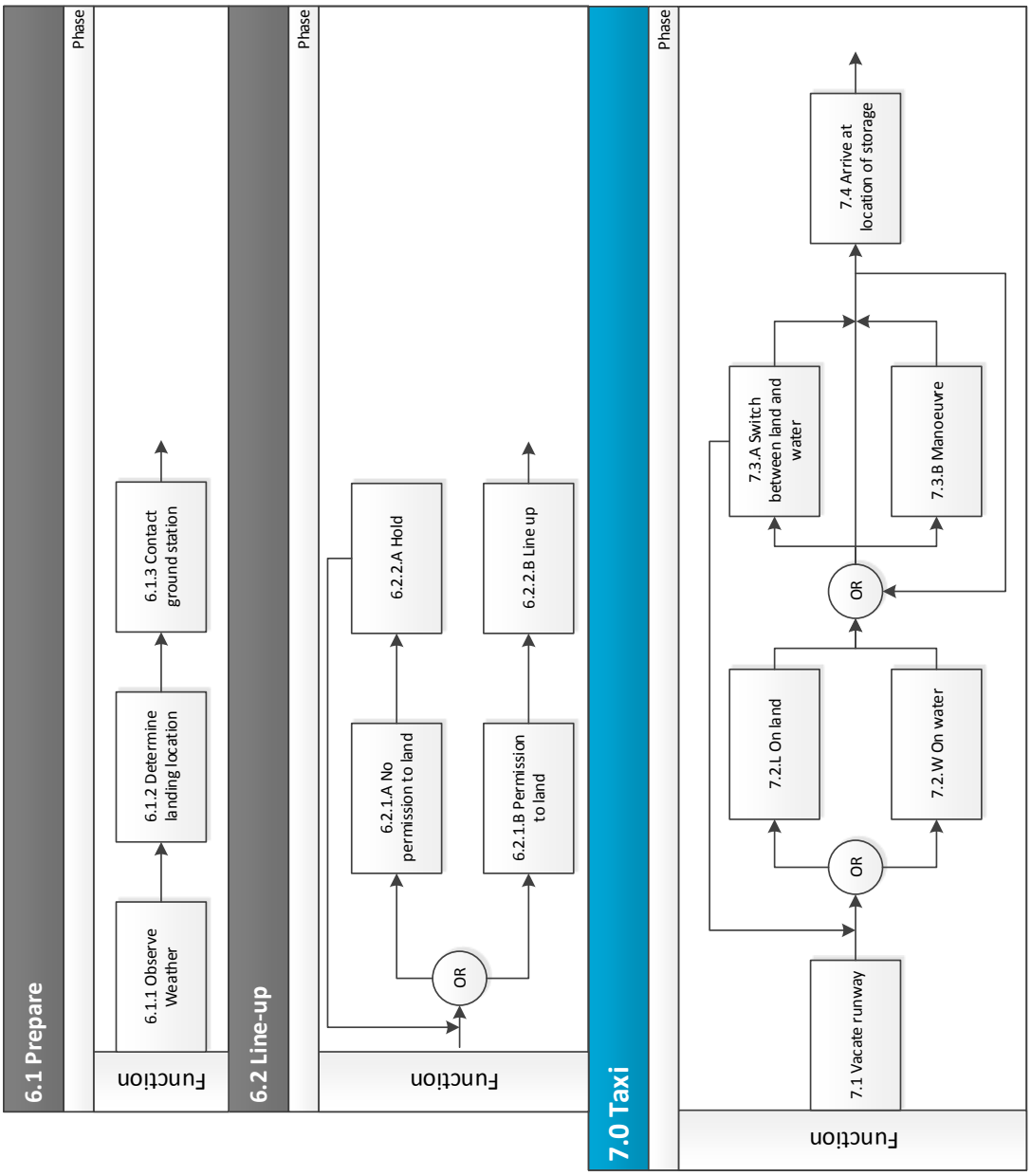

Figure A.6: Functional Flow Diagram (part 5) of Parashuttle 2, as referred to in chapter 4.

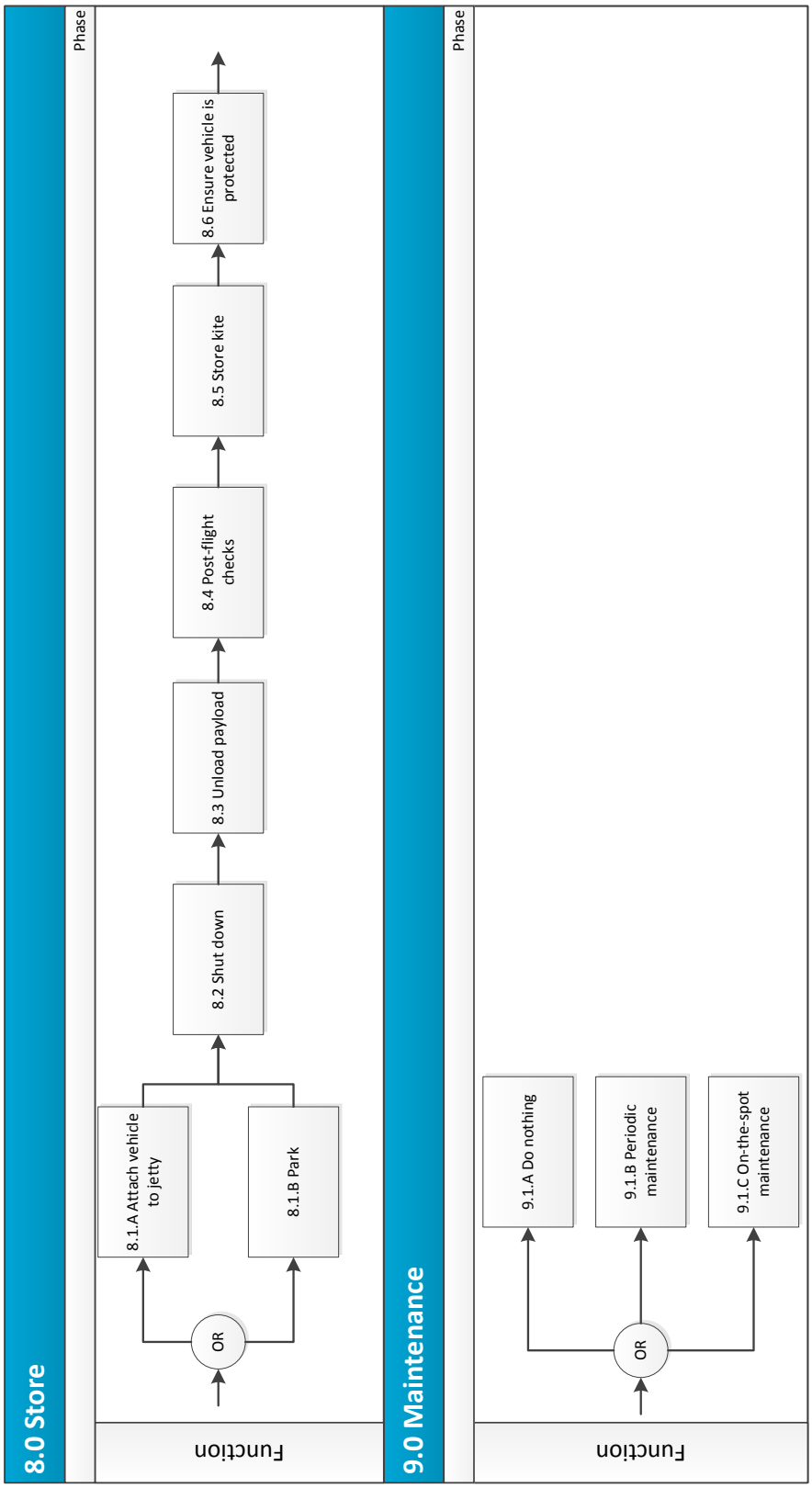

Figure A.7: Functional Flow Diagram (part 6) of Parashuttle 2, as referred to in chapter 4.

Appendix B | Requirements

This appendix presents the full set of requirements imposed on Parashuttle 2, referred to in chapter 4. All requirements have been ordered in a requirements discovery tree, shown in Figure B.1. For completeness all requirements have been stated below the figure.

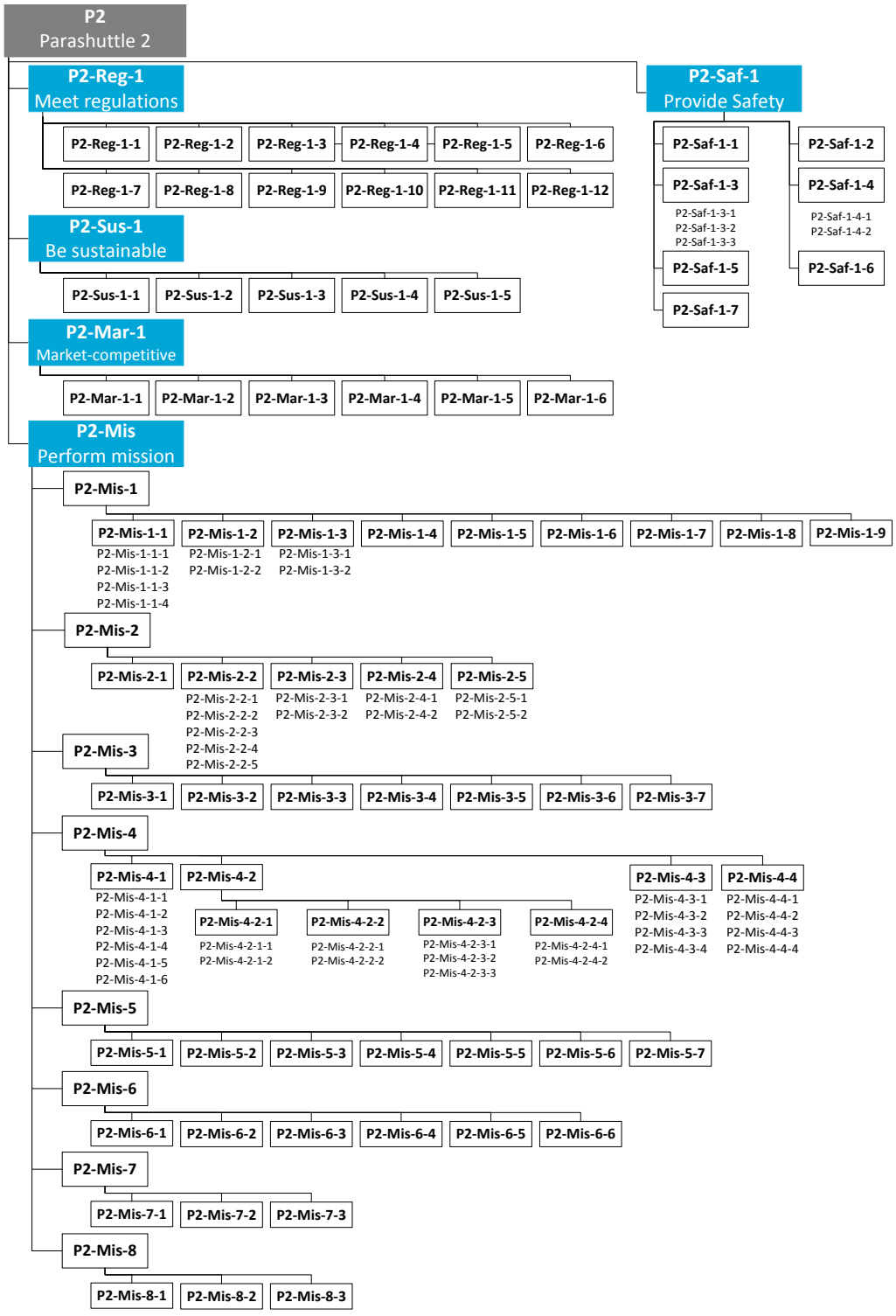

Figure B.1: Requirements discovery tree for Parashuttle 2, as referred to in chapter 4.

The full set of requirements is given below. Precise locations of the identifiers in the Requirements Discovery Tree can be found in Figure B.1. Requirements which are met by the final design are marked with a check, as discussed in chapter 29.

Table B.1: Overview of requirements of Parashuttle 2, including indications of the requirements having been met.

Identifier	Requirement	Met?
P2	Parashuttle 2 shall meet all regulations, be sustainable, be able to fulfil its entire mission and be market-competitive.	✓
P2-Reg-1	Parashuttle 2 shall meet all MLA-regulations imposed by aviation authorities and governments.	✓
P2-Reg-1-1	Parashuttle 2 shall have a maximum take-off weight not exceeding 495 kg in amphibian mode.	✓
P2-Reg-1-2	Parashuttle 2 shall have a maximum take-off weight not exceeding 450 kg in ground mode.	✓
P2-Reg-1-3	Parashuttle 2 shall be statically and dynamically stable during all operations.	✓
P2-Reg-1-4	Parashuttle 2 shall have a stall speed not exceeding 65 km/h.	✓
P2-Reg-1-5	Parashuttle 2 shall have a clearly recognisable audiovisual stall warning signal.	✓
P2-Reg-1-6	Parashuttle 2 shall be used for non-aerobatic purposes only.	✓
P2-Reg-1-7	Parashuttle 2 shall be powered by a single engine.	✓
P2-Reg-1-8	Parashuttle 2 shall perform visual flight rules (VFR) flights only.	✓
P2-Reg-1-9	Parashuttle 2 shall have a wing loading not exceeding 25kg/m^2.	✓
P2-Reg-1-10	Parashuttle 2 shall not produce noise levels exceeding 60 dB at 150 metres distance with full engine power and engine RPM.	✓
P2-Reg-1-11	In the Netherlands Parashuttle 2 shall be used for non-commercial activities only.	✓
P2-Reg-1-12	In the Netherlands Parashuttle 2 shall perform only non-work related activities.	✓
P2-Sus-1	Parashuttle 2 shall be sustainable.	✓
P2-Sus-1-1	Parashuttle 2 shall have emissions lower than or equal to those of Parashuttle 1.	✗
P2-Sus-1-2	Parashuttle 2 shall be made of durable materials.	✓
P2-Sus-1-3	Parashuttle 2 shall save on material used wherever possible.	✓
P2-Sus-1-4	Parashuttle 2 shall have an operational empty weight of at most 110% of Parashuttle 1.	✗
P2-Sus-1-5	Parashuttle 2 shall have low drag.	✓
P2-Mar-1	Parashuttle 2 shall be market-competitive.	✓
P2-Mar-1-1	Parashuttle 2 shall have a maximum sales price of €35,000.	✗
P2-Mar-1-2	Parashuttle 2 shall be available in countries with a very high human development index [175] and China.	✓
P2-Mar-1-3	Parashuttle 2 shall fit in a 1TEU ISO container [174].	✗
P2-Mar-1-4	The design of Parashuttle 2 shall be able to adjust to future market demands.	✓

Continued on next page

Table B.1 – continued from previous page

Identifier	Requirement	Met?
P2-Mar-1-5	Parashuttle 2 should have operating costs lower than or comparable to those of comparable priced LSA aircraft.	✓
P2-Mar-1-6	Parashuttle 2 shall stand out in the market due to two unique features: a closed cockpit and amphibian capabilities.	✓
P2-Saf-1	Parashuttle 2 shall be safe to operate in all mission phases.	✓
P2-Saf-1-1	Parashuttle 2 shall ensure that the passenger and pilot stay fixed in their seats in case of an impact.	✓
P2-Saf-1-2	Parashuttle 2 shall have a means of landing safely when the main parachute fails.	✗
P2-Saf-1-3	Parashuttle 2 shall be be able to safely recover from a bird-strike.	-
P2-Saf-1-3-1	Parashuttle 2 shall be be able to safely recover from a bird-strike with the parachute.	-
P2-Saf-1-3-2	Parashuttle 2 shall be be able to safely recover from a bird-strike with the fuselage.	-
P2-Saf-1-3-3	Parashuttle 2 shall be be able to safely recover from a bird-strike with the engine.	-
P2-Saf-1-4	Parashuttle 2 shall allow the crew to escape the vehicle without serious injury in case of an emergency.	✓
P2-Saf-1-4-1	Parashuttle 2 shall allow the crew to escape the vehicle without serious injury in case of fire.	✓
P2-Saf-1-4-2	Parashuttle 2 shall allow the crew to escape the vehicle without serious injury in case of a crash.	✓
P2-Saf-1-5	Parashuttle 2 shall be able to safely land in case of a fire during flight.	✓
P2-Saf-1-6	Parashuttle 2 shall cause no harm to its external environment.	✓
P2-Saf-1-7	Parashuttle 2 shall be able to withstand a load factor of 3 without detrimental effects on the vehicle.	✓
P2-Mis	Parashuttle 2 shall be able to perform its mission.	✓
P2-Mis-1	Parashuttle 2 shall be transportable.	✓
P2-Mis-1-1	Parashuttle 2 shall fit on an internationally road-legal trailer.	✓
P2-Mis-1-1-1	Parashuttle 2 shall have an empty weight of at most 500 kg [176–179].	✓
P2-Mis-1-1-2	Parashuttle 2 shall have a maximum length of 7.0 m in transport mode [176–179].	✓
P2-Mis-1-1-3	Parashuttle 2 shall have a maximum width of 2.44 m in transport mode [176–179].	✓
P2-Mis-1-1-4	Parashuttle 2 shall have a maximum height of 4.0 m in transport mode [176–179].	✓
P2-Mis-1-2	Parashuttle 2 shall be able to be prepared for flight by one person.	✓
P2-Mis-1-2-1	Parashuttle 2 shall be able to be fully inspected by one person on land.	✓
P2-Mis-1-2-2	Parashuttle 2 shall be able to be fully inspected by one person on water.	✓
P2-Mis-1-3	Parashuttle 2 shall not be damaged during transporting.	✓
P2-Mis-1-3-1	Parashuttle 2 shall not be damaged by vibrations during transporting.	✓
P2-Mis-1-3-2	Parashuttle 2 shall not be damaged by impact during loading onto the transport vehicle.	✓
P2-Mis-1-4	Parashuttle 2 shall be able to be loaded unto a transport vehicle by 1 person.	✓

Continued on next page

Table B.1 – continued from previous page

Identifier	Requirement	Met?
P2-Mis-1-5	Parashuttle 2 shall be able to be refuelled/recharged by one person.	✓
P2-Mis-1-6	Parashuttle 2 shall be able to carry 180 kg of payload, including passengers.	✓
P2-Mis-1-7	Parashuttle 2 shall be able to carry 2 persons inside the cockpit.	✓
P2-Mis-1-8	Parashuttle 2 shall be able to communicate with ground authorities.	✓
P2-Mis-1-9	Parashuttle 2 shall allow for engine start-up from within the cockpit.	✓
P2-Mis-2	Parashuttle 2 shall manoeuvrable on ground.	✓
P2-Mis-2-1	Parashuttle 2 shall be fully stable during all ground operations for all loading conditions.	✓
P2-Mis-2-2	Parashuttle 2 shall be drivable over both land and water.	✓
P2-Mis-2-2-1	Parashuttle 2 shall have a floating capacity of 180% of MTOW [96, 140].	✓
P2-Mis-2-2-2	Parashuttle 2 shall be manoeuvrable in 'sea state 2' conditions.	✓
P2-Mis-2-2-3	Parashuttle 2 shall have a maximum velocity of over 3 m/s on land.	✓
P2-Mis-2-2-4	Parashuttle 2 shall have a maximum velocity of over 2 m/s on water.	✓
P2-Mis-2-2-5	Parashuttle 2 shall be able to withstand both fresh and salt water.	✓
P2-Mis-2-3	Parashuttle 2 shall be able to brake during ground manoeuvring.	✓
P2-Mis-2-3-1	Parashuttle 2 shall come to a standstill from 3 m/s within 5 m on land.	✓
P2-Mis-2-3-2	Parashuttle 2 shall come to a standstill from 2 m/s within 5 m on water.	✗
P2-Mis-2-4	Parashuttle 2 shall be able to turn during ground manoeuvring.	✓
P2-Mis-2-4-1	Parashuttle 2 shall have a maximum turn radius of 6 m on land.	✓
P2-Mis-2-4-2	Parashuttle 2 shall have a maximum turn radius of 8 m on water.	✓
P2-Mis-2-5	Parashuttle 2 shall be able to switch from land to water and vice versa.	✓
P2-Mis-2-5-1	Parashuttle 2 shall be able to drive up a 15° ramp.	✓
P2-Mis-3-1:	Parashuttle 2 shall be able to take off from both land and water.	✓
P2-Mis-3-1-1	Parashuttle 2 shall be able to take off in 'sea state 2' conditions [180].	✓
P2-Mis-3-1-2	Parashuttle 2 shall be able to take off from unprepared surfaces on land.	✓
P2-Mis-3-1-3	Parashuttle 2 shall have a maximum take-off distance of 40 m on land.	✓
P2-Mis-3-1-4	Parashuttle 2 shall have a maximum take-off distance of 60 m on water.	✓
P2-Mis-3-1-5	Parashuttle 2 shall have a kite that is deployable by 1 person on both land and water.	✓
P2-Mis-3-1-6	Parashuttle 2 shall be able to raise its kite while accelerating.	✓
P2-Mis-3-1-7	Parashuttle 2 shall have a minimum take-off speed of 1.1 V_{stall}.	✓
P2-Mis-4	Parashuttle 2 shall be able to be flown by one pilot.	✓
P2-Mis-4-1	Parashutle 2 shall be able to perform steady and level flight.	✓
P2-Mis-4-1-1	Parashuttle 2 shall be fully stable in all flight conditions.	✓
P2-Mis-4-1-2	Parashuttle 2 shall be able to operate between ground altitude and 1500 metres altitude [181].	✓
P2-Mis-4-1-3	Parashuttle 2 shall have a cruise speed of at least 45 km/h.	✓
P2-Mis-4-1-4	Parashuttle 2 shall have a maximum velocity of at least 50 km/h.	✓
P2-Mis-4-1-5	Parashuttle 2 shall have a range of at least 100 kilometres.	✓
P2-Mis-4-1-6	Parashuttle 2 shall have an endurance of at least 2.5 hours.	✓
P2-Mis-4-2	Parashuttle 2 shall be able to perform in-flight manoeuvres.	✓

Continued on next page

Table B.1 – continued from previous page

Identifier	Requirement	Met?
P2-Mis-4-2-1	Parashuttle 2 shall be able to climb.	✓
P2-Mis-4-2-1-1	Parashuttle 2 shall have a minimum climb rate of 3.0 m/s at ground altitude.	✓
P2-Mis-4-2-1-2	Parashuttle 2 shall achieve a climb angle of 25° at ground altitude.	✗
P2-Mis-4-2-2	Parashuttle 2 shall be able to descend.	✓
P2-Mis-4-2-2-1	Parashuttle 2 shall have a maximum descent rate of 7 m/s.	✗
P2-Mis-4-2-2-2	Parashuttle 2 shall be able to sustain a 30° descent angle.	✗
P2-Mis-4-2-3	Parashuttle 2 shall be able to perform turning manoeuvres.	✓
P2-Mis-4-2-3-1	Parashuttle 2 shall be able to perform a rate 4 (12 °/s) turn.	✓
P2-Mis-4-2-3-2	Parashuttle 2 shall be able to have an in-flight turn radius of at most 40 metres.	✓
P2-Mis-4-2-3-3	Parashuttle 2 shall be able to sustain a bank angle of 60°.	-
P2-Mis-4-2-4	Parashuttle 2 shall be able to accelerate and decelerate during flight.	✓
P2-Mis-4-2-4-1	Parashuttle 2 shall be able to control its velocity during flight.	✓
P2-Mis-4-2-4-2	Parashuttle 2 shall be able to achieve a velocity change from 25 to 45 km/h in 5 seconds.	✓
P2-Mis-4-3	Parashuttle 2 shall be able to deal with disturbances.	✗
P2-Mis-4-3-1	Parashuttle 2 shall be able to handle 10 km/h gusts.	-
P2-Mis-4-3-2	Parashuttle 2 shall be able to safely land in case of an engine failure.	✓
P2-Mis-4-3-3	Parashuttle 2 shall be able to safely land in case one of the parachute attachment lines fails.	✗
P2-Mis-4-3-4	Parashuttle 2 shall be able to recover from parachute stall/loss of lift with an altitude loss of at most 100 metres.	-
P2-Mis-4-4	Parashuttle 2 shall allow the pilot to deal with the external environment.	✓
P2-Mis-4-4-1	Parashuttle 2 shall allow the pilot to observe the weather conditions.	✓
P2-Mis-4-4-2	Parashuttle 2 shall provide the pilot with 360 degrees of view in the local horizontal plane and 60 degrees top view.	✓
P2-Mis-4-4-3	Parashuttle 2 shall allow the pilot to communicate with other aerial vehicles.	✓
P2-Mis-5	Parashuttle 2 shall be able to land on both land and water.	✓
P2-Mis-5-1	Parashuttle 2 shall be able to land on a different surface than the surface it took off from.	✓
P2-Mis-5-2	Parashuttle 2 shall be able to abort its landing procedure up to an altitude of 10 metres.	✓
P2-Mis-5-3	Parashuttle 2 shall be able to land on (un-prepared) land.	✓
P2-Mis-5-3-1	Parashuttle 2 shall be able to come to a standstill on land within 180 metres after clearing a 15 m obstacle.	✓
P2-Mis-5-4	Parashuttle 2 shall be able to land on water under sea state 2 conditions[180].	✓
P2-Mis-5-4-1	Parashuttle 2 shall have a maximum landing distance of 180 metres on water after clearing a 15 m obstacle.	✓
P2-Mis-5-5	Parashuttle 2 shall have an minimum approach speed equal to 1.1 times the stall speed.	✓
P2-Mis-5-6	Parashuttle 2 shall be able to sustain a ground impact when landing with a vertical velocity of 2 m/s	✓
P2-Mis-5-7	Parashuttle 2 shall be able to flare before touch-down.	✓

Continued on next page

Table B.1 – continued from previous page

Identifier	Requirement	Met?
P2-Mis-6	Parashuttle 2 shall be able to be stored between flights.	✓
P2-Mis-6-1	Parashuttle 2 shall be able to be secured on land with a running engine by one person.	✓
P2-Mis-6-2	Parashuttle 2 shall be able to be secured on water with a running engine by one person.	✓
P2-Mis-6-3	Parashuttle 2 shall be able to be shut down from the cockpit by one person.	✓
P2-Mis-6-4	Parashuttle 2 shall allow for post-flight checks to be performed by one person.	✓
P2-Mis-6-5	Parashuttle 2 shall allow for the kite storage to be done by one person.	✓
P2-Mis-6-6	Parashuttle 2 shall be able to be stored over an extended period without major degradation.	✓
P2-Mis-7	Parashuttle 2 shall be able to be maintained by one person.	✓
P2-Mis-7-1	Parashuttle 2 shall allow for easy access to all components.	✓
P2-Mis-7-2	Parashuttle 2 shall allow for replacing of components by one person.	✓
P2-Mis-7-3	Parashuttle 2 shall be able to be used directly after maintenance (plug & play).	✓
P2-Mis-8	Parashuttle 2 shall provide comfort to the passengers.	✓
P2-Mis-8-1	Parashuttle 2 shall have a closed-cockpit fuselage.	✓
P2-Mis-8-2	Parashuttle 2 shall be able to thermally control the fuselage.	✓
P2-Mis-8-3	Parashuttle 2 shall have a cockpit with high visibility.	✓

Appendix C | Instruments

This appendix lists what instruments are integrated in the standard version and the deluxe version of the cockpit. In Table C.1 the price, mass and power usage of the instruments are shown. In the two righthand columns it can be seen what instruments are used in which version of the cockpit. In Table C.2 data on the two versions is summarised.

Table C.1: Instrument data

Instrument	**Function(s)**	**Cost** [€]	**Mass** [gr]	**Current drain** [mA]	**Standard**	**Deluxe**
Alinco DR-635 Radio [182]	Communication	400	1,000	700	✓	
Stratomaster V10 Radio [183]	Communication	990	1,088	1,500		✓
Stratomaster ASX-1 [184]	Altimeter, Airspeed Indicator	215 [185]	100	50	✓	
Stratomaster FF-1 [184]	Fuel Management System	115 [185]	100	70	✓	
Stratomaster EMS-582 [184]	Engine Monitoring System	230 [185]	100	45	✓	
Xtreme EFIS (incl. RDAC XF, SP-6 and SP-7) [186]	Engine Monitoring System GPS Attitude Altimeter Airspeed Indicator Fuel Management System Magnetic Heading Direction G-Force Indicator Outside Air Temperature Vertical Speed Indicator Wind Speed and Direction Indicator	3,300	1,250	450		✓

Table C.2: Standard version and Deluxe version information.

Version	**Cost** [€]	**Mass** [kg]	**Current drain** [mA]
Standard	960	1.3	865
Deluxe	4,290	2.3	1,950

Appendix D | Frame member details

The fuselage truss structure of Parashuttle 2 is depicted in figures D.1 and D.2. The accompanying red numbers serve to identify the beams, of which details are given in tables D.1 and D.2.

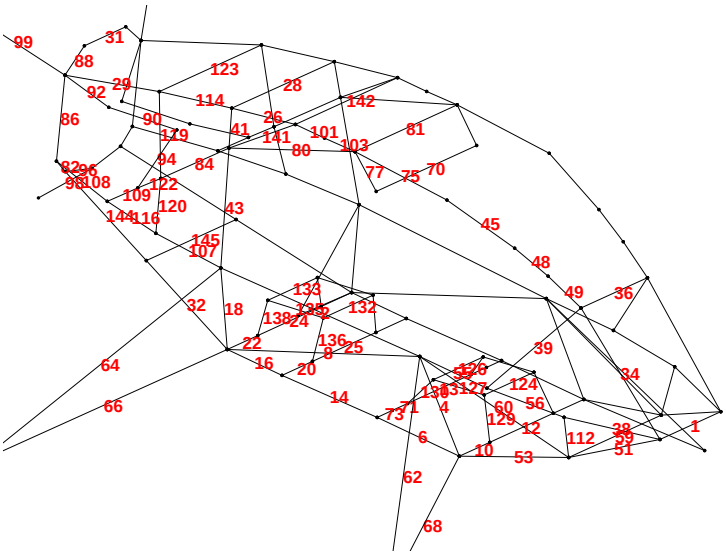

Figure D.1: Beam locations

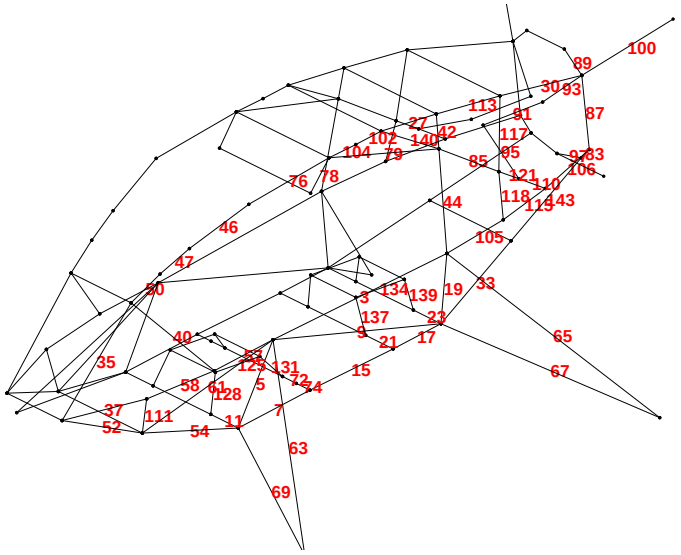

Figure D.2: Beam locations (2)

Table D.1: Details of the frame members

Element	Inner radius [mm]	Outer radius [mm]	Length [m]	Mass [kg]	Maximum stress [MPa]	Normal stress[MPa]
1	17.3	18.8	0.440	0.192	85.5	85.2
2	17.3	18.8	1.199	0.524	136.3	135.8
3	17.3	18.8	1.199	0.524	143.7	143.6
4	8.4	9.9	0.505	0.113	190.9	168.6
5	8.4	9.9	0.505	0.112	177.7	152.6
6	11.3	12.8	0.510	0.149	247.6	230.2
7	11.3	12.8	0.510	0.149	246.4	223.7
8	12.9	14.4	1.229	0.405	136.9	76.6
9	14.0	15.5	1.229	0.439	155.2	89.9
10	9.4	10.9	0.220	0.054	257.3	257.2
11	9.4	10.9	0.220	0.054	270.7	266.4
12	9.4	10.9	0.460	0.113	79.3	79.3
13	9.1	10.6	0.460	0.110	105.3	93.0
14	11.3	12.8	0.589	0.173	223.2	219.0
15	11.3	12.8	0.589	0.173	225.7	215.7
16	11.3	12.8	0.340	0.100	291.1	275.4
17	11.3	12.8	0.340	0.100	271.0	254.4
18	20.6	22.1	0.435	0.228	289.4	237.5
19	20.6	22.1	0.435	0.228	245.8	191.4
20	8.7	10.2	0.220	0.050	282.9	278.4
21	8.7	10.2	0.220	0.050	206.4	199.8
22	20.6	22.1	0.220	0.115	229.6	195.4
23	20.6	22.1	0.220	0.115	175.8	142.2
24	20.6	22.1	0.460	0.241	195.6	151.8
25	8.7	10.2	0.460	0.105	100.4	84.8
26	22.6	25.0	0.393	0.368	292.8	284.5
27	22.6	25.0	0.391	0.366	284.7	272.2
28	20.6	22.1	0.740	0.388	100.4	99.3
29	22.6	25.0	0.681	0.638	48.8	47.1
30	22.6	25.0	0.681	0.638	91.1	89.0
31	16.6	18.1	0.300	0.126	171.6	170.6
32	11.3	12.8	0.666	0.195	148.7	148.4
33	11.3	12.8	0.666	0.195	138.0	138.0
34	22.6	25.0	0.722	0.677	54.1	47.6
35	22.6	25.0	0.722	0.677	105.2	89.7
36	8.6	10.1	0.480	0.108	72.4	65.1
37	17.3	18.8	0.476	0.208	110.4	108.2
38	17.3	18.8	0.476	0.208	90.6	90.2
39	8.7	10.2	0.636	0.145	135.4	132.3
40	8.4	9.9	0.636	0.141	133.3	130.2
41	20.6	22.1	0.193	0.101	222.9	179.5
42	20.6	22.1	0.193	0.101	260.8	243.6
43	20.6	22.1	0.579	0.304	288.3	286.7
44	20.6	22.1	0.579	0.304	220.5	205.6
45	22.6	25.0	0.404	0.378	44.6	37.2
46	22.6	25.0	0.404	0.378	58.2	41.6
47	22.6	25.0	0.209	0.196	87.6	70.7
48	22.6	25.0	0.209	0.196	54.0	46.6
49	22.6	25.0	0.218	0.204	57.5	50.1
50	22.6	25.0	0.218	0.204	104.3	87.2
51	11.3	12.8	0.513	0.150	69.4	34.9
52	11.3	12.8	0.513	0.150	75.0	44.8
53	11.3	12.8	0.599	0.175	129.5	104.9
54	11.3	12.8	0.599	0.175	129.1	102.7
55	17.3	18.8	0.417	0.182	95.3	92.4
56	17.3	18.8	0.434	0.190	79.9	76.4
57	17.3	18.8	0.417	0.182	101.0	101.0
58	17.3	18.8	0.434	0.190	113.7	112.9
59	8.2	9.7	0.670	0.145	60.3	46.3
60	8.8	10.3	0.887	0.205	54.0	53.4
61	9.1	10.6	0.887	0.212	60.4	60.4
62	11.3	12.8	1.192	0.349	73.8	64.6
63	12.3	13.8	1.192	0.378	76.8	76.2
64	21.2	22.7	1.532	0.818	130.5	130.4
65	20.3	21.8	1.532	0.782	120.2	120.2
66	19.6	21.1	1.306	0.644	250.1	151.5
67	21.1	22.6	1.306	0.692	261.8	179.3
68	12.5	14.0	0.843	0.272	155.2	155.0
69	14.4	15.9	0.843	0.310	204.0	204.0
70	8.4	9.9	0.727	0.162	90.5	89.8
71	9.1	10.6	0.110	0.026	282.4	280.5
72	9.1	10.6	0.110	0.026	275.2	272.6

Table D.2: Details of the frame members- continued

Element	Inner radius [mm]	Outer radius [mm]	Length [m]	Mass [kg]	Maximum stress [MPa]	Normal stress[MPa]
74	9.1	10.6	0.110	0.026	140.0	138.4
75	22.6	25.0	0.574	0.538	113.2	106.8
76	22.6	25.0	0.574	0.538	287.6	272.7
77	17.6	19.1	0.212	0.094	283.9	282.0
78	22.2	25.0	0.212	0.224	292.4	292.4
79	16.6	18.1	0.769	0.324	284.3	155.7
80	12.4	13.9	0.770	0.245	182.9	182.9
81	9.2	10.7	0.740	0.179	75.4	64.6
82	16.6	18.1	0.110	0.046	260.1	241.6
83	16.6	18.1	0.110	0.046	153.8	132.6
84	9.3	10.8	0.493	0.120	122.3	70.0
85	14.4	15.9	0.495	0.182	147.8	138.6
86	16.6	18.1	0.456	0.192	120.3	117.4
87	16.6	18.1	0.456	0.192	182.3	180.4
88	16.6	18.1	0.169	0.071	292.5	290.1
89	16.6	18.1	0.169	0.071	221.8	220.8
90	18.5	20.0	0.420	0.197	291.2	273.5
91	8.6	10.1	0.420	0.095	260.9	254.3
92	18.8	20.3	0.323	0.153	291.1	258.6
93	23.4	24.9	0.323	0.189	284.2	283.3
94	9.6	11.1	0.395	0.099	276.5	266.2
95	19.5	21.0	0.395	0.196	287.8	277.4
96	16.6	18.1	0.206	0.087	101.3	101.3
97	16.6	18.1	0.206	0.087	121.8	120.7
98	8.6	10.1	0.409	0.093	149.7	147.4
99	11.6	13.1	0.654	0.196	146.5	146.5
100	11.5	13.0	0.654	0.194	148.2	148.2
101	22.6	25.0	0.181	0.169	180.8	132.8
102	22.6	25.0	0.181	0.169	175.9	128.5
103	22.6	25.0	0.189	0.177	100.0	81.6
104	22.6	25.0	0.189	0.177	88.3	74.7
105	17.3	18.8	0.430	0.188	202.3	201.0
106	17.3	18.8	0.441	0.193	209.9	209.7
107	17.3	18.8	0.430	0.188	124.5	124.3
108	17.3	18.8	0.441	0.193	188.3	151.8
109	9.3	10.8	0.223	0.054	283.4	225.4
110	14.4	15.9	0.223	0.082	268.5	256.1
111	8.6	10.1	0.243	0.055	133.4	126.8
112	8.7	10.2	0.243	0.056	130.0	126.8
113	22.6	25.0	0.451	0.423	154.5	151.8
114	22.6	25.0	0.449	0.421	87.0	86.6
115	17.3	18.8	0.369	0.161	149.1	148.9
116	17.3	18.8	0.369	0.161	101.0	101.0
117	9.0	10.5	0.422	0.099	221.8	221.7
118	9.0	10.5	0.262	0.062	121.0	113.7
119	8.7	10.2	0.422	0.097	130.8	102.1
120	8.7	10.2	0.262	0.060	112.7	97.9
121	14.4	15.9	0.176	0.065	290.2	282.7
122	9.3	10.8	0.176	0.043	198.7	129.3
123	8.8	10.3	0.740	0.171	79.1	58.2
124	9.0	10.5	0.360	0.085	44.0	43.5
125	8.6	10.1	0.313	0.071	149.0	149.0
126	8.7	10.2	0.360	0.082	62.3	62.3
127	8.3	9.8	0.313	0.068	175.3	175.3
128	8.6	10.1	0.224	0.051	167.5	167.3
129	8.9	10.4	0.224	0.052	198.1	197.9
130	8.7	10.2	0.187	0.043	237.1	236.1
131	9.0	10.5	0.187	0.044	220.3	218.9
132	8.8	10.3	0.360	0.084	37.6	37.6
133	9.3	10.8	0.360	0.088	49.2	49.0
134	8.5	10.0	0.343	0.077	53.6	50.4
135	9.0	10.5	0.343	0.081	59.7	56.8
136	8.3	9.8	0.220	0.048	217.2	216.2
137	8.7	10.2	0.220	0.050	175.7	175.0
138	8.8	10.3	0.177	0.041	273.3	270.0
139	8.7	10.2	0.177	0.041	272.6	270.0
140	8.7	10.2	0.438	0.100	205.4	92.4
141	15.9	17.4	0.439	0.177	247.2	162.4
142	8.3	9.8	0.740	0.162	38.3	36.3
143	11.3	12.8	0.666	0.195	88.0	88.0
144	11.3	12.8	0.666	0.195	102.8	102.7
145	8.6	10.1	0.650	0.147	33.7	33.5

Appendix E | Mass and cost breakdown

In Table E.1 the complete mass and cost breakdown of Parashuttle 2 is shown.

Table E.1: The mass and cost breakdown of Parashuttle 2

	Mass breakdown		Cost breakdown		
System	**Mass** [kg]	**Uncertainty** [kg]	**Material cost** [€]	**Labour cost** [€]	**Uncertainty** [€]
Propulsion	**86.6**	**1.5**	**8,096**	**504**	**0**
Engine & accessories	63.2	0	7,000	-	0
Fuel tank	5.7	1	13	84	0
Propeller	4.5	0	800	-	0
Duct	13.2	0.5	283	420	0
Kite	**16.7**	**4**	**5,100**	**-**	**1,000**
Kite	16	4	5,000	-	1,000
Kite connection	0.7	0	100	-	0
Undercarriage	**42.3**	**1.8**	**1,580**	**2,688**	**88**
Floats	28.2	0.6	72	2,240	3
Wheels & connection	12	1	1506	-	85
Rudders	2.1	0.2	2	448	0
Control System	**14.2**	**2.4**	**690**	**-**	**61**
Kite control	8.1	1	365	-	1
Engine control	0.2	0.1	63	-	10
Wheel control	3.3	0.7	190	-	34
Rudder control	2.6	0.6	72	-	16
Fuselage	**66.2**	**3.4**	**526**	**924**	**12**
Frame structure	31.5	0.5	360	-	5
Outer skin	16.5	2.5	41	224	1
Windows	11.4	0	60	700	1
Floor panels	3.1	0.2	25	-	1
Door frame	3.7	0.2	40	-	4
Cockpit	**32.4**	**3.3**	**2,199**	**-**	**120**
Instruments	1.3	0	1,000	-	0
Seats	5.4	0	288	-	0
Seat belts	1.5	0.1	400	-	50
Electrical system	6.1	0.2	180	-	0
Heating	10	2	200	-	50
Upholstering	8.1	1	131	-	20
Extra	**5.5**	**2**	**260**	**-**	**50**
Paint	5	2	200	-	50
Life vests	0.5	0	60	-	0

Table E.2: Total mass and cost for Parashuttle 2.

Mass [kg]		**Cost** [€]	
OEW	264.7	Components	18,574
Fuel mass	30	Labour cost manufacturing parts	4,116
Payload mass	180	Labour cost assembly	7,000
MTOW	474.7	Total	29,690
Uncertainty	±19	Uncertainty	±1321

Appendix F | Technical drawings

The technical drawings of the final design of Parashuttle 2 are shown below: